8-2016

Computational Labeling, Partitioning, and Balancing of Molecular Networks

Biaobin Jiang
Purdue University

Graduate School Form
30 Updated 12/26/2015

PURDUE UNIVERSITY
GRADUATE SCHOOL
Thesis/Dissertation Acceptance

This is to certify that the thesis/dissertation prepared

By Biaobin Jiang

Entitled
COMPUTATIONAL LABELING, PARTITIONING, AND BALANCING OF MOLECULAR NETWORKS

For the degree of Doctor of Philosophy

Is approved by the final examining committee:

Michael Gribskov
Chair

Daisuke Kihara

Henry C. Chang

Jennifer Neville

To the best of my knowledge and as understood by the student in the Thesis/Dissertation Agreement, Publication Delay, and Certification Disclaimer (Graduate School Form 32), this thesis/dissertation adheres to the provisions of Purdue University's "Policy of Integrity in Research" and the use of copyright material.

Approved by Major Professor(s): Michael Gribskov

Approved by: Daoguo Zhou 7/6/2016

Head of the Departmental Graduate Program Date

COMPUTATIONAL LABELING, PARTITIONING, AND BALANCING OF MOLECULAR NETWORKS

A Dissertation

Submitted to the Faculty

of

Purdue University

by

Biaobin Jiang

In Partial Fulfillment of the

Requirements for the Degree

of

Doctor of Philosophy

August 2016

Purdue University

West Lafayette, Indiana

Dedicated to my family

ACKNOWLEDGMENTS

It is my great honor to be surrounded by many inspirational and friendly people during my whole graduate study at Purdue. I first would like to thank my Ph.D. advisor Michael Gribskov, for his unlimited encouragement over the years. His educational philosophy fosters a truly academic freedom that supports me to think about the questions I am really interested in. I am also grateful to my committee members: Daisuke Kihara, Henry Chang, and Jennifer Neville for their helpful comments. I am also indebted to David Gleich for his numerous discussions on many technical details of my research since he came to Purdue in 2011. I would also like to thank Chun-Ju Chang for offering the collaboration opportunity which widens the scope of my research. Of course, I cannot forget the supports from my research collaborators: Yong Wang who led me to the field of bioinformatics, and Kyle Kloster for his patient discussions and revision of our manuscript. Most of all, I owe my deepest gratitude to my family for their endless love in my whole life.

PREFACE

Computational biology is still in its infancy. It had not been included in any college curriculum until the end of last century. That means every young researcher in computational biology has his/her own story about how to transition to this new field of study. Here, I would like to share my story about how I become a computational biologist step by step.

My major in college was pharmaceutical engineering whose curriculum is a combination of chemistry, chemical engineering and pharmacology. At that time, I had very poor ability to keep tons of chemical reaction formulas in mind, and therefore gained very little academic achievement in my major. In 2007, I accidentally registered a course on mathematical modeling when I was a sophomore. The first project was to use mathematical models to predict the Chinese population in the future. I still remember I used a logistic regression model to fit the given population data in the past. As a result, my report received a top grade, which deeply encouraged me to do something bigger in this field. In that summer, I founded a team with Yuanhai Xue from computer science and Yongzhuo Li from optoelectronics to participate in a five-round campus-wide competition in order to represent our college for the international contest. One of the problems we were given was to design a power supply network that connects hundreds of villages with minimal lengths. Yuanhai taught me Kruskal's algorithm, a classical algorithm in graph theory for finding the minimal spanning tree in a graph, to solve this problem. This was the beginning of my journey in graph theory, and eventually led me to my graduate research: using network models to understand molecular functions and behaviors. Our team was finally awarded meritorious winner in the international Mathematical Contest in Modeling in 2008, and the two teammates become my lifelong friends.

After graduating from college, I went to the Academy of Mathematics and Systems Science in the Chinese Academy of Sciences as a research intern for one year, under Yong Wang's supervision. During that time, I utilized the PageRank algorithm to study the relevance of proteins to Type 2 Diabetes in different tissues. At that time, I wrote my first PageRank program using a very time-consuming power method. Two years later, I took David Gleich's class: Network and Matrix Computation, and learned how to accelerate PageRank by formulating it as a linear system and solving it faster by taking advantage of network sparseness. All these experiences benefit my graduate research in this thesis about how to use PageRank to predict protein functions and to partition a network into small modules. I suddenly realize that everything is ultimately interconnected, which reminds me of a speech given by Steve Jobs at Stanford University in 2005:

> *"Again, you can't connect the dots looking forward; you can only connect them looking backwards. So you have to trust that the dots will somehow connect in your future. You have to trust in something—your gut, destiny, life, karma, whatever. Because believing that the dots will connect down the road will give you the confidence to follow your heart even when it leads you off the well-worn path and that will make all the difference."*

Biaobin Jiang

West Lafayette, Indiana

July 22, 2016

TABLE OF CONTENTS

Page

Page

LIST OF TABLES

LIST OF FIGURES

Figure Page

ABSTRACT

Jiang, Biaobin Ph.D., Purdue University, August 2016. Computational Labeling, Partitioning, and Balancing of Molecular Networks. Major Professor: Michael Gribskov.

Recent advances in high throughput techniques enable large-scale molecular quantification with high accuracy, including mRNAs, proteins and metabolites. Differential expression of these molecules in case and control samples provides a way to select phenotype-associated molecules with statistically significant changes. However, given the significance ranking list of molecular changes, how those molecules work together to drive phenotype formation is still unclear. In particular, the changes in molecular quantities are insufficient to interpret the changes in their functional behavior. My study is aimed at answering this question by integrating molecular network data to systematically model and estimate the changes of molecular functional behaviors.

We build three computational models to label, partition, and balance molecular networks using modern machine learning techniques. (1) Due to the incompleteness of protein functional annotation, we develop AptRank, an adaptive PageRank model for protein function prediction on bilayer networks. By integrating Gene Ontology (GO) hierarchy with protein-protein interaction network, our AptRank outperforms four state-of-the-art methods in a comprehensive evaluation using benchmark datasets. (2) We next extend our AptRank into a network partitioning method, BioSweeper, to identify functional network modules in which molecules share similar functions and also densely connect to each other. Compared to traditional network partitioning methods using only network connections, BioSweeper, which integrates the GO hierarchy, can automatically identify functionally enriched network modules. (3) Finally, we conduct a differential interaction analysis, namely difFBA, on protein-protein interaction networks by simulating protein fluxes using flux balance analysis

(FBA). We test difFBA using quantitative proteomic data from colon cancer, and demonstrate that difFBA offers more insights into functional changes in molecular behavior than does protein quantity changes alone. We conclude that our integrative network model increases the observational dimensions of complex biological systems, and enables us to more deeply understand the causal relationships between genotypes and phenotypes.

1. INTRODUCTION

The whole is greater than the sum of its parts.

—Aristotle (384–322 BC)

1.1 Network as a Language of Functions

A central goal of molecular biology is to understand molecular functions based on sequences and structures. Sequences determine structures, and structures determine functions, as a three-layer pyramid from bottom to the top. Sequences are molecular identifiers indicating who the molecules are; structures are molecular appearances showing what they look like; and functions are molecular vocations designating what they do. Ultimately, evolution sheds light on why they do one thing and not another. Understanding molecular functions serves as a genotype-phenotype mapping, since a phenotype is a product of multiple molecular functions. Mapping genotypes to phenotypes is not an easy task: one genotype may cause multiple phenotypes, while one phenotype can originate from multiple genotypes. This many-to-many relationship has been systematically mapped onto the Human Disease Network [1], in which nodes are either a gene or a disease and edges are gene-disease associations. The research group in this study published a drug-target network later in the same year, which displays a similar intertwined relationship between drugs and their targeted proteins [2]. Taken together, this disease-gene-protein-drug network implies that characterizing molecular functions can close the gap between diseases and drugs to transform traditional medicine with a one-disease-one-drug paradigm to precision medicine with accurate diagnosis, personalized treatment, and predictive prevention.

How do molecular biologists investigate molecular functions? Half a century ago, researchers believed that one gene genetically determines one enzyme that acts with

one function [3]. This simple concept leads to a *reductionist* research philosophy, which has been dominant in molecular biology for a long time. A main reductionist strategy in experimental design is to study the function of a single gene by deleting the gene from the genome, and then comparing the phenotypic differences between the mutant and a wild type control. On one hand, molecular biologists can manipulate genomic sequences to investigate the effects of genetic variants of many disease-associated genes, especially for Mendelian diseases, a.k.a., monogenic diseases. On the other hand, structural biologists can investigate structural variants of proteins that cause diseases due to misfolding. However, this strategy fails if the expected phenotypic difference is masked by compensation of another redundant gene with the same function as the deleted one [4]. This property of robustness is one of the consequences of evolution, which shapes the survival capability of organisms by exposure to various deleterious environments, and builds up a living organism as an inseparable whole. This suggests that a *holistic* strategy, which considers the living organism as a whole, or as least as not just a single component, might be an alternative approach to reductionism.

What is a holistic strategy, and how does molecular functional characterization benefit from it? By definition, a holistic strategy is to study the interactions of the multiple components of a complex system as an integrated system, rather than to break it apart and study each part individually. The idea of holism was introduced long ago, in the late 1940s, when scientists tried to interpret a systematic cellular behavior: differentiation [5, 6]. Their question was "how can two cells, having exactly the same genetic material, differentiate into two functionally different cells?" The scientists interpreted differentiation as a positive feedback circuit in which two molecules mutually activate each other. This system exhibits the property of *bistability*: it tends to remain "on" once it is activated, and in contrast, remain "off" once it is inactivated. This profound concept explains why two differentiated cells are not interchangeable, and why the process of differentiation is rarely reversible. Understanding a gene regulatory circuit, or gene regulatory network at large scale,

implies that understanding systematic cellular behaviors requires deep knowledge of the complex interconnections between macromolecules, which brings up an emerging field of study: systems biology.

The aim of systems biology is to study how complex interconnections between macromolecules give rise to emergent cellular behaviors. There are no stringent definition of the scale and boundaries of a biological system. And therefore, a system can be either as small as a signaling pathway, or as large as a whole organism. At local levels, for instance, when one studies the function of a single transmembrane receptor in detail, it can be beneficial to have a functional understanding of the binding ligands in upstream and downstream signaling cascades in the pathway [7]. At intermediate levels, a well-known example is the biochemical network in which nodes are metabolites and edges represent biochemical reactions. Systems biologists use *flux* in the biochemical network to denote reaction rates, and construct a linear programming model called flux balance analysis (FBA, [8]) to simulate a steady state, or equilibrium, of the total network flux [9]. At the whole-cell level, the task becomes more challenging since systems biologists need to consider not only a homogeneous network wherein nodes are the same type (e.g., a metabolic network), but also a heterogeneous network wherein nodes are of more than one type (e.g., transcription factors and their targeted DNA sequences), or even networks of networks when simulating the entire cell cycle [10].

Studying biomolecular networks can benefit pathology research by elucidating the consequences of genetic variants. As mentioned above, the Human Disease Network implies that dysfunction of one gene may result in multiple different diseases, and conversely, one multigenic disease may result from multiple genes. A common dilemma in the study of disease-associated genotypes is that identical genetic variants are rarely found across multiple patient samples with the same phenotype [11]. To this end, Ciriello *et al.* proposed a computational method, called MEMo (Mutual Exclusivity Modules), to identify highly recurrent genetic variants in the same biological process (i.e., functional module, a subset of a biomolecular network) that are mutually exclu-

sive between different patients [12]. They claimed that, even though those variants are not commonly found in all patients, they alter the same biological process, and therefore, result in the same phenotype. Another example of using computational network biology methods to address this dilemma is to infer tumor evolutionary trajectories that illustrate which genetic variants drive the occurrence of others [13]. This method infers sequential networks between variants from longitudinal data, and then performs network integration across different patient samples and uses network deconvolution to determine a final resulting trajectory. Besides tumor heterogeneity, systems biologists also study the effects of genetic variants using protein-protein binding interface data to increase the resolution of network interactions [14]. In a profound study, Zhong *et al.* proposed a novel concept, namely edge-specific genetic perturbation (*edgetic* perturbation) to denote a set of genetic variants that specifically disrupt protein-protein interactions [15]. This study for the first time systematically demonstrates how disease-associated variants cause loss of function at protein structure resolution (see Chapter 1.4.1 for details).

Given the effects of disease-associated genetic variants, as seen through the lens of network data, systems biologists next seek a systematic treatment capable of restoring the perturbations of those effects, which gives rise to a new field of study, namely systems pharmacology or network medicine [16, 17]. To effectively develop drugs targeting complex diseases, we may need to rewire signaling networks perturbed by multiple genetic variants using a combinatorial treatment strategy. Irish *et al.* utilized single-cell flow cytometry to monitor signaling activities of phospho-proteins, and showed that there is dramatic remodeling of signaling networks between healthy and acute myeloid leukemia patient samples [18]. Komurov *et al.* investigated a set of breast cancer cells that are resistant to lapatinib treatment, an EGFR/ErbB2 inhibitor, and found that those cells receiving the treatment overly upregulate the glucose deprivation network [19]. They next treated those cells with other drugs targeting this network, which significantly reduces the survival rate of those resistant cells. Furthermore, Lee *et al.* investigated this EGFR inhibition using a combina-

torial treatment strategy as well, and found that a sequential treatment of multiple anticancer drugs, rather than simultaneous treatment, significantly enhances the treatment effect of rewiring apoptotic signaling networks [20]. These successful examples suggests that modeling molecular networks can guide the design of multi-drug combinatorial treatment to cure complex diseases caused by multiple genetic variants.

In summary, I have given a brief introduction to network biology, and how it enhances our understanding of multigenic diseases and provides therapeutic clues in the development of combinatorial treatment. I next will further introduce how to construct a molecular network via high throughput techniques, and how to computationally analyze network topological structure, and its dynamics in disease progression.

1.2 Network Construction

A molecular network consists of multiple molecules and their interactions. In this section, I will introduce several primary high throughput techniques for molecular quantification and measurement of their interactions. In addition, I will introduce computational methods for inference of virtual networks that cannot be measured directly via experimental techniques.

1.2.1 Molecular Quantification

Proteins are primary functional units in a cell. Researchers are dedicated to developing a collection of qualitative and quantitative techniques to determine which protein exits in the cell and how many copies it has. These techniques includes cellular imaging, electron microscopy, array and chip platforms, and mass spectrometry (MS) [21]. Unlike the other methods, mass spectrometry is a *de novo* analytic technique that examines complex protein populations, and it has been widely used in pharmaceutical development, disease diagnosis and food safety control. In 2002, the Nobel Prize in chemistry was jointly rewarded to John B. Fenn and Koichi Tanaka for their exceptional contribution to the development of molecular ionization in mass

spectrometry. A generic mass spectrometry experiment consists of five steps [21]: (1) isolate the proteins to be analyzed from cells or tissues; (2) digest the proteins to peptides by trypsin; (3) ionize the peptides by electrospray or soft laser desorption; (4) collect the mass/charge spectrum of the peptides; and (5) process the spectrum and match the peaks against protein sequence databases to determine the identity of the peptides. MS studies quickly go beyond qualitative to quantitative measurements, enabling comparison of the same peptide under different experimental conditions. Stable-isotope labeling by amino acids in cell culture (SILAC) tags peptides with stable isotopes, such as ^{13}C, ^{15}N and ^{2}H, to produce predictable mass differences between peptides from two conditions [22]. Another quantitative method is targeted MS techniques, e.g., Selected reaction monitoring (SRM) [23, 24]. This method monitors particular ions (ionized peptides) of an *a priori* known protein throughout a tandem MS measurement over time, which enables the detection of low-copy number proteins, and the quantitative study of its signaling behaviors.

Although detection and quantification of low-copy proteins is challenging [25], and proteome-wide measurement based on current proteomic protocols are highly laborious, large-scale proteome-wide measurements are technically possible for model organisms, and even for human cells. Kim *et al.* introduced a draft map of the human proteome using high-resolution Fourier-transform mass spectrometry [26]. Uhlén *et al.* presented a map of the human tissue proteome including 44 major tissues and organs in the human body using the integration of transcriptomics and antibody-based proteomics [27]. The Cancer Proteome Atlas project has generated protein expression data for many tumor samples using reverse-phase protein arrays (RPPAs), which provides researchers with an insightful functional landscape of cancer proteomes [28].

In addition to proteins, messenger RNAs (mRNAs) can also be measured in a high throughput manner. RNA sequencing is a powerful technique for accurately measuring gene expression at single-base resolution, and identifying different isoforms as well [29]. Briefly, it first converts a long mRNA into a complementary DNA (cDNA),

and then fragments the cDNA into short sequences. After adding adaptors to the two ends of each sequence, it utilizes high-throughput next-generation sequencing technology to obtain the sequence of each cDNA fragment, a.k.a. reads. These reads then can be mapped back to the reference genome, or are assembled together into longer contigs in a *de novo* manner for species without reference genomes. The key computational analysis in this RNA-seq transcriptomics pipeline is to accurately map the reads to reference genomes. Numerous computational tools for RNA-seq assembly and quantification have been developed in the past decade. A comprehensive assessment has been conducted to evaluate the performances of 14 independent computational methods using benchmark datasets [30]. It turns out that the current tools can successfully identify transcript components with high accuracy, whereas accurate identification of complete isoform structures still needs further improvement due to the tremendous combinations of exons. Recently, a new ultra-fast method, namely kallisto, has been proposed to quantify gene expression level from RNA-seq reads data using pseudoalignment to avoid base-to-base exact alignment of reads to a reference genome [31]. Experimental tests using both simulated and real datasets show that kallisto achieves comparably accurate quantification with other four state-of-the-art methods, but shortens the computational time by nearly 10 to 400 fold.

Another large class of biomolecules are metabolites. Metabolites can be measured and quantified using liquid chromatography and flow injection analysis-mass spectrometry [32]. One computational analysis in metabolomics is to first identify the associated proteins (e.g., enzymes) of the metabolites in the Human Metabolome Database (HMDB) [33] , and then to analyze the regulatory pathways at the protein level. This method is suitable for small-scale studies of hundreds of metabolites. Another method for large-scale studies is to reconstruct a metabolic network from thousands of biochemical reactions, which usually requires community efforts [34]. The reconstruction of the global human metabolic network enables computational analysis of each reaction rate using FBA, under the balanced assumption that the

current concentration of one metabolite is equal to the produced amount minus the consumed amount.

Ultimately, systems biologists expect to comprehensively model and analyze the physiological states of an individual using multi-omics data to fulfill the mission of personalized medicine. Chen *et al.* presented an integrative personal omics profile (iPOP) including genomic, transcriptomic, proteomic, metabolomic, and autoantibody profiles of an individual during 14 months [35]. This extensive study is the first attempt to monitor an individual's health using multi-omics data, and uncovers various potential disease risks for useful guidance of prevention in advance.

1.2.2 Interaction Measurement

In order to understand the emergent properties of complex biological systems, measuring molecular quantities alone is insufficient, since a biological system does not run via simple summation of individual molecular functions, but via collective behaviors mediated by molecular interactions.

The primary macromolecular interaction is protein-protein physical interactions since proteins are the primary functional units in a cell. In 1989, Fields and Song invented the yeast two-hybrid (Y2H) assay to successfully measure binary protein-protein interactions [36]. The Y2H concept makes use of a reporter gene in yeast for detecting the interaction of pairs of proteins inside yeast cell nucleus. First, a bait protein and a prey protein are fused to a DNA-binding domain and a transcriptional activation domain of a transcription factor (e.g., Gal4) via DNA recombination techniques, respectively. Then if the bait protein binds to the prey protein, the two domains of the transcription factor are linked to activate the expression of a reporter gene (LacZ, encoding enzymes of galactose utilization) [36]. After a decade, two research groups in 2000 presented large-scale Y2H screens identifying protein-protein interactions in *Saccharomyces cerevisiae* (budding yeast) [37] and *Caenorhabditis elegans* (a roundworm) [38]. Giot *et al.* in 2003 and Rual *et al.* in 2005 used Y2H to

systematically map the first large-scale *Drosophila melanogaster* (fruit fly) and human protein interactomes, respectively [39, 40]. With continuous refinement and efficiency improvement of the Y2H assays, researchers successfully map at larger scales the protein interactomes of *S. cerevisiae* in 2008 [41], *C. elegans* [42] and humans in 2014 [43]. Vo *et al.* presented a proteome-wide binary protein interactome for *S. pombe* (fission yeast) comprising 2,278 interactions, conducted cross-species analysis of protein interactomes, and identified more evolutionarily conserved interacting proteins between *S. pombe* and humans, other than *S. cerevisiae* [44]. Marc Vidal and Stanley Fields reviewed the history of Y2H from 1989, when Y2H was invented, to 2014 [45], and estimated that, so far, about 10,000 high-quality binary protein-protein interactions have been mapped, which accounts for less than 10% of the total protein interactome in human.

Another technology for measuring protein-protein interactions is affinity purification-mass spectrometry (AP-MS). This method is mainly used to measure interactions of multi-protein complexes, the stoichiometry of the protein subunits, and dynamics of the protein-complex assemblies [46]. In 1999, Bertrand Seraphin and his colleagues developed the first AP-MS protocol in yeast [47]. The basic idea of AP-MS is first to use an affinity reagent to purify a protein complex from a protein lysate, and then to identify the subunits of the purified complex by MS. Some protein complexes with a large number of subunits need to be purified multiple times using tandem affinity purification (TAP) tags. Gavin *et al.* and Krogan *et al.* used the TAP-tag approach followed by MS to comprehensively identify high-confidence interactions of protein complexes in yeast [48, 49]. Hutchins *et al.* used AP-MS approach to systematically identify human protein complexes during chromosome segregation [50]. Havugimana *et al.* identified 622 human soluble protein complexes comprising 3,006 proteins and 13,993 high-confidence physical interactions [51]. The key difference between AP-MS and Y2H is that AP-MS only gives a list of proteins physically associated with the bait protein. How those subunits of protein complexes bind to each other cannot be

specified by AP-MS. That is why the interactions identified by Y2H are called binary interactions.

In addition to identification of protein-protein interactions by Y2H and AP-MS in single species, systems biologists utilize various high throughput techniques to identify protein interactions between different species, or interactions of proteins with other biomolecules. Rozenblatt-Rosen *et al.* used Y2H to map the interactions between tumor virus proteins and host proteins, and found that tumor virus proteins systematically perturb the host interactome [52]. Breitkreutz *et al.* used MS-based approaches to identify a kinase and phosphatase interaction (KPI) network comprising 1,844 interactions in budding yeast [53]. Saliba *et al.* presented a liposome microarray-based assay (LiMA) to systematically characterize protein-lipid interactions [54]. Gu *et al.* invented a novel method for detecting protein-protein interactions by taking advantage of powerful DNA sequencing technology [55]. Their single-molecule-interaction sequencing (SMI-seq) attaches DNA barcodes to proteins so that the DNA barcodes can next be amplified, sequenced and quantified by next-generation sequencing (NGS) technology. To understand transcriptional regulation via binding of transcription factors and their direct targeting of DNA sequences, Johnson *et al.* presented a high throughput method called chromatin immunoprecipitation followed by sequencing (ChIPseq) for performing genome-wide mapping of protein-DNA interactions [56]. All these experimental methods aim to generate a global map of biomolecules, which serves as the basis for further modeling and analysis of complex biological processes.

1.2.3 Virtual Network Inference

The biomolecular networks mapped by high throughput experimental assays are still incomplete, and therefore, computational systems biologists attempt to construct computational models to predict the interactions that have not been mapped by the experimental assays using partially known interactions in current databases. Zhang *et al.* devised a computational approach to predict protein-protein interactions using

three-dimensional structural information [57]. La and Kihara presented a phylogenetic framework, namely BindML, to predict protein-protein binding sites using information from evolutionary conservation [58].

Another example of biological network inference is the identification of gene regulatory networks (GRNs). The interactions are "virtual", which means that those interactions do not necessarily imply a physical interaction between two genes, rather than indirect interactions that arise from correlated patterns of gene expression [59]. Bansal *et al.* presented a comprehensive review on gene network inference algorithms, and divided them into four classes: coexpression and clustering, Bayesian networks (BNs), information-theoretic approaches, and ordinary differential equations (ODEs) [59]. Calculating Pearson correlation coefficients (PCCs) between each pair of gene profiles is a straightforward method to construct a gene network. This analytical framework is normally followed by a hierarchical clustering analysis to group genes with similar expression profiles [60,61]. BNs are a graphical presentation of the joint multivariate probability distribution that captures conditional independence between random variables. Friedman *et al.* first constructed a BN to analyze gene expression data in yeast, and successfully inferred several gene interactions that are supported by biological evidences [62]. Information-theoretic approaches rely on a statistical metric called Mutual Information (MI), which measures the degree to which one random variable is non-randomly associated with another. Butte and Kohane used MI to construct a relevance network using 79 expression measurements of 2,467 genes in yeast, and then detected 22 clusters of genes with significant biological relevance [63]. ODEs are normally used to model time-series expression data without considering statistical dependencies, in contrast to BN or MI. D'Haeseleer *et al.* used ODEs to infer gene interactions given the expression of 65 genes at 28 time points, and demonstrated how to use the resulting network to generate hypotheses and direct further experiments [64]. To accelerate the development of novel methods for gene network inference, systems biologists organized the Dialogue on Reverse Engineering Assessment and Methods (DREAM) project, and integrated the inferred networks

from over 30 methods to produce a high-confidence network [65]. They further experimentally tested the ensemble network, and showed that 23 out of 53 previously unreported interactions are supported by the experimental evidences.

To understand the properties of emergence and robustness of biological systems, systems geneticists study the functional dependency of two genes by examining whether the effects of simultaneously knocking out two genes is equal to the sum of the effects of the individual knockouts. This kind of functional dependency is referred to as genetic interaction, or epistasis [66]. Tong *et al.* presented a high throughput assay, termed synthetic genetic array (SGA) to systematically map the genetic interaction network in yeast comprising 204 genes and 291 interactions in 2001 [67]. They continuously conducted the assays for a larger scale mapping of the yeast genetic interactions including about 1,000 genes and 4,000 interactions later in 2004 [68]. In 2010, they finally created a global reference map for the yeast genetic interaction network comprising 5.4 million gene-gene pairs using high throughput double knockout assays [69]. Bandyopadhyay *et al.* further perturbed the yeast genetic interaction network with a DNA-damaging agent, and found that the network rewires to adapt to the external perturbation [70]. Another team utilized an RNA interference (RNAi) strategy to comprehensively map the genetic interaction network in mammalian cells, and created a functional map of chromatin complexes in mouse fibroblasts [71]. Those extensive maps of functional dependency serve as a basis for system biologists to further understand functional organization and adaptive properties of a cell.

1.3 Network Topology

Given a network, scientists have defined many topological properties from different perspectives. Here, I will briefly introduce three basic network concepts: centrality, distance, and modularity, and their applications to biological networks. In particular, built on these three basic concepts, network scientists introduce the three most robust

measures of network topology: degree distribution, average path length and clustering coefficient.

1.3.1 Centrality

The first and most straightforward network property is degree, the number of connections (neighbors) that a node has in a network. Mathematicians and statistic physicists attempted for a long time to find a probability distribution to fit the degree distribution of a network. In 1959, the Hungarian mathematicians Erdős and Rényi proposed a pure random network model with the assumption that each connection (or edge) appears with equal probability, and is independent of any other connections [72]. This model produces a binomial distribution of network degree, or Poisson distribution in the limit of large number of nodes. However, Barabási *et al.* reported in 1999 that most real-world networks, such as the internet and social networks, follow a power-law distribution $P(k) \sim k^{-\gamma}$ with $2 < \gamma < 3$ [73], rather than the Poisson distribution in the classical Erdős-Rényi model. They named the networks following this power-law distribution *scale-free* networks, in the sense that the second (variance) and higher moments of the power-law distribution are infinite when $\gamma < 3$, and hence these networks lack a characteristic scale. In this type of network, a small set of nodes have high degree, whereas the majority of nodes have low degree. They explained this phenomenon by proposing a rule of network growth called *preferential attachment*: a new node prefers to attaching to the nodes with higher degree, called *hubs* in the network [73]. This principle is commonly known as "the rich get richer". Several years later, many researchers showed that protein-protein interaction networks are scale-free, following a power-law distribution [39–41, 49], even though this statement is currently still in debate [74, 75]. These hub proteins were later found to be essential in yeast: knockouts of hub genes frequently lead to lethality, compared to non-essential genes/proteins with fewer links, whose removals are non-lethal and tolerable [76]. Han *et al.* further defined two types of hubs: *party* hubs,

which interact with their partners at the same time and location, and *date* hubs, which bind their neighbors at different times or locations [77]. By computationally removing nodes to identify their topological importance, they found that both types of hubs are indispensable to connectivity of the whole network, and date hubs are even more significantly important than party hubs. Taylor *et al.* extended this concept into intramodular hubs and intermodular hubs, and found that besides their topological importance, intermodular hubs have more signaling domains and more cancer-associated mutations than intramodular hubs [78].

1.3.2 Distance

The second basic network measure is the topological distance between two nodes in a network. In a connected network without any isolated "islands", one node can reach any other node through many possible paths. Among these paths, the shortest one is widely used to define the distance between two nodes. Occasionally, there may be multiple shortest paths between two nodes with equal lengths. In the simplest network, one without weights and directions on edges, the length of the shortest path between two nodes is defined as the number of the traversed edges connecting the source node, destination node and intermediate nodes along the path. Given a network, finding the shortest path between two nodes is a classical problem in graph theory. The classical algorithm to find the shortest path, given a single source node to any other nodes, is Dijkstra's algorithm [79]. This algorithm, in fact, adopts the idea of dynamic programming: it finds the shortest path from source node to each intermediate node at each iteration. This strategy breaks down an optimization problem into several sub-problems, and the optimality of the solution to each sub-problem can be guaranteed according to the *Principle of Optimality* which was proposed by Richard E. Bellman in 1952 [80].

Many other network characteristics are built on the shortest path. One of them is average path length, a.k.a., characteristic path length (CPL), defined as the average

length of all pairwise shortest paths in a network. CPL is widely used to characterize the small-world phenomenon [81], popularly known as six degrees of separation [82]. Watts and Strogatz used CPL and clustering coefficient (see Chapter 1.3.3) to characterize three real-world networks [83], and reported that the small-world networks have longer CPL than the random networks (generated by the Erdős-Rényi model), but smaller clustering coefficients than in lattice networks where each node connects to its k nearest neighbors. In particular, a small-world network is defined as a network whose CPL, termed L, increases proportionally to the logarithm of the number of nodes N in the network, i.e., $L \propto \log N$. Telesford *et al.* proposed a unified small-world measurement $\omega = L_{\text{rand}}/L - C/C_{\text{latt}}$ where C denotes clustering coefficient and the subscripts "rand" and "latt" indicate random networks and lattice networks, respectively [84]. CPL is widely used to quantify the topological importance of one node in retaining the small-world property. A node is topologically important in retaining the small-world property if its removal increases the CPL of the network. As mentioned previously, Taylor *et al.* used the change in CPL to show that intermodular hubs are more important in retaining the small-world property than intramodular hubs [78].

Another network characteristic built on shortest paths is betweenness centrality, another widely used centrality measure. The betweenness centrality of a node in a network is defined as the number of all pairwise shortest paths that pass through that node [85]. A node with high betweenness centrality is analogous to a bridge between two big cities. And every time people would like to travel from one city to the other, they have to pass through the bridge. Proteins with high betweenness are likely to be essential: knocking out those genes tends to result in lethality [86]. Furthermore, proteins with high betweenness but low degree tend to have low expression correlation with their neighbors [86]. These proteins are likely to be key regulators in cross-talk between two pathways. For example, cyclin-dependent protein kinase-activating kinase 1 (CAK1) gene, encodes the protein Cak1p, which regulates two key signaling-

transduction pathways: the mitotic cell cycle, and the MAP kinase pathway which regulates spore morphogenesis in yeast [86].

1.3.3 Modularity

A third network topological property is clustering coefficient, an indicator of modularity that partitions a global network into densely connected subnetworks. Even though a holistic strategy attempts to investigate all molecules and their connections as a whole, a global network sometimes may be too large to be analyzed without loss of details. Partitioning a large network into several relatively independent modules is a feasible compromise.

There are two different clustering coefficients: global clustering coefficient (GCC) and local clustering coefficient (LCC). GCC is a characteristic of a network. Define a triplet as three connected nodes in a network. A closed triplet is three nodes that are fully connected by three edges, whereas an open triplet is three nodes that are connected by two edges, without connection between one pair of nodes (open). Three nodes in which one node lacks of connection are not considered to be a triplet. In 1949, Luce and Perry defined GCC as the ratio of number of closed triplets over the total number of triplets (both open and closed) [87]. GCC ranges from 0, indicating no triplets, to 1 for a fully connected network. Similarly, LCC is a characteristic of nodes in a network. LCC is defined as the ratio of number of edges between the neighbors of a node over all possible edges between these neighbors. That is, a node having k neighbors will have $(k-1)k/2$ possible edges for the case of undirected networks. A node whose neighbors are not connected to each other, like a spoke, will have an LCC of 0, whereas a node with a fully connected neighborhood will have an LCC of 1. As mentioned previously, Watts and Strogatz defined a small-world network using CPL and average LCC of all nodes, and demonstrated that a small-world network has significantly higher average LCC than a random network [83].

Biological systems have proven to be modular [88]. Clustering coefficients can only indicate whether a network is modular, and therefore, automatically finding functional modules in biological networks has become a long-term goal in systems biology. Ravasz *et al.* decomposed the metabolic networks of 43 distinct organisms into several small but densely connected modules using an average-linkage hierarchical clustering algorithm [60], and showed that those metabolic networks have higher average LCC than module-free networks [89]. Girvan and Newman reviewed the shortcomings of traditional hierarchical clustering methods in finding network modules. Based on this, they proposed an alternative method using edge-betweenness [90]. They defined the edge-betweenness of an edge as the number of pairwise shortest paths traversing that edge divided by the number of all-pair shortest paths. And then they detected modules by sequentially removing the edges with high edge-betweenness. They further proposed *modularity*, a score for quantifying the quality of functional modules [91]. It is defined as the observed number of edges within a module minus the expected number of edges within the module. Assuming that each edge appears uniformly at random, the expected number of edges between node i and j can be estimated as $k_i k_j/2m$, where k_i and k_j are the degrees of nodes i and j, and m is the total number of edges in the network. Newman later proposed a spectral algorithm to maximize the modularity score, and demonstrated that the proposed algorithm can detect better modules with larger modularity scores than other modularity-based methods [92].

This problem has also gained the attention of computer scientists, since module detection has become a general task not only in biological networks, but also social networks and others. Fortunato gave a comprehensive review on the progress of this study [93].

1.4 Network Dynamics

Network topology is primarily applied to characterizing static networks. However, biological networks in many cases are not static, but dynamic [94]. Even though

high-throughput experimental technology for the interrogation of biological network dynamics is still limited, accumulating evidence shows that biological networks rewire when perturbed by genetic variants, or changes of post-translational modification (PTM). Time-dependent molecular quantification can reveal quantitative changes in interaction frequency and strength in signaling pathways. In this section, I will briefly review experimental and computational techniques for examining biological network rewiring and dynamics.

1.4.1 Edgetic Perturbation

As mentioned in Chapter 1.1, the concept of *edgetic perturbation* sheds light on how genetic variants located in protein-protein binding interfaces disrupt specific interactions rather than the entire protein structure [15]. Dreze *et al.* presented an integrated method using the reverse Y2H system to systematically characterize edgetic alleles of the gene CED-9, whose mutations can alter its protein-protein interactions and result in different phenotypes in *C. elegans* [95]. Wang *et al.* investigated 62,663 genetic variants and their disruptive effects on 4,222 high-quality binary human protein-protein interactions, and showed that different mutations in the same protein can cause distinct disorders by altering different interactions [96]. In 2015, Sahni *et al.* published a more comprehensive investigation with over 100,000 disease-associated variants, and systematically characterized the effects of those human disease missense mutations into two classes: protein folding/stability changes and protein interaction perturbations [97]. In 2016, Yang *et al.* conducted a large-scale investigation on how alternative splicing alters protein interactions, and demonstrated that besides genetic mutations, different isoforms made by different combinations of exons, interact with distinct functional partners in a tissue-specific manner [98]. This research team, led by Marc Vidal at the Dana-Farber Cancer Institute, claimed in one review article that the study of edgetics provides an insightful way to partially interpret genotype-

to-phenotype relationships as the loss or gain of protein interactions [99]. And they named these edgetics-associated phenotypes as *edgotypes*.

Enlightened by the concept of edgetics, systems biologists have further explored how genetic mutations alter signaling networks, e.g., phosphorylation-dependent interactions between kinases and their substrates. Rune Linding and his colleagues developed a computational method named KINspect to predict which amino acids in the kinase domain determine substrate specificity [100], and then presented a computational framework called ReKINect, to analyze how genetic mutations of those alleles, termed network-attacking mutations, rewire phosphorylation-dependent signaling networks leading to the associated phenotypes such as cancers [101]. AlQuraishi *et al.* described an analytic framework based on multiscale statistical mechanics (MSM) to estimate the effects of genetic mutations on the SH2 domains of human kinases, and showed how those cancer-associated mutations mediate signaling pathways by activating or disrupting interactions [102]. All these studies demonstrate that the concept of edgetics is not only applicable to common protein-protein physical interactions, but also kinase-substrate transient interactions.

1.4.2 Temporal Dynamics

In addition to genetic mutations and PTMs, many other factors can alter molecular interactions, such as molecular abundance, binding affinity, binding ratio (stoichiometry), conditional regulation and so on. With the advance of high-throughput molecular quantification during the past five years, it has become feasible to systematically quantify macromolecular abundance over time, even at the single-cell level. In 2011, Tony Pawson and his colleagues designed an MS-based method named AP-SRM, to quantify the changes in protein interactions with GRB2 (growth factor receptor bound protein 2), an adaptor protein in the downstream of the epidermal growth factor receptor (EGFR) pathway [103]. They successfully totally identified 90 proteins interacting with GRB2 in HEK293T cells at five different time points

after stimulation of cells with epidermal growth factor (EGF). This GRB2-centered protein-interaction network displays a time-dependent map comprising upregulated, downregulated, and unchanged interactions, and reveals the dynamic signaling behaviors from stimulation to activation of effectors.

In 2013, Ruedi Aebersold and his colleagues proposed another MS-based method, called affinity purification combined with sequential window acquisition of all theoretical spectra (AP-SWATH), to investigate how the 14-3-3β scaffold protein changes its interaction frequency with its binding partners after stimulation by insulin-like growth factor 1 (IGF1) [104]. Lambert *et al.* at the same time developed the corresponding statistical analysis pipeline for AP-SWATH, and applied it to investigating the dynamics of another protein interactome centered at CDK4 (cyclin-dependent kinase 4) under three different conditions: wild type, two mutants R24C and R24H, and treatment by NVP-AUY922, an experimental drug candidate for cancers [105].

In 2014, Dana Pe'er, Garry Nolan and their colleagues pushed the study of molecular interaction dynamics forward to single-cell resolution [106]. They utilized mass cytometry, combined with the statistical models, to establish quantitative estimation of signaling interaction strengths and the resulting signaling response functions in naïve and antigen-exposed $CD4^+$ T lymphocytes. They also experimentally validated their estimated interaction strengths and demonstrated the utility of their method in systematically mapping quantitative signaling networks.

1.5 Thesis Road Map

In this thesis, I develop three computational tools to investigate three topics in network biology: labeling, partitioning, and balancing molecular networks. Due to the incompleteness of protein functional annotations, I develop AptRank, a classification-based method, to integrate molecular network data to predict protein functions. With full molecular functional profiles, I next develop BioSweeper, a clustering-based method, to partition the networks into functional modules in which molecules share

similar functions. Finally, I develop difFBA, a linear-programming-based method to estimate the balanced state of protein fluxes throughout the network, and compare the balanced states using proteomic data from healthy and colon cancer samples. The organization of the three thesis projects is outlined in Table 1.1.

Table 1.1
Thesis Outline

Chapter	Topic	Aim	Tool
2	network labeling	protein function prediction	AptRank
3	network partitioning	functional module detection	BioSweeper
4	network balancing	differential flux balance analysis	difFBA

At the end, I briefly describe two side projects in Chapter 5, and summarize all the works in Chapter 6.

2. NETWORK LABELING: PROTEIN FUNCTION PREDICTION

Diffusion-based network models are widely used for protein function prediction using protein network data and have been shown to outperform neighborhood-based and module-based methods. Recent studies have shown that integrating the hierarchical structure of the Gene Ontology (GO) data dramatically improves prediction accuracy. However, previous methods usually either used the GO hierarchy to refine the prediction results of multiple classifiers, or flattened the hierarchy into a function-function similarity kernel. No study has taken the GO hierarchy into account together with the protein network as a two-layer network model.

We first construct a Bi-relational graph (Birg) model comprising protein-protein association and function-function hierarchical networks. We then propose two diffusion-based methods, BirgRank and AptRank, both of which use PageRank to diffuse information on this two-layer graph model. BirgRank is a direct application of traditional PageRank with fixed decay parameters. In contrast, AptRank utilizes an adaptive diffusion mechanism to improve the performance of BirgRank. We evaluate the ability of both methods to predict protein function on yeast, fly, and human protein datasets, and compare with four previous methods: GeneMANIA, TMC, ProteinRank and clusDCA. We design three different validation strategies: missing function prediction, *de novo* function prediction, and guided function prediction to comprehensively evaluate predictability of all six methods. We find that both BirgRank and AptRank outperform the previous methods, especially in missing function prediction when using only 10% of the data for training.

AptRank naturally combines protein-protein associations and the GO function-function hierarchy into a two-layer network model without flattening the hierarchy into a similarity kernel. Introducing an adaptive mechanism to the traditional, fixed-

parameter model of PageRank greatly improves the accuracy of protein function prediction. All the datasets and Matlab codes are available in our GitHub repository at `https://github.rcac.purdue.edu/mgribsko/aptrank`.

2.1 Introduction

Given a set of functionally uncharacterized genes or proteins from a Genome-Wide Association Study, or differential expression analysis, experimental biologists often have little *a priori* information available to guide the design of hypothesis-based experiments to determine molecular functions. For example, what is the expected phenotype if a particular gene is removed? It would greatly improve hypothesis formation if biologists had prior insight from predicted functions of interesting genes or proteins in databases. Computational annotation of genes or proteins with unknown functions is thus a fundamental research area in computational biology.

In the past decade, there has been much work to accurately predict functional annotations of genes or proteins using heterogeneous molecular feature data [107, 108]. The collected molecular features include gene expression, sequence patterns, evolutionary conservation profiles, protein structures and domains, protein-protein interactions (PPIs), and phenotypes or disease associations. In one comprehensive assessment [107], one of the methods, GeneMANIA [109] slightly outperformed the other eight methods by integrating the multiple molecular features into a functional association network (a.k.a., a kernel). The success story of GeneMANIA suggests two important ideas. First, we can significantly improve prediction methods that rely on a single data type by integrating data of many types. And second, kernel integration is a particularly powerful approach to combining multiple types of data.

Given an integrated functional association network, methods for protein function prediction can be divided into three different types: neighborhood-based, module-assisted, and diffusion-based [110]. Neighborhood-based methods [111] predict the function of one protein by using the functions of its neighbors in the network, i.e.,

the guilt-by-association approach. This approach has two obvious drawbacks. On one hand, it ignores the functional information from all the other proteins outside the neighborhoods of the query proteins, which leads to a low true-positive rate. On the other hand, it may also have high false-positive rates when the query protein has a single function but is surrounded by many multi-functional proteins.

Module-assisted methods operate by first partitioning a network or a kernel into functional modules [112,113]. Biologically, a functional module in a PPI network is a group of physically interacting proteins engaged in a biological activity, e.g., to form a scaffold or to relay signals. In network science, a good module is commonly defined as a densely connected subgraph with loose connections to the outside [91]. This definition is naturally coincident with protein complexes, but not signaling cascades. Obtaining a high-quality graph partition is challenging, and this field of study is still highly active.

Diffusion-based methods generally simulate propagating information from functionally known proteins to unknown ones through network connectivity. Nabieva *et al.* [114] constructed a network flow model with fixed diffusion distances and capacities on network edges. This method was claimed to capture both global network topology as well as local network structure to improve the function predictability over the first two domains of methods mentioned above. Freschi devised a tool called ProteinRank by utilizing PageRank [115], the method used by Google to rank webpages, to diffuse functional annotation information throughout a network without setting a fixed diffusion distance or edge capacities [116]. Mostafavi *et al.* utilized the Label Propagation algorithm [117] to develop GeneMANIA [109] as a classification model with multiple heterogeneous network datasets using weighted kernels and labeled negative samples. The method achieved approximately $70 \sim 90\%$ accuracy in three-fold cross validation using a benchmark dataset [107]. Yu *et al.* [118] developed the Transductive Multilabel Classifier (TMC), based on a Bi-relational graph [119] consisting of a protein interactome and cosine similarities in a protein functional profile as two

kernels in each graph layer. Then they used PageRank on this two-layer graph to diffuse functional information to predict protein functions.

Functional annotation data are usually organized in a *tree-like* ontological structure with general terms at the root and specific terms on the leaves [120]. However, the majority of previous methods disregard this intrinsic hierarchical structure by assuming that the relationships between functions are independent. Recently, several methods have been proposed in order to take into account the interdependent relationships between functional terms in the hierarchical structure. King *et al.* [121] predicted gene functions using decision trees and Bayesian networks while taking advantage of the annotation dependency between different branches of the GO hierarchy. Notably, when they trained and tested the association of functional terms with genes, they excluded the information from any ancestors and descendants of the terms in question. This ensures a fair cross validation in which prediction does not benefit from the GO annotation rule: if one gene is annotated by a term, then that gene is automatically annotated by all the ancestors of that term. Barutcuoglu *et al.* [122] and Valentini [123] proposed a hierarchical Bayesian framework and a True Path Rule, respectively, to perform ensemble learning of the classification results yielded by multiple Support Vector Machines (SVMs). They demonstrated that the accuracy of protein function prediction can be significantly improved by integrating the functional hierarchy [124]. Tao *et al.* [125] and Pandey *et al.* [126] utilized Lin's similarity [127] to flatten the functional hierarchy, and then predicted protein functions using a k-Nearest Neighbor (k-NN) method. Sokolov and Ben-Hur [128] directly modeled the hierarchical structure of functional ontology using structured SVM [129], and showed that their method outperformed k-NN and other binary classifiers without taking the hierarchy into account. Recently, Yu *et al.* [130] combined Lin's similarity of protein functional profiles with an ontological hierarchy using downward random walks with restarts, so as to improve the TMC model [118], which can predict functions of a protein that are not in its neighborhood, but are present in the hierarchy. Wang *et al.* proposed clusDCA [131] for protein function prediction by integrating

protein networks and a functional hierarchy, using PageRank for network smoothing and low-rank matrix approximation to de-noise the network data.

In this study, we propose two methods that directly diffusing information on the functional hierarchy other than a flat functional similarity constructed by Lin's method [127]. The first method, which we call BirgRank, constructs a Bi-relational graph model with a protein-protein functional association network as one layer and an unflattened ontological hierarchy as a second layer, and then directly applies PageRank to diffuse annotation information across the two-layer network. The second method, which we call AptRank, employs an adaptive version of PageRank that replaces the standard PageRank parameters with values dynamically chosen to better fit the training data. The main differences between our methods and other diffusion-based methods are (1) we do not require any negative labeled samples since our method is not a traditional classification model; (2) we take full advantage of the functional hierarchy as a two-way directed graph, and do not use Lin's similarity [127], or any kernel trick, to flatten the hierarchy; and (3) we avoid using the annotation of a particular term to predict the annotation of its parental terms, we train and test our methods using the direct annotations only (see Figure 2.3(B) and (C)), which guarantees that the functional terms to be tested for each protein are mutually neither ancestors nor descendants in the GO hierarchy.

To avoid the inflated accuracies of network-based methods in protein function prediction noted by Gillis and Pavlidis [132–135], we conduct a large and strict evaluation of our methods against the other state-of-the-art methods. In addition to three small benchmark datasets, we use an up-to-date protein interaction network dataset and exclude the functional annotations inferred from protein interactions (evidence code: IPI). Rather than two-fold [116], three-fold [109, 131] or five-fold [118] cross validation, we design three different validations: missing function prediction, *de novo* function prediction, and a hybrid of the two strategies, namely guided function prediction. For each of the three types of validation, we perform the validation method using 20% or 10% of the data in training. To overcome the drawback of using Area

Under the ROC curve (AUROC) as a criterion in evaluating performance on imbalanced data with a small number of positive samples, we also utilize Mean Average Precision (MAP) which focuses on the ranking of positive samples only, and is widely used in the field of information retrieval.

2.2 Methods

2.2.1 Problem Statement

This study is motivated by the fact that there are still many proteins whose functions are poorly characterized. To examine the extent to which each protein has been experimentally annotated, we downloaded three benchmark datasets of yeast, fly and human proteins maintained by GeneMANIA-SW since 2010 from their website `http://morrislab.med.utoronto.ca/~sara/SW/`, and also the human Gene Ontology Annotation (GOA) data [136] in March 2015. For the human GOA data, we only consider the annotations in the Biological Process (BP) category, regardless of Molecular Function (MF) and Cellular Component (CC) terms. Also, we only use annotations with experimental evidence codes, within which we remove the terms inferred by physical interaction (evidence code: IPI). All of these four datasets will be used for evaluation later in this study. We illustrate the proportion of the number of functional annotations of each protein in Figure 2.1. We can see that there are a large number of proteins with fewer than 3 functional annotations. This is primarily due to bias in biological research interests and the difficulty of experimentally determining protein functions.

The aim of this study is to predict protein functions given a protein-protein association network and a hierarchically structured set of functional terms. The hypothesis is that associated proteins in the protein network are likely to share similar functions. Here, we define a protein-protein association network as pairwise quantitative relationships of proteins. This network either can be sparse and binary, e.g., a protein-

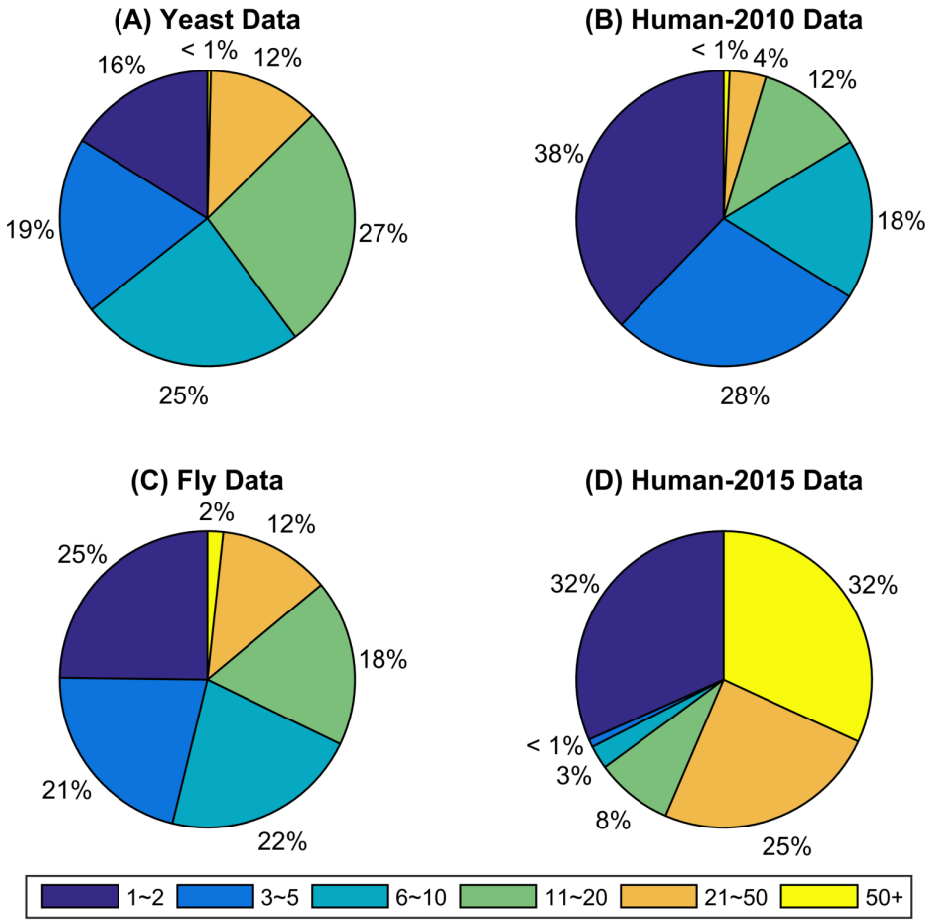

Fig. 2.1. Distribution of Annotated Functions of Proteins. (A) yeast, (B) human collected in 2010, (C) fly and (D) human collected in 2015. The yeast, human-2010, and fly datasets are collected from and maintained by the GeneMANIA developers.

protein physical interaction network, or weighted and dense, e.g., a pairwise similarity of protein sequences.

2.2.2 Preliminaries of Personalized PageRank

PageRank is a well-studied model in network analysis that simulates how information diffuses across a network [115]. It is also called Random Walk with Restart (RWR) in other literature [137]. We will use PageRank to diffuse annotation infor-

mation from well-annotated proteins through a functional association network to less well-annotated proteins. In particular, we use a "personalized" variation of PageRank [138], which models the flow of information from a small number of specific objects, called source nodes (in our case, a single protein) to the remainder of a network. And we use this model to quantify which functions are most relevant to a source protein.

Intuitively, personalized PageRank operates on a network of interconnected nodes by placing a quantity of "dye" at a source node of interest, then letting the dye diffuse across the edges of the network, decaying as it spreads. Once the diffusion process decays to zero, the network regions where the largest amount of dye has concentrated are then the most important regions to the source node. See Figure 2.2 for a visualization of the dye diffusing from a source node.

Mathematically, on a network with n objects, the network is modeled by an adjacency matrix $\boldsymbol{A} \in \mathbb{R}^{n \times n}$ such that $\boldsymbol{A}_{ij}$ is 1 if node j has an edge to node i, and is 0 otherwise. To model the diffusion process beginning with "dye" at a source node, we use a vector $\mathbf{v} \in \mathbb{R}^{n \times 1}$ that is all 0s except for a 1 in the entry corresponding to the source node. This vector $\mathbf{v}$ is called the personalization vector. Let $\mathbf{x} \in \mathbb{R}^{n \times 1}$ be a vector representing the amount of dye at each node in the network at some point during the diffusion process. We then model the diffusion of the dye across the graph by multiplying $\mathbf{x}$ by a column-stochastic version of $\boldsymbol{A}$; this represents the dye on node j being distributed in equal parts to each neighbor i of node j. We denote the column-stochastic version of any nonnegative matrix $\boldsymbol{M}$ as $\overline{\boldsymbol{M}}$; this is computed by dividing each column of the matrix $\boldsymbol{M}$ by the sum of the entries in that column.

Finally, the decay of the diffusion process is controlled by the so-called PageRank teleportation parameter, $\alpha \in (0, 1)$. During each stage of the diffusion, the dye that spreads across the network decays proportionally to α, so that the amount of dye still diffusing after k steps is α^k. Then the PageRank vector $\mathbf{x}$ is given by the solution of the linear system

$$(\boldsymbol{I} - \alpha\overline{\boldsymbol{A}})\mathbf{x} = (1 - \alpha)\mathbf{v}. \tag{2.1}$$

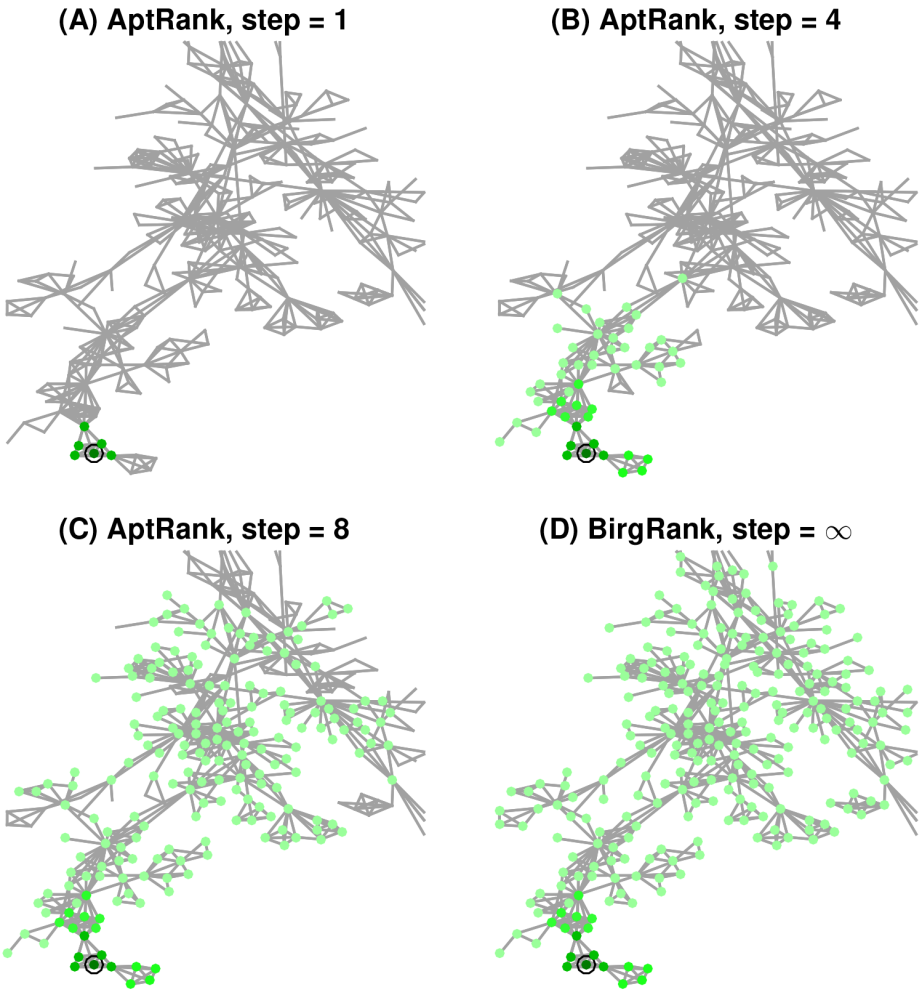

Fig. 2.2. Diffusion Patterns of Personalized PageRank. Diffusion starts from the node circled in black. The green dye diffuses from the black circled node. Nodes where the diffusion concentrates the most appear the darkest green; this indicates the nodes that are most strongly connected to the black circled node. (A), (B) and (C) illustrate our AptRank diffusion with different step sizes. (D) displays our BirgRank diffusion once the associated Markov chain has converged to its stationary distribution.

Recall our intuition that the PageRank vector indicates how much of the dye flows from the source node (i.e. the nonzero entry in the vector $\mathbf{v}$) to each node in the graph. In our context, this means that $\mathbf{x}$ will indicate how much of the functional information flows from the protein of interest to each other protein in the graph.

In our model, we combine proteins and functions into a single network so that the PageRank vector can indicate diffusion flow between proteins and functions.

The solution to the Personalized PageRank linear system in Equation (2.1) can be expressed as

$$\mathbf{x} = \sum_{k=0}^{\infty} (1-\alpha)\alpha^k \overline{\boldsymbol{A}}^k \mathbf{v}. \tag{2.2}$$

This expression will become useful when we introduce the idea of using adaptive coefficients in place of α^k to optimize prediction quality (see Section 2.2.4). We note that, although PageRank has an interpretation as a Markov chain, and Markov chains must meet certain conditions to guarantee convergence to a stationary distribution, this matrix power series (2.2) always converges for any $\alpha \in (0, 1)$ and stochastic matrix $\overline{\boldsymbol{A}}$. Thus, the existence of the unique solution $\mathbf{x}$ is guaranteed regardless of the structure of the matrix $\boldsymbol{A}$. We emphasize this because the form of linear system that we use differs from the traditional PageRank setting, which uses Markov chain analysis in the proof of its convergence; in contrast, our computations do not rely on this Markov chain analysis.

2.2.3 BirgRank: Bi-relational graph PageRank model

We denote the number of proteins by m and the number of function terms by n. Then the three given datasets (protein-protein association network, protein-function annotations, and function-function hierarchy) are denoted by the following matrices:

- $\boldsymbol{G} \in \mathbb{R}^{m \times m}$, a symmetric matrix where $G(i, j)$ denotes to which extent protein i is associated with protein j;
- $\boldsymbol{R} \in \mathbb{R}^{m \times n}$, a binary matrix where $R(i, j) = 1$ if protein i is annotated by function j, 0 otherwise; and
- $\boldsymbol{H} \in \mathbb{R}^{n \times n}$, a binary matrix where $H(i, j) = 1$ if functional term i is the child of term j, 0 otherwise.

We illustrate these three components in Figure 2.3(A), (B) and (C), using a small example with 6 proteins and 7 functional terms. For simplicity, Figure 2.3(A) shows a protein-protein binary interaction network, but it can be replaced by any protein-protein association network. Functional terms are hierarchically structured in a Gene Ontology (Figure 2.3(C)) like an upside down "tree", where the terms on the top (root) are more general and the ones in the bottom (leaves) are more specific. The annotation rule is that if one gene/protein is annotated by one term, then this gene/protein is automatically annotated by all the parental terms of that term in the hierarchy. However, note that in this study we only consider training and predicting the direct annotations of each protein, and do not propagate the corresponding parental annotations using the annotation rule, as shown in Figure 2.3(B). This ensures that our prediction does not benefit from the annotation rule.

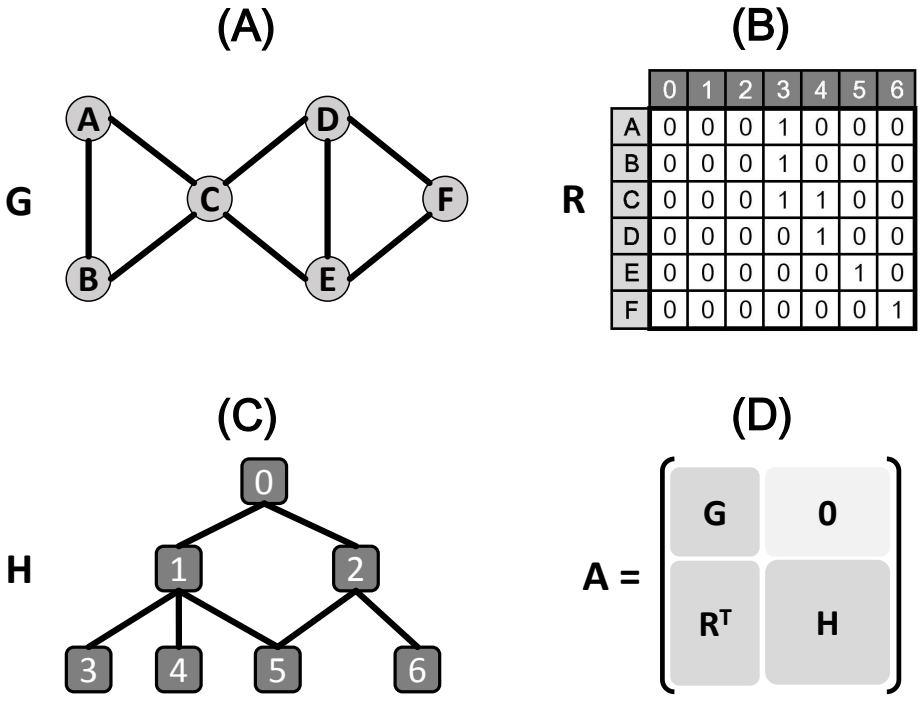

Fig. 2.3. Visualization of Given Data in a Simple Case. (A) protein-protein binary interaction network, (B) protein-function reference matrix, (C) function-function hierarchy, (D) adjacency matrix $\boldsymbol{A}$ of a bi-relational graph.

Next, we construct a bi-relational graph [119] that incorporates these three datasets into a single network (Figure 2.3(D)). To evaluate prediction performance, we split all the annotations in $\boldsymbol{R}$ into $\boldsymbol{R}_T$, which we use for training during model construction, and $\boldsymbol{R}_E$, which we use for evaluating predictions (see Figure 2.4). For each protein i, we predict its functions using Equation (2.1) by setting it as the diffusion source, i.e., by computing the diffusion using $\mathbf{v} = \mathbf{e}_i$. To predict the functions of all proteins, we extend the linear system in Equation (2.1) to a matrix form:

$$\left(\begin{bmatrix} \boldsymbol{I}_m & \mathbf{0} \\ \mathbf{0} & \boldsymbol{I}_n \end{bmatrix} - \alpha \overline{\begin{bmatrix} \boldsymbol{G} & \mathbf{0} \\ \boldsymbol{R}_T^T & \boldsymbol{H} \end{bmatrix}} \right) \begin{bmatrix} \boldsymbol{X}_G \\ \boldsymbol{X}_H \end{bmatrix} = (1-\alpha) \begin{bmatrix} \boldsymbol{I}_m \\ \mathbf{0} \end{bmatrix}, \tag{2.3}$$

where the bar over the block matrix still indicates the whole matrix is normalized to be column-stochastic. The lower block of the solution, $\boldsymbol{X}_H$, is the output matrix of BirgRank for function prediction, and has the same dimensions as $\boldsymbol{R}^T$. To further control the proportion of diffusion passing between the two layers of the bi-relational graph, we parameterize the model in Equation (2.3) as

$$\left(\begin{bmatrix} \boldsymbol{I}_m & \mathbf{0} \\ \mathbf{0} & \boldsymbol{I}_n \end{bmatrix} - \alpha \overline{\begin{bmatrix} \mu\boldsymbol{G} & \mathbf{0} \\ (1-\mu)\boldsymbol{R}_T^T & \boldsymbol{H}^* \end{bmatrix}} \right) \begin{bmatrix} \boldsymbol{X}_G \\ \boldsymbol{X}_H \end{bmatrix} = (1-\alpha) \overline{\begin{bmatrix} \theta\boldsymbol{I}_m \\ (1-\theta)\boldsymbol{R}_T^T \end{bmatrix}}, \tag{2.4}$$

where $\boldsymbol{H}^* = \lambda\boldsymbol{H} + (1-\lambda)\boldsymbol{H}^T$, and λ controls the diffusion direction on $\boldsymbol{H}$. Specifically, $\lambda = 0$ indicates that the diffusion flows down the hierarchy, and 1 indicates flow up the hierarchy. The parameter $\mu \in (0, 1)$ controls the proportion of the diffusion flowing within $\boldsymbol{G}$, and $\theta \in (0, 1)$ controls the weighted sources between the proteins and functional annotations in the right-hand side of Equation (2.4).

2.2.4 Extension to AptRank

In the traditional model of PageRank, which we use in BirgRank, the teleportation parameter $\alpha \in (0, 1)$ can be thought of as controlling the rate of decay of the diffusion as it spreads from the nodes in the personalization vector $\mathbf{v}$ to the rest of the graph. After k steps the diffusion has decayed by a factor of α^k, for $k = 1, \cdots, \infty$

(Equation (2.2)). There are a variety of other empirical weighting schemes [139–142], each with slightly different theoretical properties.

In this section, we seek to replace the standard, fixed diffusion coefficients α^k at each step with an adaptive parameter, denoted by $\gamma^{(k)}$, to optimize the predictive power of the Markov chain. To do this we repeatedly split the training set of protein function annotations, $\boldsymbol{R}_T$, into different subsets to use in fitting and validating the coefficients. We denote the matrix used for fitting by $\boldsymbol{R}_F$, and the matrix used in validation by $\boldsymbol{R}_V$. These matrices have the same dimensions as $\boldsymbol{R}_T$ and consist of entries of $\boldsymbol{R}_T$, i.e., $\boldsymbol{R}_T = \boldsymbol{R}_F + \boldsymbol{R}_V$.

To determine the adaptive coefficients $\gamma^{(k)}$ so that they bias predictions toward the training data, we proceed as follows. The AptRank method begins by computing terms in the following sequence:

$$\boldsymbol{X}^{(k)} = \begin{bmatrix} \boldsymbol{X}_G^{(k)} \\ \boldsymbol{X}_H^{(k)} \end{bmatrix} = \overline{\begin{bmatrix} \boldsymbol{G} & \boldsymbol{R}_F^* \\ \boldsymbol{R}_F^T & \boldsymbol{H}^* \end{bmatrix}}^k \boldsymbol{X}^{(0)}, \tag{2.5}$$

where the bar over the block matrices still denotes column-stochastic normalization,

$$\boldsymbol{X}^{(0)} = \begin{bmatrix} \boldsymbol{X}_G^{(0)} \\ \boldsymbol{X}_H^{(0)} \end{bmatrix} = \begin{bmatrix} \boldsymbol{I}_m \\ \boldsymbol{0} \end{bmatrix}, \tag{2.6}$$

and

$$\boldsymbol{R}_F^* = \begin{cases} \boldsymbol{0} & \text{to use a one-way diffusion} \\ \boldsymbol{R}_F & \text{to use a two-way diffusion} \end{cases}.$$

We denote AptRank using a one-way diffusion and a two-way diffusion as AptRank-1 and AptRank-2, respectively. These two variations can have significant differences in prediction performance when the underlying networks have different sparsities.

To compute the optimal set of coefficients $\gamma^{(k)}$ that best fits the validation set $\boldsymbol{R}_V$, we solve the following constrained least squares model,

$$\begin{aligned} \underset{\gamma}{\text{minimize}} \quad & \left\| \text{vec}(\boldsymbol{R}_V^T) - \sum_{i=k}^{K} \gamma^{(k)} \text{vec}(\boldsymbol{X}_H^{(k)}) \right\|_2^2 \\ \text{subject to} \quad & \sum_{k=1}^{K} \gamma^{(k)} = 1, \\ & \gamma^{(k)} \geq 0, \end{aligned} \tag{2.7}$$

where $\text{vec}(\cdot)$ is a matrix-to-vector transformation that stacks the columns of the matrix into a single column vector.

The entire AptRank framework is summarized in Algorithm 1. We perform this fitting-validating process multiple times, each time splitting $t\%$ of entries in $\boldsymbol{R}_T$ into new matrices $\boldsymbol{R}_F$ and $\boldsymbol{R}_V$ by choosing entries from $\boldsymbol{R}_T$ uniformly at random. Each such iteration generates a new set of coefficients $\gamma^{(k)}$, which we store. We call these iterations "shuffles" because in essence they consist of shuffling the entries of $\boldsymbol{R}_T$ into the two matrices $\boldsymbol{R}_F$ and $\boldsymbol{R}_V$. Again, we note that the annotations in each row (for each protein) of $\boldsymbol{R}_F$ and $\boldsymbol{R}_V$ do not share parental ontology terms. The number of shuffles performed, denoted as S, is an input parameter; after the prescribed number of shuffles is completed, we compute the average $\gamma^{*(k)}$ of the $\gamma^{(k)}$ across all shuffles, and use those averaged $\gamma^{*(k)}$ to compute the final diffusion values $\boldsymbol{X}_{\text{AptRank}}$. This prediction solution will be compared against the evaluation set $\boldsymbol{R}_E$ (see Section 2.3).

2.2.5 Connection with Other Methods

To investigate the similarities and differences of our methods and the other four previous methods used for evaluation, we perform a theoretical analysis and comparison here, and summarize the features of each method in Table 2.1.

The linear system of BirgRank in Equation (2.3) can be expanded into

$$\begin{cases} (\boldsymbol{I} - \alpha\tilde{\boldsymbol{G}})\boldsymbol{X}_G = (1-\alpha)\boldsymbol{I} \\ \alpha\tilde{\boldsymbol{R}_T}^T \boldsymbol{X}_G = (\boldsymbol{I} - \alpha\tilde{\boldsymbol{H}})\boldsymbol{X}_H, \end{cases} \tag{2.8}$$

Algorithm 1: AptRank

Input : $\boldsymbol{G}$,$\boldsymbol{R}_T$,$\boldsymbol{H}^*$,K,S,t

Output: $\boldsymbol{X}_{\text{AptRank}}$

for $s \leftarrow 1$ **to** S **do**

  $[\boldsymbol{R}_F, \boldsymbol{R}_V] \leftarrow \texttt{splitR}(\boldsymbol{R}_T, t)$

  // Choose t% of nonzero entries in $\boldsymbol{R}_T$ uniformly at random and split to $\boldsymbol{R}_F$, and derive $\boldsymbol{R}_V = \boldsymbol{R}_T - \boldsymbol{R}_F$.

  Initialize $\boldsymbol{X}^{(0)}$ using Equation (2.6)

  for $k \leftarrow 1$ **to** K **do**

    Compute $\boldsymbol{X}^{(k)}$ using Equation (2.5)

    $\boldsymbol{A}[:, k] \leftarrow \texttt{vec}(\boldsymbol{X}_H^{(k)})$

  end

  $[\boldsymbol{Q}_A, \boldsymbol{R}_A] \leftarrow \texttt{qr}(\boldsymbol{A})$ // QR decomposition

  $\mathbf{b} \leftarrow \texttt{vec}(\boldsymbol{R}_V)$

  Solve $\underset{\boldsymbol{\gamma}^{(s)}}{\text{minimize}} \quad \|\boldsymbol{Q}_A^T \mathbf{b} - \boldsymbol{R}_A \boldsymbol{\gamma}^{(s)}\|_2^2$ subject to $\sum_k \gamma_k^{(s)} = 1, \gamma_k^{(s)} \geq 0$

  // Equivalently as Equation (2.7).

end

$\boldsymbol{\gamma}^* \leftarrow \texttt{median}(\boldsymbol{\gamma}^{(s)})$

// Take the median over all $s = 1$ to S for each k.

$$\begin{bmatrix} \boldsymbol{X}_G^* \\ \boldsymbol{X}_H^* \end{bmatrix} \leftarrow \sum_{k=1}^{K} \gamma_k^* \begin{bmatrix} \boldsymbol{G} & \boldsymbol{R}_T^* \\ \boldsymbol{R}_T^T & \boldsymbol{H}^* \end{bmatrix}^k \begin{bmatrix} \boldsymbol{I}_m \\ \mathbf{0} \end{bmatrix}$$

Output $\boldsymbol{X}_{\text{AptRank}} \leftarrow \boldsymbol{X}_H^*$ for use in prediction.

where $\tilde{\boldsymbol{G}}$, $\tilde{\boldsymbol{R}}_T$, and $\tilde{\boldsymbol{H}} = \overline{\boldsymbol{H}}$ denote the submatrices of the column-stochastic matrix in Equation (2.3). By solving Equations (2.8) for $\boldsymbol{X}_H$, we get

$$\boldsymbol{X}_H = \alpha(1-\alpha)(\boldsymbol{I} - \alpha\overline{\boldsymbol{H}})^{-1} \tilde{\boldsymbol{R}}_T^{\,T} (\boldsymbol{I} - \alpha\tilde{\boldsymbol{G}})^{-1}. \tag{2.9}$$

In contrast, ProteinRank [116] uses only the protein-protein association network $\boldsymbol{G}$ as a one-layer network model — and does not directly take into consideration the functional hierarchy $\boldsymbol{H}$ — and then computes PageRank using $\boldsymbol{R}_T$ as the personalization vectors (matrix). ProteinRank constructs a regression model and solves the linear system

$$\boldsymbol{X}_{\text{ProteinRank}} = (1-\alpha)(\boldsymbol{I} - \alpha\overline{\boldsymbol{G}})^{-1}\boldsymbol{R}_T, \tag{2.10}$$

which can cause poor prediction quality due to the assumption of independence between functions (see Section 2.3). Our method BirgRank is closely related to ProteinRank: if we plug $\overline{\boldsymbol{H}} = \boldsymbol{I}$ into Equation (2.9), then the resulting BirgRank solution differs from the ProteinRank solution (Equation (2.10)) only by a scalar coefficient and a slightly different normalization of $\boldsymbol{G}$.

Similar to ProteinRank, GeneMANIA [109] models protein function prediction as a multiclass-multilabel classification problem by integrating multiple heterogeneous network datasets and then using the Label Propagation algorithm [117] as

$$\boldsymbol{X}_{\text{GeneMANIA}} = (\boldsymbol{I} - \boldsymbol{L})^{-1}\boldsymbol{R}^{*T}, \tag{2.11}$$

where $\boldsymbol{L} = \boldsymbol{D} - \boldsymbol{W}$ is the Laplacian matrix, $\boldsymbol{W}$ is a weighted sum of multiple kernel matrices from heterogeneous network data sets, and $\boldsymbol{D}$ is a diagonal matrix with $D_{ii} = \sum_j W_{ij}$. Additionally, GeneMANIA extends the binary matrix $\boldsymbol{R}_T^T$ to $\boldsymbol{R}^{*T}$ by introducing negative samples in which $R^*_{i,j} = -1$ if protein i is known not to have function j. The developers of GeneMANIA further accelerated their algorithm by introducing Simultaneous Weights (hereafter GeneMANIA-SW) [143].

Yu *et al.* proposed the Transductive Multilabel Classifier (TMC) [118] by directly applying a Bi-relational graph model used in image annotation [119] to protein function prediction, without consideration of the functional hierarchy. Instead, they use the cosine similarity of functional annotations to construct a function-function similarity matrix to replace $\boldsymbol{H}$. The key difference between TMC and BirgRank is that TMC allows information to diffuse from functional terms to proteins, but not

proteins to functional terms, as in BirgRank. Mathematically, the transition matrix of PageRank used in TMC is

$$\overline{\boldsymbol{A}_{\text{TMC}}} = \begin{bmatrix} \overline{\boldsymbol{W}_G} & \boldsymbol{W}_R \\ \mathbf{0} & \boldsymbol{W}_F \end{bmatrix}, \tag{2.12}$$

where the matrix $\boldsymbol{W}_F$ is the degree-weighted function-function cosine similarity, i.e., $\cos(\boldsymbol{R}_T^T, \boldsymbol{R}_T)$, $\boldsymbol{W}_G$ is a degree-weighed graph kernel of protein-protein association network, and $\boldsymbol{W}_R$ is a normalized function profile derived from $\boldsymbol{R}_T$. The developers of TMC suggest further flattening the functional hierarchy by using a random walk with restart approach [130]. But this method, called dRW, does not use a bi-relational graph model, and was tested only using a very small data set [130].

Wang *et al.* proposed clusDCA [131] by extending their original Diffusion Component Analysis (DCA) method [144]. The clusDCA algorithm first uses PageRank to smooth both of the graphs, denoted as $\boldsymbol{G}$ and $\boldsymbol{H}$ in this study. Next, it computes Singular Value Decomposition (SVD) for the two smoothed matrices for low-rank matrix approximations. Finally, it attempts to find the optimal projection between the two low-rank matrices.

2.3 Results

2.3.1 Experimental Setup

We present a comprehensive evaluation of the six methods using the three benchmark datasets from yeast, human and fly that can be downloaded from the GeneMANIA-SW website. All three datasets were collected by the developers of GeneMANIA in 2010. We collected one more dataset for human proteins from public databases in March 2015 in order to test all the methods using up-to-date data with a larger size than those collected in 2010 (see Table 2.2). In this human dataset, denoted as human-2015, the network $\boldsymbol{G}$ was downloaded from BioGRID [145], and the annotations $\boldsymbol{R}$ and the hierarchy $\boldsymbol{H}$ from the Gene Ontology Consortium [136]. The number of direct GO (Table 2.2, 3rd column) indicates the number of annotations of

individual proteins directly downloaded from the Gene Ontology Annotation (GOA) database. This does not reflect the implied inclusion of parental terms (see the total number of terms in Table 2.2, 4th column for comparison). The multiple kernels (Table 2.2, 5th column) from heterogeneous molecular data were directly downloaded from the GeneMANIA-SW website, and combined into a single network (i.e., $\boldsymbol{G}$) with the weights provided in the datasets.

To evaluate the quality of each method in protein function prediction, we conducted cross validation using three different strategies to split the given functional annotation data $\boldsymbol{R}$ into $\boldsymbol{R}_T$ used for training and $\boldsymbol{R}_E$ used for evaluation (see Section 2.3.2). The three strategies are:

1. missing function prediction
2. *de novo* function prediction
3. guided function prediction.

All three validation strategies ensure that the matrices $\boldsymbol{R}$, $\boldsymbol{R}_T$ and $\boldsymbol{R}_E$ have the same dimensions, and $\boldsymbol{R} = \boldsymbol{R}_T + \boldsymbol{R}_E$. To measure the prediction quality of each method, we use two evaluation metrics: AUROC (Area Under the Receiver Operating Characteristic curve) which is widely used in protein function prediction, and MAP (Mean Average Precision) which is widely used in information retrieval (Figure 2.4). The key advantage of MAP is that MAP does not take true negatives into account, and is thus a more informative metric than AUROC when negative samples outnumber positive samples. This is true in our case since in the human-2015 dataset, for example, we attempt to predict 45 functions on average from $11,519$ possible annotations (feature space, see Table 2.2).

We determined parameter settings as follows. For the four methods other than our BirgRank and AptRank, we mostly used the default settings specified in the corresponding literature. We only tuned the reduced dimensionality d in clusDCA to be 500, rather than the parameter setting $2,500$ specified by the authors [131], since this parameter is a key factor in time complexity of clusDCA. Empirically, we found

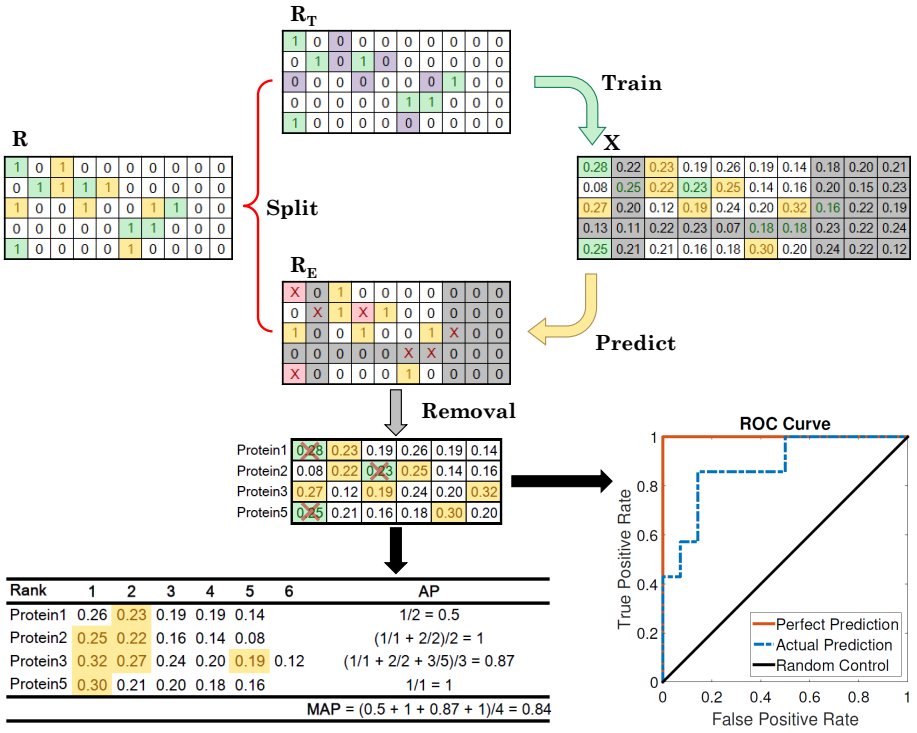

Fig. 2.4. Validation Strategy of Missing Function Prediction. Split the given annotations $\boldsymbol{R}$ by putting 50% into the training set $\boldsymbol{R}_T$ and 50% into the evaluation set $\boldsymbol{R}_E$. Then compare the predictions against $\boldsymbol{R}_E$ and evaluate the performance of each method using AUROC and MAP.

that clusDCA is the most time-consuming method as shown in Table 2.4, and a large d value dramatically increases running time. For the parameters in BirgRank, we set $\lambda = 0.5$ in determining $\boldsymbol{H}^*$, to allow equal diffusion upward and downward the hierarchy. For the other three parameters α, θ, and μ in BirgRank (See Equation (2.4)), we observed that different settings of these three parameters did not yield significant differences in performance, and found that a value of 0.5 empirically achieved good results. For the parameters in AptRank, we set the total iteration number K to be 8, the splitting parameter t to be 50%, and the number of shuffles S to be 5. These setting may vary depending on the validation strategies and the data sizes, which we discuss in Section 2.3.2.

2.3.2 Comparison of Prediction Performances

Missing Function Prediction

We first conducted a numerical experiment to evaluate the ability of the six methods in predicting missing protein functions as follows. We uniformly select a certain percentage of non-zero entries in $\boldsymbol{R}$ at random, move them to a matrix $\boldsymbol{R}_T$ for training, and let $\boldsymbol{R}_E = \boldsymbol{R} - \boldsymbol{R}_T$ be the evaluation set. Figure 2.4 illustrates how to split matrix $\boldsymbol{R}$ with 14 entries into $\boldsymbol{R}_T$ and $\boldsymbol{R}_E$ when the splitting percentage is specified as 50%. We carried out this random sampling with replacement 5 times for each specified splitting percentage. This is not a circular cross validation since it does not guarantee that each functional annotation is tested once and only once. This strategy aims to test whether the methods can restore incomplete functional annotations for each protein and is unbiased with respect to how many annotations each protein has.

We start with 10% split for training and increase by increments of 10% up to 80% (Figure 2.5). Generally, the resulting AUROCs and MAPs of the six methods show that both BirgRank and AptRank outperform the other four previous methods in all 8 groups of experiments with different amounts of training data. In the 10% group of human-2010 and fly datasets, clusDCA slightly outperforms our methods in AUROC, but its MAP is lower than those of our methods (Figure 2.5 (C) and (E)). When more data are given for training, our methods outperform the other four methods in terms of MAP with approximately 2- to 3-fold improvement.

To investigate the effect of the GO functional hierarchy in prediction, we compare the performance of non-hierarchy-integrated methods (GeneMANIA-SW, TMC and ProteinRank) with hierarchy-integrated methods (clusDCA, BirgRank and AptRank). We find that the integration of the functional hierarchy clearly improves the prediction accuracy (Figure 2.5). Furthermore, our methods, for the most part, perform better than clusDCA, which suggests that using a bi-relational graph framework (Figure2.3) to integrate the hierarchy is better than seeking for projection between the protein network and the functional hierarchy.

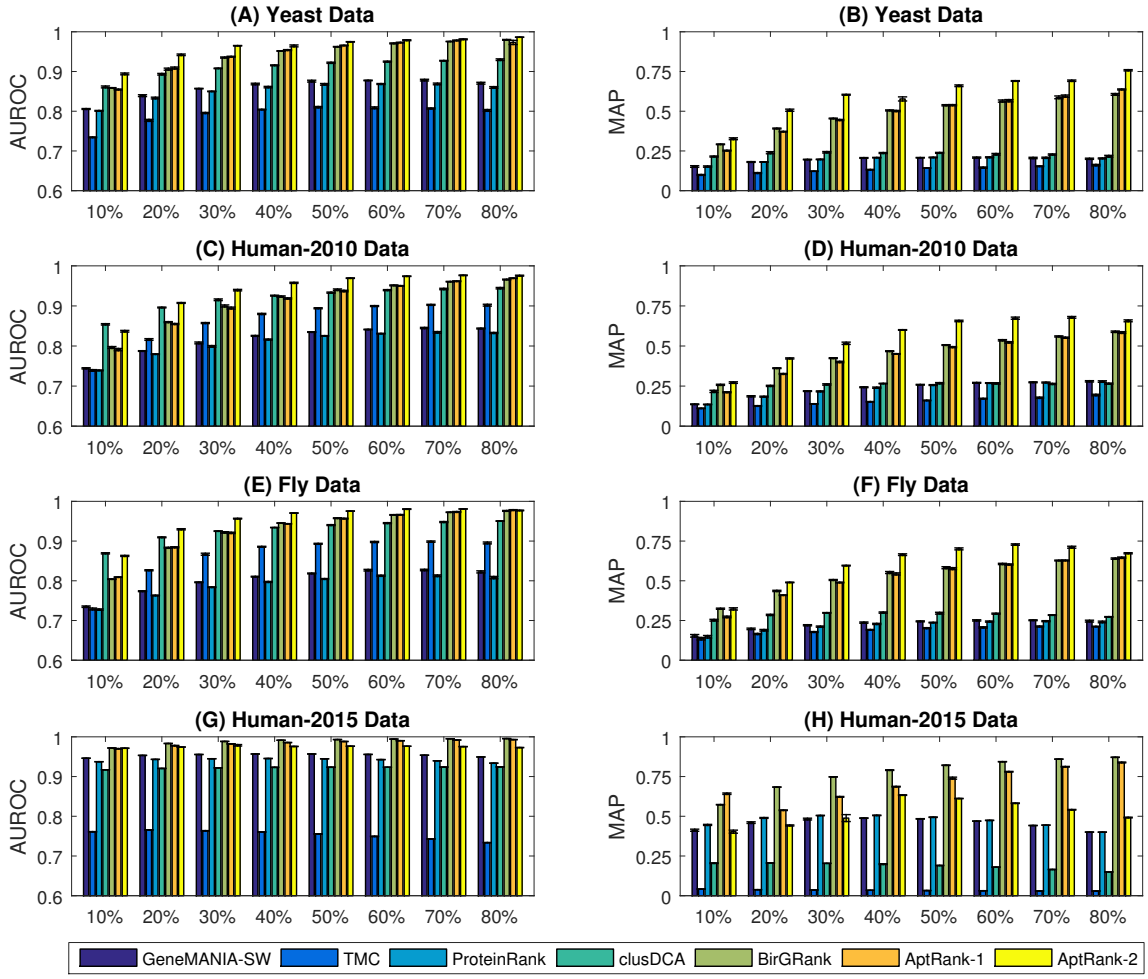

Fig. 2.5. Missing Function Prediction. The x-axis represents the percentages of data used in training. The error mark on top of each bar indicates the standard deviation of AUROCs or MAPs over 5 repetitions of each experiment.

Comparing the performances of BirgRank and AptRank, we find that the performance of the algorithms differs as the network sparsity varies (Figure 2.5 (B), (D), (F) vs. (H)). The three benchmark datasets are smaller and denser than Human-2015 dataset due to the integration of multiple kernels (Table 2.2). We can see that AptRank with a two-way diffusion performs better on the dense network, while BirgRank is better on the sparse network. This could be because a dense network restricts network diffusion within a local region of the source node, and two-way diffusion forms a

feedback loop that enhances the contributions of the annotations within local regions. However, the two-way diffusion spreads out of this local region in a sparse network and provides irrelevant feedback to the source node.

In addition, we find that GeneMANIA-SW and ProteinRank achieve similar performance in both AUROC and MAP. The key difference between these two models is that GeneMANIA-SW requires negative samples in its classification framework. This demonstrates that negative samples have a very limited contribution to the performance of GeneMANIA-SW on these datasets. This could be in part because it can be difficult to confirm that a protein does not have a function.

Lastly, we find that BirgRank outperforms TMC. Theoretically, the models of TMC and BirgRank are quite similar, differing mainly in how the two methods direct the diffusion between the two network layers, $\boldsymbol{G}$ and $\boldsymbol{H}$. BirgRank diffuses information from $\boldsymbol{G}$ to $\boldsymbol{H}$, while TMC does the reverse. Our results support the idea that diffusion from proteins to functional terms is the more useful direction in the context of protein function prediction.

De novo Function Prediction

To investigate whether the six methods can accurately predict the functions of one protein without any annotation for training, we design a *de novo* circular cross validation as follows. Uniformly partition a certain percentage, denoted as c, of proteins into b groups at random. Letting $[v]$ denote the nearest-integer operation, we can calculate

$$b = \begin{cases} [1/c] & \text{if } 0 < c \leq 0.5 \\ [1/(1-c)] & \text{if } 0.5 < c \leq 1 \end{cases}.$$

In practice, we set c as 20%, 50% and 80% as shown in the x-axis of Figure 2.6. When $c = 80\%$, it is equivalent to a conventional five-fold cross validation with 80% of proteins as the training set and the complementary 20% as the evaluation set. On the contrary, $c = 20\%$ means we only use 20% of proteins for training and evaluate the

prediction performance by the complementary 80%. Lastly, $c = 50\%$ is equivalent to a two-fold cross validation. Normally, three-fold cross validation ($c = 66.7\%$) is used in the four reference methods. Here, our cross validation design is aimed to explore the potential predictive power of all of the methods with a more stringent criterion.

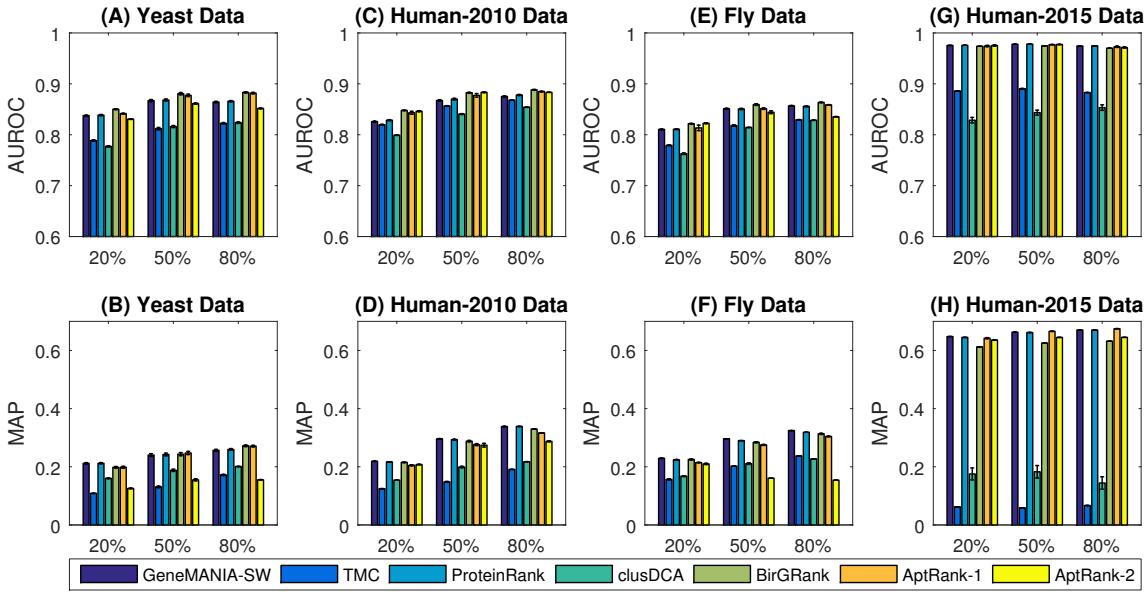

Fig. 2.6. *De novo* Function Prediction. The x-axis represents the percentages of data used in training. The error mark on top of each bar indicates the standard deviation of AUROCs or MAPs over 3 repetitions of each experiment.

As shown in Figure 2.6, our methods generally perform no worse than the four reference methods. Interestingly, GeneMANIA has nearly the same performance as ProteinRank in both AUROC and MAP metrics, which occurs in our missing function prediction experiment as well (Figure 2.5). Furthermore, they both perform better than the other two reference methods, TMC and clusDCA. Our methods perform slightly better than GeneMANIA and ProteinRank in AUROC, but do slightly worse in MAP. This leads us to conclude that (1) a classification model that includes negative samples (GeneMANIA) is little different from a diffusion model (ProteinRank) in *de novo* function prediction; and (2) integrating the GO hierarchy (BirgRank and

AptRank) cannot significantly improve the accuracy in function prediction for newly found proteins without known functional information.

Guided Function Prediction

To examine the extent to which our methods benefit from limited known annotations of tested proteins, we devise a validation strategy called guided function prediction which is a hybrid of the missing function prediction (Section 2.3.2) and the *de novo* prediction (Section 2.3.2) strategies. In this validation, the strategy of partitioning training and evaluation sets is identical to that used in *de novo* prediction except that it gives *one* functional annotation as guidance for each evaluated protein that has more than one annotation. The proteins in the evaluation set with only one or no annotation are not taken into account.

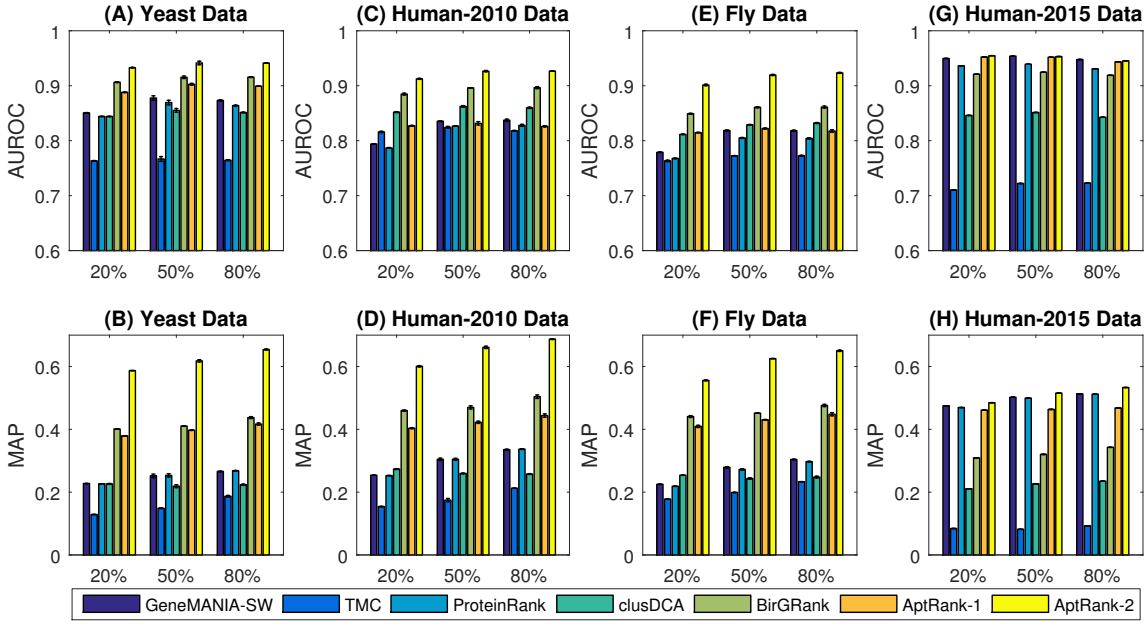

Fig. 2.7. Guided Function Prediction. The x-axis represents the percentages of data used in training. The error mark on top of each bar indicates the standard deviation of AUROCs or MAPs over 3 repetitions of each experiment.

We can see in Figure 2.7 that in the evaluations using the three benchmark datasets with dense network data, our methods, especially AptRank-2, can take full advantages of the single given annotation to improve prediction performance by approximately 2-fold in AUROC and 3-fold in MAP, compared to the other four methods. In the sparse network data (Human-2015), we find that the given annotations worsen the performances of all the methods (Figure 2.6 (G,H) vs. Figure 2.7 (G,H)). We conclude that sparse network datasets may cause underfitting of our model training, and reducing the model complexity can alleviate this problem, e.g., setting a small α in BirgRank or a small K in AptRank. On the contrary, we also find that in some experiments, the more data we provide for training, the worse the testing accuracy is (e.g., AptRank-2 in Figure 2.6(F)). In these cases, Verleyen *et al.* proposed using sampling of the training data to overcome this overfitting [146].

Finally, all three validations show that AUROC is always higher than MAP in the evaluation of the same prediction result. This suggests that MAP is a better metric when the number of negative samples is much larger than the number of positive samples, as is the case in protein function prediction.

2.3.3 Analysis of Adaptive Coefficients

The adaptive coefficients of AptRank (γ) are the unique feature that differs from traditional PageRank. To investigate their behaviors in prediction, we list the medians of γ over the different shuffles in the prediction of yeast and human-2015 datasets in Table 2.3. We can see that there are three main features of γ's behaviors,

(1) $\gamma^{(1)}$ is always zero, since the information diffusing within $\boldsymbol{G}$, from proteins at the first step, has not yet reached the hierarchy;

(2) as shown in the yeast dataset, the distribution of γ is not uniform, but concentrates on specific terms of Markov chains, which demonstrates that AptRank can adaptively select the most predictive terms rather than weighting all terms with power-decays like traditional PageRank; and

(3) in comparison of γ in yeast and human-2015 datasets, we find that AptRank mostly selects the 2nd term in the human-2015 dataset, but a few more terms in the yeast dataset, which is due to the different network densities of the two datasets. The yeast dataset is smaller but denser, since it integrates 44 different kernels into $\boldsymbol{G}$; the human-2015 dataset is larger but sparser, and all the entries in the raw human-2015 dataset are binary. This implies that for a sparse dataset, our AptRank might be equivalent to neighbor-voting methods.

2.3.4 Comparison of Runtimes

The average computational time of the six methods compared in this study are shown in Figure 2.4. In this comparison, the computational time is recorded for the prediction using the largest dataset, human-2015. We can clearly see AptRank requires the third longest computational time, likely because it involves many dense matrix operations. The SVD computations required in clusDCA are likely responsible for clusDCA having the longest running time. Without a parallel implementation of SVD, clusDCA might be impractical unless we sacrifice prediction accuracy by using a small d value. GeneMANIA-SW is the second most computationally expansive method, since it computes the prediction scores function by function. This is extremely expensive when the number of functions is large, even though we only used direct GO terms in GeneMANIA-SW. BirgRank and TMC both use bi-relational graphs, and take only several minutes to solve the PageRank linear system. ProteinRank has the most simple model, and it takes the shortest time, since it needs only to solve a PageRank linear system with approximately half the dimension of the systems involved in BirgRank and TMC.

2.4 Conclusion

In this paper we present two network-diffusion-based methods for protein function prediction. Our first method, BirgRank, uses PageRank on a bi-relational graph

model that incorporates protein-protein and function-function networks. Our second method, AptRank, introduces an adaptive mechanism to the PageRank framework that computes an optimal set of weights for the first several steps of diffusion so as to maximize recovery of a subset of known function annotations. We show that both methods outperform the four existing state-of-the-art methods in almost all cases, and in particular, outperform those methods that do not incorporate information about the functional hierarchy. Our results also suggest that diffusion-based methods are still among the most competitive in network-based protein function predictions, compared to classification-based and decomposition-based methods.

Furthermore, our methods provide a theoretical framework in data integration, which may benefit multi-omics studies in complex diseases, or multi-species metabolic network modeling in microbiome studies. From a general view outside bioinformatics, our methods can be used to develop multi-class recommendation systems in social media with inter-dependent labels. For example, the protein-protein association network in this study can be viewed as similar to the professional social network between LinkedIn users, and the functional hierarchy can be seen as generalizing to an individual's skill set. Those skill sets are typically inter-dependent. For instance, a user with knowledge of Perl programming is likely to have bioinformatics expertise.

Table 2.1
Summary of the Six Methods

Method Name	**Method Type**	**Functional Hierarchy**	**Bi-relational Graph**	**Negative Samples**	**Random Walk**	**Stationary PageRank**	**Reference**
GeneMANIA-SW	kernel integration & classification			✓	✓	✓	[109] [143]
TMC	diffusion		✓		✓	✓	[118]
ProteinRank	regression				✓	✓	[116]
DCA-clusDCA	diffusion & decomposition	✓		✓	✓	✓	[144] [131]
BirgRank	diffusion	✓	✓		✓	✓	this study
AptRank	diffusion	✓	✓		✓		this study

Table 2.2
Statistics of Data Sets

Data Set	No. of proteins	No. of direct GO	No. of all GO	No. of kernels
Yeast	3904	1188	1695	44
Human-2010	13281	1952	2919	8
Fly	13562	2195	2919	38
Human-2015	14515	11519	27106	1

Table 2.3
Medians of γ in Prediction of Yeast and Human-2015 Data Sets

Data Set	Training (%)	Markov chain iteration							
		1st	2nd	3rd	4th	5th	6th	7th	8th
Yeast	**10%**	0	0	0	0	0	0	0.08	0.92
	20%	0	0.11	0	0	0	0	0.23	0.66
	30%	0	0.34	0	0.08	0	0	0.58	0
	40%	0	0	0	0	0	0	1	0
	50%	0	0	0	0	0.84	0	0.16	0
	60%	0	0	0	0	1	0	0	0
	70%	0	0	0.09	0	0.91	0	0	0
	80%	0	0	0.64	0	0.36	0	0	0
Human 2015	**10%**	0	0.20	0	0	0	0	0.31	0.49
	20%	0	0.65	0	0	0	0	0.11	0.24
	30%	0	1	0	0	0	0	0	0
	40%	0	1	0	0	0	0	0	0
	50%	0	1	0	0	0	0	0	0
	60%	0	1	0	0	0	0	0	0
	70%	0	1	0	0	0	0	0	0
	80%	0	1	0	0	0	0	0	0

Table 2.4
Runtimes of the Six Methods in Minutes (Human-2015 Dataset)*

Methods	Training Data Proportion					
	10%	**20%**	**40%**	**50%**	**70%**	**80%**
GM-SW	252.52	214.47	232.02	231.65	225.54	234.56
TMC	6.71	7.10	7.52	7.58	7.37	7.12
ProteinRank	0.85	0.87	0.87	0.87	0.88	0.88
clusDCA	1054	1019	1072	1061	1025	1050
BirgRank	9.42	9.46	9.46	9.45	9.42	9.49
AptRank-1	51.79	53.48	55.82	55.28	57.85	58.69

*The runtimes of 30% and 60% is not shown due to space limit. The AptRank-1 uses 12-core parallel computing for matrix multiplication.

3. NETWORK PARTITIONING: FUNCTIONAL MODULE DETECTION

Real-world networks are usually too large to be investigated in details. For example, given a global protein-protein interaction network with thousands of proteins, molecular biologists may get lost in this big data set. Network scientists overcome this challenge by breaking down large networks into several small subnetworks according to some intrinsic patterns. In biological networks, computational biologists often partition a molecular network into several functional modules within which molecules are densely connected and also share similar biological functions.

In this Chapter, we extend our AptRank model described in Chapter 2 for biological network partitioning. In particular, we develop a computational tool, namely BioSweeper, for joint clustering of multilayer biological networks. BioSweeper first adopts localized PageRank to diffuse information from a set of seed nodes, which generates, for each seed node, a ranking list of nodes in the network representing the proximity to the seed nodes. Next, BioSweeper detects a network cluster with the minimal conductance by sweeping over all cuts induced by the ranking list. We test the performance of BioSweeper against two state-of-the-art methods, MCL and ClusterONE, in protein complex detection using a benchmark dataset from the MIPS database. Experimental results show that, given an appropriate seed set, BioSweeper outperforms the other methods in terms of identifying gold-standard protein complexes. We then apply BioSweeper to detecting long-range regulatory modules in which genes are strongly co-expressed and their genomic regions have highly frequent contacts.

The main contributions of BioSweeper are the capabilities of (1) detecting overlapping clusters; (2) integrating heterogeneous datasets for multimodal cluster identification; and (3) tuning cluster sizes between small and large.

3.1 Background

Most of biological networks are too large to be investigated at molecular levels. And those networks are usually organized in hierarchical and modular structures [88,89]. Thus, partitioning those networks into small subnetworks using computational methods becomes a daunting challenge in systems biology [147]. Many computational methods have been developed to automatically identify functional modules in biological networks, including Markov CLuster (MCL, [112]), Molecular COmplex DEtection (MCODE, [113]), Restricted Neighborhood Search Clustering algorithm (RNSC, [148]), CFinder [149, 150], Affinity Propagation [151], Repeated Random Walks (RRW, [152]), linkcomm [153,154], ClusterONE [155], and so on. Wiwie *et al.* conducted a comprehensive comparison of multiple clustering algorithms using many benchmark data sets, but could not find a universal best performer across all the data sets [156].

The original definition of biological network partitioning is similar to that of community detection in social network analysis, i.e., to seek for subnetworks with dense connections inside and loose connections to the outside, given the network connections only. The subnetworks detected following this definition may be insufficiently meaningful in biology, in the sense that a densely connected subnetwork is likely to be a protein complex (e.g., proteasome), but rarely to be a signaling cascade with linear structure (e.g., mitogen-activated protein kinase (MAPK) cascade). And therefore, only can combining functional annotations with network connectivity detect more biologically meaningful functional modules including protein complexes and signaling cascades. Lubovac *et al.* developed SWEMODE (Semantic WEights for MODule Elucidation, [157]) to detect functional modules from protein interactome using a weighted version of clustering coefficient on the weighted protein interactome with Lin's semantic similarity [127] of protein function profiles. Cho *et al.* presented a flow-based modularization algorithm on a weighted protein interactome combined with functional semantic similarity to detect functional modules [158]. Marcus Dit-

trich and his colleagues extended their integer-linear programming model for protein functional module detection, LiSA [159], by integrating semantic similarity of protein functional profiles [160]. These integrative methods let the protein interactome convey rich functional information, and have demonstrated that integrating functional information to protein interactome directly yields functional enriched modules after the network partitioning.

Most network partitioning algorithms produce disjoint subnetworks. However, there are many multi-functional proteins playing different roles in distinct biological processes. Those *critical nodes* [161] usually have more than one isoform, and can be highly regulated either positively or negatively to generate signaling divergence in downstream regulation. To this end, computational biologists attempt to partition a network by allowing the subnetworks having overlapping regions, so that those multi-functional proteins can be partitioned into more than one functional module. Palla *et al.* presented CFinder [149, 150] to detect functional modules by seeking for overlapping k-clique communities, i.e., complete subgraphs of size k. They claimed that overlapping communities are prevalent in a variety of real-world networks, and traditional clustering strategies such as divisive and agglomerative methods cannot identify such overlapping structures. Ahn *et al.* proposed a novel concept, *link community*, to identify overlapping communities using hierarchical clustering in a *line graph* where each *node* represents an edge in the original graph, and two *nodes* are connected if the corresponding two edges share a common node in the original graph [153]. If two edges are connected to one node but belong to two different link communities, then that node belongs to the two communities as well. Nepusz *et al.* presented ClusterONE, a fast method to search for protein complexes on protein-protein interaction networks using a greedy strategy to grow a seed module in order to maximize a cohesiveness score [155]. The score is defined as the weights of within-module edges over the sum of within-module edges, boundary edges, and a penalty term. They claimed that ClusterONE can naturally adapt to weighted graphs, and

that the accuracy of identifying protein complexes is higher than those of the other clustering methods, such as MCL, MCODE, RNSC, Affinity Propagation, and RRW.

Network data are sometimes heterogeneous, in which nodes present more than one type of objects. Those heterogeneous data are usually described as a multilayer network with the same of type of objects in the same layer. How to perform network partition in those multilayer networks is still elusive. Mucha *et al.* modified the traditional modularity score [91] to obtain a multislice generalization of modularity for time-dependent community detection in social networks [162]. In terms of biological network, Xianghong Jasmine Zhou and her colleagues proposed a series of methods [163, 164] to identify gene regulatory modules in a multilayer network comprising multiple types of genomic data: copy number variation, DNA methylation, mRNA expression, and microRNA expression. Wang *et al.* constructed a similarity network of cancer patients using multiple types of genomic data, and then partitioned the network using similarity network fusion to divide the patients into different cancer subtypes [165].

In this study, we extend our AptRank (described in Chapter 2) to partition multilayer molecular networks into overlapping functional modules. In particular, our method, namely BioSweeper, identifies network modules using the following three stages: (1) diffuse information throughout the two-layer network from a set of seed nodes using a localized PageRank algorithm [166]; (2) for each diffusion from a seed node, sort each node in the network in descending order of information intensity, and then *sweep* over the ranking list of the nodes to find a partition with the minimal conductance value; and (3) merge two groups of nodes together if their overlapping region is above a threshold. For evaluation, we first use BioSweeper to partition a protein-protein interaction network interconnected with the Gene Ontology hierarchical structure as the second layer. Unlike the existing methods, MCL and ClusterONE, BioSweeper automatically detects functionally enriched modules by partitioning the two-layer network. We also test BioSweeper by partitioning a gene co-expression network interconnected with a Hi-C contact network between genomic regions, which can

identify long-range regulatory modules in which the genes are strongly co-expressed and their genomic regions have strong Hi-C contacts.

3.2 Methods

Before describing the methodology of BioSweeper, we first describe the notations for the primary data elements and the problem we attempt to solve. We use the same notations in AptRank (see Chapter 2) to describe a two-layer network with two distinct types of nodes at each layer. The adjacency matrix of the first-layer network with m type-1 nodes is denoted as $\boldsymbol{G} \in \mathbb{R}^{m \times m}$. The second layer network with n type-2 nodes is denoted as $\boldsymbol{H} \in \mathbb{R}^{n \times n}$. And the interconnections between type-1 and type-2 nodes are indicated as a matrix $\boldsymbol{R} \in \mathbb{R}^{m \times n}$. The task is to partition $m + n$ nodes in this two-layer network into ℓ overlapping modules such that each module has at least one type-1 node and one type-2 node. In this Chapter, the terms *module*, *cluster*, and *community* have the same meaning, and hence are used interchangeably.

3.2.1 Localized PageRank Diffusion

As described in Chapter 2, the adjacency matrix of a two-layer network with two-way diffusion is

$$\boldsymbol{A} = \begin{bmatrix} \boldsymbol{G} & \boldsymbol{R} \\ \boldsymbol{R}^T & \boldsymbol{H} \end{bmatrix}. \tag{3.1}$$

Using Personalized PageRank with seeds at each node at a time, we obtain the following linear system,

$$\left(\begin{bmatrix} \boldsymbol{I}_m & \boldsymbol{0} \\ \boldsymbol{0} & \boldsymbol{I}_n \end{bmatrix} - \alpha \begin{bmatrix} \overline{\sigma \boldsymbol{G}} & \overline{(1-\tau)\boldsymbol{R}} \\ \overline{(1-\sigma)\boldsymbol{R}^T} & \overline{\tau \boldsymbol{H}} \end{bmatrix} \right) \begin{bmatrix} \boldsymbol{X}_G \\ \boldsymbol{X}_H \end{bmatrix} = (1-\alpha) \begin{bmatrix} \boldsymbol{I}_m \\ \boldsymbol{0} \end{bmatrix}, \tag{3.2}$$

where $\overline{\boldsymbol{A}}$ denotes column-wise normalization of matrix $\boldsymbol{A}$. The parameters σ and τ, ranging from 0 to 1, control the proportion of information diffusion between the two layers of the network. In this diffusion system, the information diffuses from each

node, as denoted by $\boldsymbol{I}_m$ in the right-hand term, through the connectivity within $\boldsymbol{G}$, or the connectivity of $\boldsymbol{R}^T$ between the two layers, to the second layer $\boldsymbol{H}$, and then goes back to $\boldsymbol{G}$ through $\boldsymbol{R}$. In AptRank for protein function prediction, the solution to functional prediction is $\boldsymbol{X}_H$, whereas for partitioning of this two-layer network, we need to use the whole solution $\boldsymbol{X} \in \mathbb{R}^{(m+n)\times m}$. The i-th column of $\boldsymbol{X}$, denoted as $\mathbf{x}_i$, represents the information intensity after the Personalized PageRank starting from a type-1 node i.

In order to obtain a good partition, we need to prevent the information diffusion from going too far away from the source node. There are many techniques to restrict information diffusion by modifying the traditional PageRank. One of them is to use *heat kernel* in place of the fixed-decay parameter α used in the traditional PageRank [141, 167]. Compared to the fixed-decay coefficient α^k at k-th step diffusion, the heat kernel coefficient $t^k/k!$ decays much more quickly, and strongly weights early steps of diffusion. Another method to localize PageRank is to obtain a sparse and approximate solution $\mathbf{x}_\epsilon$ to Equation 3.2 such that $\|\mathbf{x}_\epsilon - \mathbf{x}\|_1 \leq \epsilon$. This sparse solution with localized behaviors in diffusion proved to be able to provide a good network partition [166, 168]. We utilize the algorithm described in ref. [166] to obtain a sparse solution to the Equation 3.2. Generally, this algorithm adopts Gauss-Southwell iteration to solve a PageRank linear system $(\boldsymbol{I} - \alpha\boldsymbol{P})\mathbf{x} = (1-\alpha)\mathbf{e}_s$ where $\mathbf{e}_s$ is an all-zero vector except the s-th entry as 1 that represents the seed node. First, initialize the solution $\mathbf{x}^{(0)} = \mathbf{0}$ and the residual $\mathbf{r}^{(0)} = (1-\alpha)\mathbf{e}_s$. Denote the approximate solution as $\mathbf{x}^{(k)}$ at k-step iteration, and the corresponding residual as $\mathbf{r}^{(k)}$. The Gauss-Southwell iteration then updates the entry j of $\mathbf{x}^{(k)}$ that corresponds to the largest entry j of $\mathbf{r}^{(k)}$, denoted as $r = \mathbf{r}_j^{(k)}$, as follow:

$$\begin{aligned} \mathbf{x}^{(k+1)} &= \mathbf{x}^{(k)} + r\mathbf{e}_j \\ \mathbf{r}^{(k+1)} &= \mathbf{r}^{(k)} - r(\boldsymbol{I} - \alpha\boldsymbol{P})\mathbf{e}_j. \end{aligned} \tag{3.3}$$

Next we describe how to use these sparse PageRank vectors to obtain optimal partitions of the two-layer network.

3.2.2 Finding Min-conductance Partition

Given a traditional Personalized PageRank vector, Andersen *et al.* proposed a method to identify a network partition with small *conductance* around the starting node [169]. The details of this procedure is visualized in Figure 3.1 using a small network with 9 nodes and 14 edges. We adopt this method to identify optimal modules given our localized PageRank vectors $\mathbf{x}_i, i = 1, 2, \cdots, m$ from a two-layer network diffusion. To define the *conductance*, the quality score of a module, let us define several preliminary concepts first. Denote the whole set of nodes in a graph as $\mathcal{V}$. For two arbitrary modules $\mathcal{C}_p, \mathcal{C}_q \subseteq \mathcal{V}$, define $\texttt{links}(\mathcal{C}_p, \mathcal{C}_q)$ as the sum of edge weights between the node sets $\mathcal{C}_p$ and $\mathcal{C}_q$. The *cut* of a module $\mathcal{C}_i$ is defined as the sum of edge weights between the nodes in $\mathcal{C}_i$ and its complement $\mathcal{V} \setminus \mathcal{C}_i$ as follows,

$$\texttt{cut}(\mathcal{C}_i) = \texttt{links}(\mathcal{C}_i, \mathcal{V} \setminus \mathcal{C}_i). \tag{3.4}$$

Then let us formally define the conductance of a module $\mathcal{C}_i$ as

$$\texttt{cond}(\mathcal{C}_i) = \frac{\texttt{cut}(\mathcal{C}_i)}{\min\left(\texttt{links}\left(\mathcal{C}_i, \mathcal{V}\right), \texttt{links}\left(\mathcal{V} \setminus \mathcal{C}_i, \mathcal{V}\right)\right)}, \tag{3.5}$$

where $\texttt{links}(\mathcal{C}_i, \mathcal{V})$ and $\texttt{links}\left(\mathcal{V} \setminus \mathcal{C}_i, \mathcal{V}\right)$ represent the number of edges incident on set $\mathcal{C}_i$ and $\mathcal{V} \setminus \mathcal{C}_i$, respectively. In implementation, we in fact compute $\texttt{links}(\mathcal{C}_i, \mathcal{V})$ for any set $\mathcal{C}_i$ as the sum of the degrees of the nodes in that set.

Taken together, the Andersen-Chung-Lang procedure [169] is to first sort the nodes in descending order of the PageRank vector normalized by the degree, $\mathbf{x}_i/\texttt{deg}(i)$, and then to calculate the conductance of each prefix set of nodes to obtain the set of nodes with lowest conductance as the partitioned module. Take a small network in Figure 3.1 as example. The PageRank diffusion starts from node-1, and finally reaches a stationary phase with the intensity distribution denoted as $\mathbf{x}$. Then the stationary intensity $\mathbf{x}$ is normalized by the degree of each node, and is sorted in descending order. We compute the conductance of each prefix set following the ranking list of nodes: $\{1\}$, $\{1, 2\}$, $\{1, 2, 3\}$, $\cdots$, $\{1, 2, 3, \cdots, 8, 9\}$. The conductance values of these 9 sets are shown in the bottom-right panel of Figure 3.1. We can see that the prefix set

$\{1, 2, 3, 4, 5, 6\}$ has the minimal conductance value, which means this set of nodes is the best partition for the diffusion from node-1. We search for the optimal partition for each localized PageRank vector $\mathbf{x}_i$ with the seed at node i, and finally output m lowest-conductance modules.

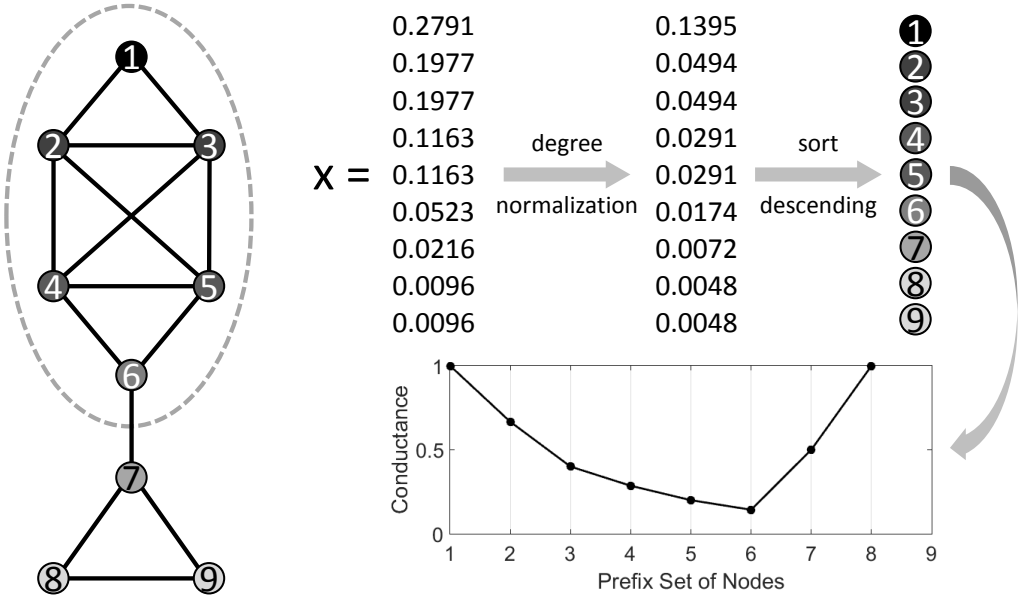

Fig. 3.1. Module Detection by Sweeping Over PageRank Vector. Left panel: a small network with 9 nodes and 14 edges. The gray dashed circle indicates the best partition. Top-right panel: $\mathbf{x}$, the stationary distribution of PageRank diffusion from node-1, is normalized by the degree of each node, and is sorted in a descending order. Bottom-right panel: the conductance value of each prefix set.

3.2.3 Post-processing

Given a set of lowest-conductance modules obtained by BioSweeper seeded on each node in the first layer network $\boldsymbol{G}$, we merge similar modules by thresholding the following pairwise module similarity score based on the Jaccard index,

$$J(\mathcal{C}_i, \mathcal{C}_j) = \frac{|\mathcal{C}_i \cap \mathcal{C}_j|}{|\mathcal{C}_i \cup \mathcal{C}_j|}. \tag{3.6}$$

If $J(\mathcal{C}_i, \mathcal{C}_j) > 0.5$, we merge $\mathcal{C}_i$ and $\mathcal{C}_j$ as one single module.

3.3 Results

We test our network partitioning algorithm, BioSweeper, on two different biological networks: a protein interactome and a gene co-expression network.

3.3.1 Partitioning Protein Interactome

We seek for protein complexes from a protein interactome of budding yeasts using BioSweeper. The protein interactome resource is from the BioGRID [145]. The functional annotations and the hierarchy are from the *Saccharomyces* Genome Database [170]. To verify whether the identified modules are truly protein complexes, we collected a gold-standard protein complex set from the MIPS (Munich Information Center for Protein Sequences, [171]). In fact, the interactome and the gold-standard reference set were directly obtained from the supplemental materials of ClusterONE [155].

Totally, there are $5,640$ proteins and $59,748$ interactions in the yeast protein interactome. We collected the GO functional annotations for these proteins, and obtained $33,922$ direct protein-function annotations between the proteins and $7,735$ GO terms. We used these datasets to construct a two-layer network with the proteins as the nodes in the first layer and the GO terms as the nodes in the second layer. We then partition this network into modules with proteins and GO terms together, which automatically produces functionally enriched modules.

In the gold-standard reference set, there are 203 yeast protein complexes ranging in size from 3 to 95 protein subunits. To evaluate our predicted protein complexes, we adopted the evaluation metric, MMR (maximum matching ratio) used in ClusterONE [155]. Unlike the original MMR based on an overlapping score between two clusters, we used the standard F_1 score in the field of machine learning to measure how good a predicted cluster is compared to a reference cluster. Suppose BioSweeper predicts p complexes, and there are $q = 203$ true complexes. We can construct a bipartite graph

with the adjacency matrix $\boldsymbol{F} \in \mathbb{R}^{p \times q}$ between these two sets of complexes whose edge weights are the F_1 score, defined as

$$F_1 = \frac{2\texttt{TP}}{2\texttt{TP} + \texttt{FP} + \texttt{FN}}, \tag{3.7}$$

where `TP`, `FP`, and `FN` represent true positives, false positives, and false negatives, respectively. The MMR is in fact the maximal matching in this weighted bipartite graph. That is to find f edges such that $\sum_{(i,j)\in f} F(i,j)$ is maximized where $f = \min(p, q)$ and only one-to-one match is allowed. Finding the optimal matching in a weighted bipartite graph can be solved by *Hungarian algorithm* [172]. We downloaded a Matlab implementation of this algorithm developed by Yi Cao from the Matlab File Exchange at `https://www.mathworks.com/matlabcentral/fileexchange/20652`.

We first partition the first-layer network $\boldsymbol{G}$ in order to compare our performance with those of MCL [112] and ClusterONE [155] using the same input protein interactome without the functional information. This experiment is denoted as `BioSweeper-1`. We used a guided seeding strategy by selecting the 203 seeds with the highest degrees within each gold-standard protein complex. After predicting 203 protein complexes by our method, we compared our predicted complexes with the gold standard set, and achieved an MMR score of 0.3258 which is comparable with the performance of ClusterONE with the MMR score of 0.3498, and outperforms MCL using inflation as 3.3 (suggested by the developers of ClusterONE in their comparison) with the MMR score of 0.2791.

We then integrated functional annotations (matrix $\boldsymbol{R}$) and the GO hierarchy (matrix $\boldsymbol{H}$) to improve the performance of BioSweeper, which is the main contribution of our method. This experiment is denoted as `BioSweeper-2` since we used two-layer network structure. A problem arises when we compare our predicted clusters against the gold-standard cluster set: BioSweeper performs clustering on the two-layer network and yields clusters containing the nodes in the both layers (proteins and GO terms), but all the nodes in the gold-standard clusters are the first-layer nodes (proteins). We did the comparison by removing the second-layer nodes from our predicted clusters, and then used the graph component containing the source node to compare

with the gold-standard cluster. This process was implemented by the Matlab function of component detection in MatlabBGL [173]. After integrating the functional information into our model with the parameters $\alpha = 0.99$, $\sigma = 0.35$ and $\tau = 0.1$, we achieved an MMR score of 0.3843 which outperformed ClusterONE by almost 10%. Besides the better performance, BioSweeper automatically detects the enriched functional terms associated with each predicted cluster. For example, BioSweeper successfully predicted a cluster with components: YBR254C, YDR246W, YDR407C, YDR472W, YEL048C, YGR166W, YKR068C, YML077W, YMR218C, YOR115C, which is identical to the gold-standard complex: TRAPPII protein complex (GO:1990071). The functional enrichment analysis verifies that the GO term, GO:1990071, is statistically enriched in our predicted cluster (p-value $= 3.27 \times 10^{-31}$, Fisher's exact test).

3.3.2 Partitioning Gene Co-expression Network

With the advance of high throughput RNA-sequencing technology, identifying gene co-expression modules is a long-term goal in systems biology. Grouping genes with similar expression pattern together gives insight into regulatory mechanisms between transcription factors and their target genes. WGCNA (Weighted Gene Co-Expression Network, [61]) is one of the classical methods to detect co-expression modules given genome-wide expression data. Here, we present how to use BioSweeper to detect co-expression modules while integrating heterogeneous data: Hi-C genomic contacts. This dataset represents the contact frequency between genomic regions in the 3D spatial chromatin structure. Hi-C genomic contact data have proved to be helpful in identification of co-factor protein complexes [174].

We construct a two-layer network with one layer as the gene co-expression network, and the other as the Hi-C genomic contact network. We downloaded an image-based measures of gene expression in mouse cortex from the Allen Brain Atlas [175], and an intra-chromosomal Hi-C contact matrix from Shen *et al.* [176]. After gene ID mapping using BioMart [177] and gene-to-genomic-region localization by BEDTools [178], we

obtain $m = 3,789$ genes and $n = 67,725$ genomic bins (genomic regions). The number of bins in each chromosome is listed in Table 3.1.

Table 3.1
Statistics of Hi-C Contact Data in Mouse Chromosomes

Chr. Index	**Chr Size**	**No. of Bins**	**Bin Size**
chr 1	195,471,971	6182	31620
chr 2	182,113,224	6074	29983
chr 3	160,039,680	4988	32085
chr 4	156,508,116	4782	32729
chr 5	151,834,684	4522	33577
chr 6	149,736,546	4273	35043
chr 7	145,441,459	3971	36626
chr 8	129,401,213	3657	35385
chr 9	124,595,110	3507	35528
chr 10	130,694,993	3385	38611
chr 11	122,082,543	3362	36313
chr 12	120,129,022	3309	36304
chr 13	120,421,639	2854	42194
chr 14	124,902,244	2660	46956
chr 15	104,043,685	2509	41469
chr 16	98,207,768	2221	44218
chr 17	94,987,271	1970	48217
chr 18	90,702,639	1903	47663
chr 19	61,431,566	1596	38491

We calculate the Pearson Correlation Coefficient (PCC) between each pair of gene expression profiles, and found that the PCC values are centered around 0.5 (Figure 3.2, blue distribution). Following the idea of WGCNA [61], we took the square of each PCC value to select strongly co-expressed pairs of genes with a threshold of

0.5 after the transformation (Figure 3.2, yellow distribution). For matrix $\boldsymbol{G} \in \mathbb{R}^{m \times m}$ in the first-layer network, $G_{ij} = 1$ if the square of PCC between gene i and j is larger than 0.5, $G_{ij} = 0$ otherwise. By setting this threshold, we obtained $426,294$ binary edges in the first-layer network.

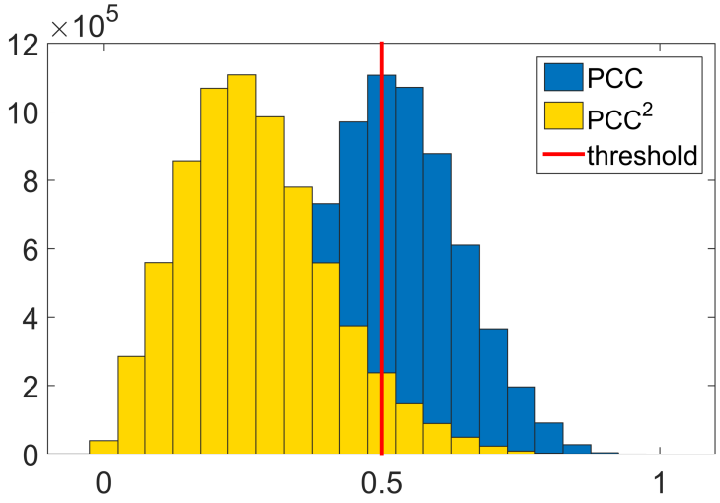

Fig. 3.2. Distribution of PCC and PCC Squared.

In terms of the Hi-C genomic contact data, the original Hi-C contact frequencies range from 0 to 557.045. Since the Hi-C data are very noisy, we converted them into binary values by setting $H_{ij} = 1$ if the frequency between region (or bin) i and j is larger than 1, and 0 otherwise. This thresholding step yields $4,365,209$ genomic contact measures.

For matrix $\boldsymbol{R} \in \mathbb{R}^{m \times n}$, the gene-bin relationship, it denotes what proportion of gene i is located in genomic bin j. One gene may span multiple bins in the genome, and we define R_{ij} as the overlapping length of gene i and bin j divided by the whole gene length from the transcription start site to the end of the last exon, which means $R_{ij} \in [0, 1]$.

We further restricted module detection to be only within each chromosome for the following reasons: (1) the co-expression network $\boldsymbol{G}$ is highly dense, containing an inseparable giant component without any modular structure; (2) no gene is known

to span more than one chromosome; and (3) no Hi-C genomic contact is measured between two regions in different chromosomes.

We highlight 3 detected co-expressed modules that meet the following criteria: (1) the module must have more than 2 genes but less than 10 genes; (2) the module must have more than 1 genomic regions; and (3) at least two genes in the module belong to different genomic regions. The details of these 3 modules are listed in Table 3.2. Note that the mouse gene annotation file is *Mus musculus* version 9 (mm9) downloaded in March 2016 from UCSC Genome Database, rather than the up-to-date version 10 (mm10).

Table 3.2
Three Highlighted Modules Detected by BioSweeper

Module	Gene Symbol and Location	Contacted Genomic Region
1	Nomo1 chr7:53289202-53339104 Nrip3 chr7:116904688-116924987 Scube2 chr7:116942767-117009100	chr7:116873567-116910192 chr7:116910193-116946818
2	Teddm3 chr16:21153006-21153890 Liph chr16:21956163-21995442 Senp2 chr16:22009715-22046768	chr16:21976347-22020564 chr16:22020565-22064782
3	Eml3 chr19:9004421-9015823 Eef1g chr19:9041704-9052592 Exosc1 chr19:41998472-42007772	chr19:9006895-9045385 chr19:9045386-9083876

3.4 Conclusion

Our multilayer network partitioning algorithm, BioSweeper, provides a joint-clustering strategy to identify meaningful network modules via heterogeneous data integration. The main contributions of BioSweeper can be summarized as follows.

- BioSweeper integrates protein functional annotations into the identification of protein complexes, which yields better predictions than ClusterONE, a state-of-the-art method in this task, and automatically identifies the statically enriched functional terms for predicted protein complexes.

- BioSweeper integrates Hi-C spatial genomic contact data to identify gene modules with similar expression profiles and high proximity in 3D chromatin structure, which implies a potential long-range regulatory mechanism within the identified modules.

4. NETWORK BALANCING: DIFFERENTIAL FLUX BALANCE ANALYSIS

Protein fluxes provide a more refined notion of protein abundance than raw counts alone by considering potential channels based on protein interaction networks. We propose a novel method, namely difFBA, to estimate protein fluxes in a protein interaction network using a linear programming model based on the framework of flux balance analysis. When we combine this estimate of protein fluxes with a protein-centric network measure, inspired by egocentric network analysis in sociology, we discover that the fluxes of proteins encoded by hypermutated genes in colon cancer have substantially higher rates of alteration in cancer cells than the protein quantities alone. These alterations remain statistically significant under different network perturbations. We conclude that the importance of a change in the quantity of a protein is determined not only by the protein itself, but also by its network neighbors.

4.1 Background

Systems biology is the interdisciplinary study of the cooperative behavior of biological molecules through complex interactions in a biological system. A fundamental task in systems biology is to uncover the rules governing how molecules select their interacting partners in a complex interaction network. Whether and how, for example, a protein changes its *friendship* under different physiological conditions given a protein physical interaction network is unclear.

High throughput technologies enable comprehensive measurements of various molecular profiles that are useful for the study of complex diseases, such as cancers [179–181]. By comparing these profiles in different conditions, one can identify both qualitative and quantitative molecular alterations, such as genetic mutations and dif-

ferential protein abundance in signaling pathways, respectively. However, identical genetic mutations are rarely identified in different patients, but rather are often found in common signaling pathways [11,182]. Attempts have been made to investigate how genetic variants disrupt protein interactions [15,97]. But these methods did not incorporate quantitative protein abundance data, and therefore cannot be used to interpret how structurally abnormal proteins caused by genetic mutations mediate interaction dynamics in signaling pathways.

Quantitative changes in protein interactions can be experimentally measured by AP-SWATH (Affinity Purification combined with Sequential Window Acquisition of all THeoretical spectra) mass spectrometry [104, 105]. However, currently the AP-SWATH technique is limited to small-scale studies due to the insufficient precision of statistical estimation for interacting protein abundances. And large-scale proteome-wide studies of quantitative changes in protein-protein interaction networks still depend on computational modeling. From a computational perspective, thermodynamic or kinetic modeling has been used to offer a precise quantitative map of transcriptional regulatory pathways [183]. However, the application scale of this method is usually limited to less than 10 transcription factors due to its high computational cost and the difficulty of obtaining the required kinetic parameters. In sum, both AP-SWATH and thermodynamic or kinetic modeling only work on small-scale studies. Extending the both methods to large-scale studies is an active research topic in systems biology community.

Linear modeling is able to model high-throughput large-scale data sets, and is widely used to study biological networks. Li *et al.* constructed a bipartite network between exon fragments and transcripts to estimate transcript abundance from mRNA sequencing data using a modified regularized least squares model [184]. Wang *et al.* reconstructed a transcriptional regulatory network from multiple microarray data sets by linear programming [185]. Duarte *et al.* utilized Flux Balance Analysis (FBA), a model based on linear programming, to reconstruct a human metabolic network [186]. However, to our knowledge, there are few studies using linear models

to analyze proteome-wide quantitative data in a large-scale protein interaction network. In fact, FBA can be extended from metabolic networks to protein interaction networks under reasonable assumptions (see Methods).

To this end, we propose difFBA, a linear programming model based on the FBA framework, to estimate *protein flux* (for definition, see Methods) in a protein interaction network, and demonstrate its use on proteome-wide quantitative data in colon cancer. In the Methods section, we make two basic assumptions to adapt the network-based proteomic model to the framework of FBA, and then mathematically describe the linear programming model and the egocentric network metric used in evaluation. In the Results section, we describe the quantitative proteomic data sets; illustrate the distribution of protein fluxes; and finally examine the predictive performance of the estimated protein fluxes within the egocentric networks of hypermutated genes, and also the performance robustness under different network perturbations.

4.2 Methods

Flux Balance Analysis (FBA) is widely used in metabolic networks [8]. It calculates the fluxes of metabolites through the network of biochemical reactions based on reaction stoichiometry. Similarly, given one protein with multiple binding partners in a protein interaction network, we would like to estimate the proportions of the protein binding to each of its partners. This binding fraction is termed *protein flux* in this study.

FBA can be viewed as a linear programming model [8]. Given a set of stoichiometric constraints, FBA aims to optimize a predefined objective function, e.g., to maximize a set of fluxes. Similarly, the goal of the proposed model in this study is to maximize the sum of all protein fluxes in the interaction network. The rationale for this objective function lies in two facts. On one hand, many proteins cannot function alone in a living cell. Instead, they bind to their network partners in a functional group to fulfill biological functions *in vivo*. On the other hand, proteins are intrinsi-

cally expensive to produce, and it is inefficient to produce proteins in excess of their binding partners.

4.2.1 Model Assumption

The proposed model is subject to the following two assumptions:

- No Stoichiometry: each protein copy can only bind one single copy of its neighboring proteins in the network. And the ratio of each binding pair of protein copies is 1:1, since currently no large-scale stoichiometric data are available. Similarly to the application of FBA in biochemical reaction networks, proteome-wide stoichiometric data can be naturally incorporated into our FBA-based model once they can be measured in high throughput manner.

- Independence: protein binding depends only on the abundance of the two proteins. Other complicated factors like protein locations, binding affinity and regulatory mechanism are not considered in this study, since these factors cannot be simplified into the linear structure of FBA. Instead, modeling protein locations, binding affinity and regulatory mechanism requires a spatial, high-order and time-varying system model. Solving this complicated model is computationally expensive, and cannot be applied to large scale proteome-wide data so far. In fact, the independence assumption is similar to assuming complete and rapid mixing of protein copies.

4.2.2 Model Construction

The model construction starts with a protein interaction network and a list of protein quantity data measured by quantitative proteomic techniques. We denote the protein interaction network as an undirected graph with a symmetric adjacency matrix $\boldsymbol{G} \in \mathbb{R}^{m \times m}$ where m is the number of proteins, and $G_{ij} = 1$ $(i, j = 1, \cdots, m)$ if protein i physically interacts with protein j, and 0 otherwise. Then the adjacency

matrix is converted into an incidence matrix $\boldsymbol{A} \in \mathbb{R}^{m \times n}$ where n is the number of edges in the graph (normally $m \ll n$), and $A_{ik} = A_{jk} = 1$ $(k = 1, \cdots, n)$ if $G_{ij} = 1$ and 0 otherwise, where $i < j$. In fact, the incidence matrix shows the relationship between nodes and edges in a graph. We denote the protein quantity data as a vector $\mathbf{b} \in \mathbb{R}^m$ and the protein flux of each interaction as $\mathbf{x} \in \mathbb{R}^n$. The model is designed to maximize the total interaction fluxes, i.e., $\mathbf{c}^T\mathbf{x}$ where $\mathbf{c}^T$ is an all-one vector. The portion of bound proteins in the flux is calculated as $\boldsymbol{A}\mathbf{x}$; this portion of any protein cannot exceed its total quantity, i.e., $\boldsymbol{A}\mathbf{x} \leq \mathbf{b}$. The estimated fluxes cannot be negative, i.e., $\mathbf{x} \geq \mathbf{0}$. In sum, we derive an FBA-like model based on linear programming as

$$\begin{aligned} \underset{\mathbf{x}}{\text{maximize}} \quad & \mathbf{c}^T\mathbf{x} \\ \text{subject to} \quad & \boldsymbol{A}\mathbf{x} \leq \mathbf{b} \\ & \mathbf{x} \geq \mathbf{0}. \end{aligned} \tag{4.1}$$

We empirically set the lower bound of $\mathbf{x}$ as 0.001 other than exact 0 for two reasons. First, to further compare the fold change of protein fluxes in two conditions, we need to calculate $\log_2(x^{c_1}/x^{c_2})$, and it has no meaning when x^{c_2} exactly equals to 0. Second, in practice we found that, given different protein abundance $\mathbf{b}$, the lower bound of $\mathbf{x}$ set to a value less than 0.001 yields different boundary values in the solutions when we use the interior point method to solve the linear programming problem.

4.2.3 Evaluation Metric

To test if differential protein flux prioritizes disease-associated genes better than differential protein quantity, we have devised a novel protein-wise metric based on an Egocentric Network (or *EgoNet*). The EgoNet of one node in a graph is defined as a local subnetwork comprising that node, its direct neighbors and the edges among them. In the literature of social and information networks, EgoNet analysis is frequently used to identify important structural and anomalous types of nodes [187,188]. In this study, similarly, the flux changes in the EgoNet of one protein help identify

how altered quantities affect a local network region centered at that protein. For a flux network, the EgoNet matrix of one protein t is defined as

$$\boldsymbol{Z}_{(t)}(i^*, j^*) = \begin{cases} x_{k^*} & \text{if } (i^*, j^*) \in EgoNet(t); \\ 0 & \text{otherwise,} \end{cases} \tag{4.2}$$

where k^* is the corresponding index of edge (i^*, j^*) in flux vector $\mathbf{x}$. Under two different conditions c_1 and c_2, the total flux change of a protein t within its EgoNet can be quantified using the Frobenius norm as $\mathbf{s}_E(t)$ (Equation 4.3). In contrast, we define two baseline scores for protein t between conditions c_1 and c_2 as the total flux change to neighbors $\mathbf{s}_N(t)$ (Equation 4.4) and the quantity change $\mathbf{s}_B(t)$ (Equation 4.5), respectively as,

$$\mathbf{s}_E(t) = \|\boldsymbol{Z}^{c_1}_{(t)} - \boldsymbol{Z}^{c_2}_{(t)}\|_F \tag{4.3}$$

$$\mathbf{s}_N(t) = \mathbf{a}_t^T |\mathbf{x}^{c_1} - \mathbf{x}^{c_2}| \tag{4.4}$$

$$\mathbf{s}_B(t) = |b_t^{c_1} - b_t^{c_2}| \tag{4.5}$$

where $\mathbf{a}_t^T$ is the t-th row of matrix $\boldsymbol{A}$.

4.3 Results

4.3.1 Data Sets

There are two data sets needed in differential FBA. One is the protein-protein physical interaction network, which can be downloaded from BioGRID [145]. The other is the protein quantity data (absolute copy numbers), which is obtained from an extensive quantitative proteome study of colon normal tissue and adenocarcinoma [189]. After ID mapping across these two data sets using BioMart [190], we identified $6,334$ proteins with measured quantities in both conditions (normal and cancerous) and $49,337$ physical interactions among them. Due to the large range of measured protein quantities (10^2 to 10^8), we performed a log-scaling, as shown in Figure 4.1(A).

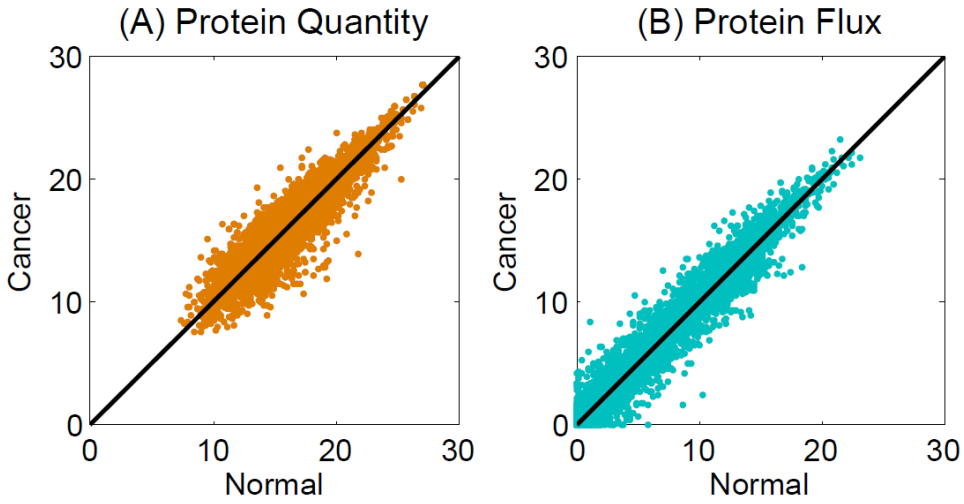

Fig. 4.1. Scatter Plot of Protein Quantities (A) and Fluxes (B) in Normal (x-axis) vs. Cancer (y-axis) Conditions.

4.3.2 Distribution of Differential Fluxes

Given the protein quantities $\mathbf{b}_n$ in normal colon tissue and $\mathbf{b}_c$ in colon cancer, respectively, the linear programming model (Equations 4.1) was solved to estimate the protein fluxes $\mathbf{x}_n$ and $\mathbf{x}_c$, respectively (Figure 4.1(B)). Comparing Figure 4.1 (A) and (B), we find that majority of protein quantities and fluxes show no change between normal and cancer conditions. However, a portion of the fluxes are close to zero, even though their linked proteins are abundant, indicating that some of the flux channels (protein interactions) are shut down under specific pathological conditions.

To highlight significant changes in protein quantities and fluxes, we illustrate the distribution of $\log_2$ fold changes of the ratios of cancerous to normal conditions in Figure 4.2. A subset of interactions show significant $\log_2$ fold changes (5+ folds) compared to the overall $\log_2$ fold changes in protein quantities (0.2+ folds). This suggests that the proposed model is able to correctly combine the changes in protein quantities and interactions. In this case, one can find an associated set of interaction fluxes that explain the change in protein quantities. For instance, given the up-

regulation of one protein, the proposed model is able to inform us which fluxes are concurrently up-regulated and which are not responsive or down-regulated.

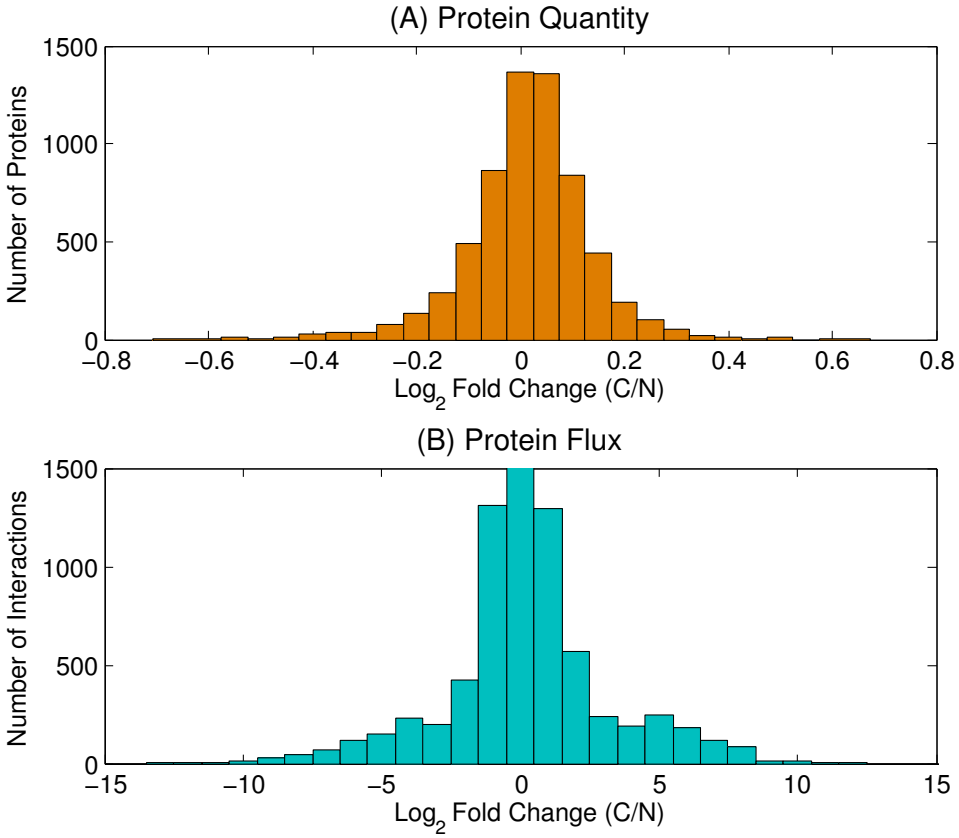

Fig. 4.2. Histogram of $\log_2$ Fold Changes (C/N, Cancer over Normal Conditions) in Protein Quantities (A) and Protein Fluxes (B). The most abundant fold change bin in (B), located within $[-0.5, 0.5]$, is truncated at $1,500$ for visualization convenience. The actual value is $43,798$ interactions.

Our FBA-based linear model is scalable for larger data sets. Using the solver, *linprog* in MATLAB, it normally takes around one minute to solve the model with our data set. We used the default algorithm in the solver, the interior point method, which has proven to be a polynomial-time algorithm in solving linear programming problems [191].

4.3.3 Identification of Known Cancer Genes

To evaluate whether significant flux changes are associated with proteins related to colon cancer, we first collected 18 hypermutated genes from a comprehensive genomic study of colon cancer reported in The Cancer Genome Atlas (TCGA) [181]. We first tested the null hypothesis that the cancer-related proteins with increasing (decreasing) quantities up-regulate (down-regulate) all the fluxes to their network neighbors. For each hypermutated gene/protein, we used a scatter plot to examine the relationship between its quantity fold-change and flux fold-changes (Figure 4.3). Generally, we can see that there is no positive relationship between the fold changes of protein quantity and protein flux. This rejects the null hypothesis and suggests that an up-regulated (or down-regulated) protein does not necessarily up-regulate (or down-regulate) all of the fluxes to its neighbors. For example, TP53, a well-known oncogene [192], is up-regulated by around 0.3 folds in quantity, whereas its flux fold changes span a wide range (± 8 folds) in cancer cells. Using our model, one can narrow down a large number of fluxes into a small set, and perform further precise modeling, or experimental validation using AP-SWATH, for example.

To further test whether flux changes in EgoNet can be used to predict these mutated genes in colon cancer, we scored each protein using the three Equations (4.3), (4.4) and (4.5), and examined the score ranks of these mutated genes using Receiver Operating Characteristic (ROC) curves (Figure 4.4). The Area Under the Curve (AUC) indicates the predictive performance of the three metrics. As shown in Figure 4.4, we find that the EgoNet-based metric achieves the AUC of 0.7327, whereas the other two baseline scores based on the difference only of protein quantity and flux changes to neighbors have the AUCs of 0.4759 and 0.7169, respectively. In particular, at a 0.2 false positive rate, the EgoNet-based metric achieves a true positive rate of around 0.55, whereas the protein quantity change and flux change to neighbors achieve only about 0.2 and 0.45, respectively. This suggests that protein quantity changes influence not only the fluxes flowing out to their network neighbors, but also the fluxes

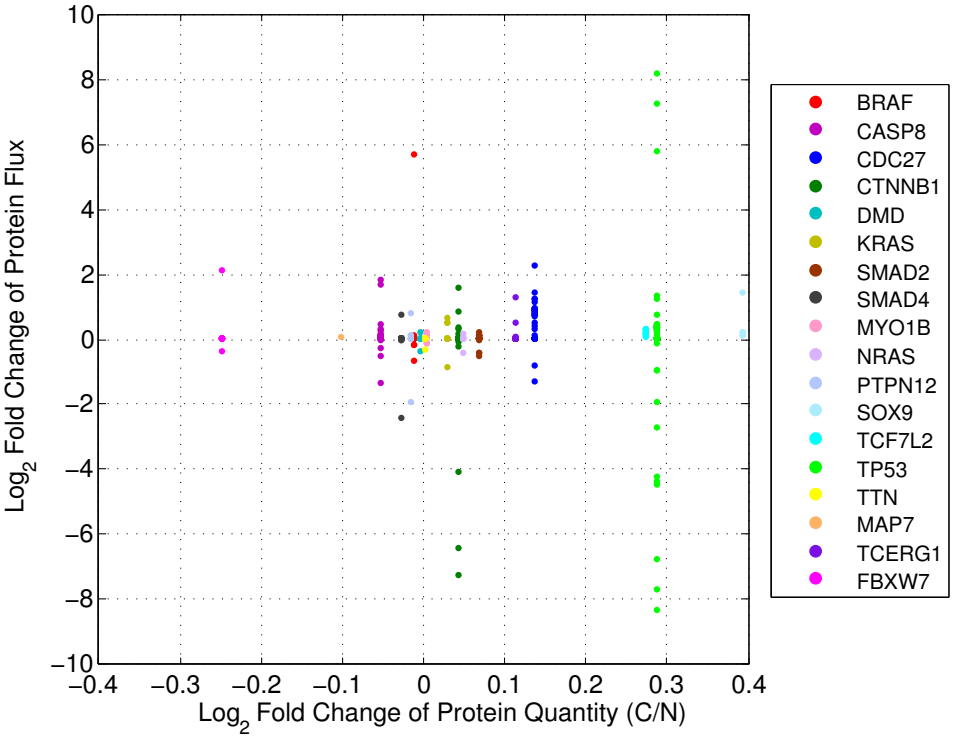

Fig. 4.3. Fold Changes of Protein Quantities (x-axis) and Fluxes (y-axis) of 18 Hypermutated Genes in Colon Cancer.

between their neighbors. In addition, it reveals that the proteins with cancer-related mutations have no significant changes in quantities. Nevertheless, using the proposed differential FBA combined with the egocentric network analysis, we discovered that genetic alterations in fact have much stronger impacts on protein fluxes within the EgoNet than protein quantities alone.

To examine the robustness of cancer-associated protein identification, we altered the protein interaction network and examined whether the prediction performance is robust to network perturbation. We first randomly reassigned the protein abundance data to different nodes in the same network, and found that the prediction performance (Area Under the ROC curve, AUROC) dramatically drops to a random level (Figure 4.5). Next, we tested whether our method is robust against network topology noise by randomly removing a proportion of edges (while ensuring that every protein

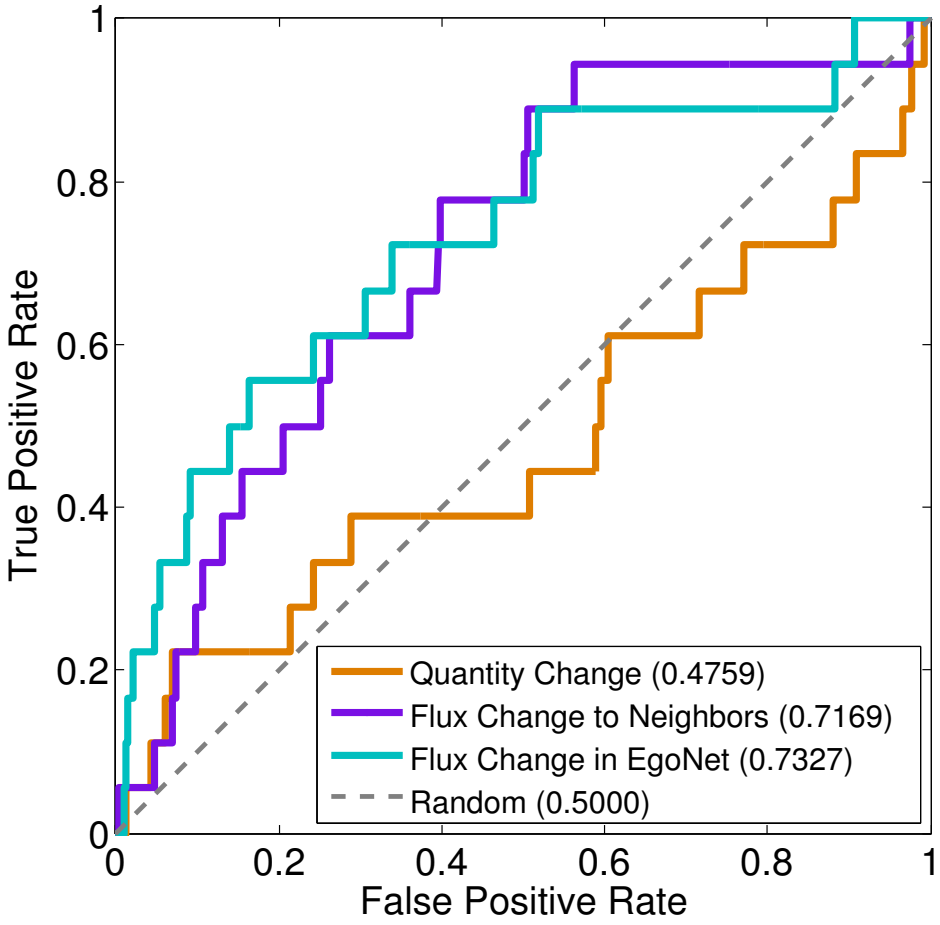

Fig. 4.4. Receiver Operating Characteristic (ROC) Curves in the Evaluation of Hypermutated Gene Prediction. The Area Under the Curves (AUCs) are shown in the brackets.

has at least one edge). We find that the performance of our method drops slowly until 30% of edges are removed (Figure 4.5). In contrast, randomly adding 10% extra edges results in a significant decline of the performance from 0.7327 to around 0.6, and even worse when 30% extra edges are added in (Figure 4.5). In sum, this perturbation test suggests that the network topology and the protein abundance data have strong associations with each other. Also, it demonstrates that our method is robust to the network data even in the presence of a relatively high false positive rate.

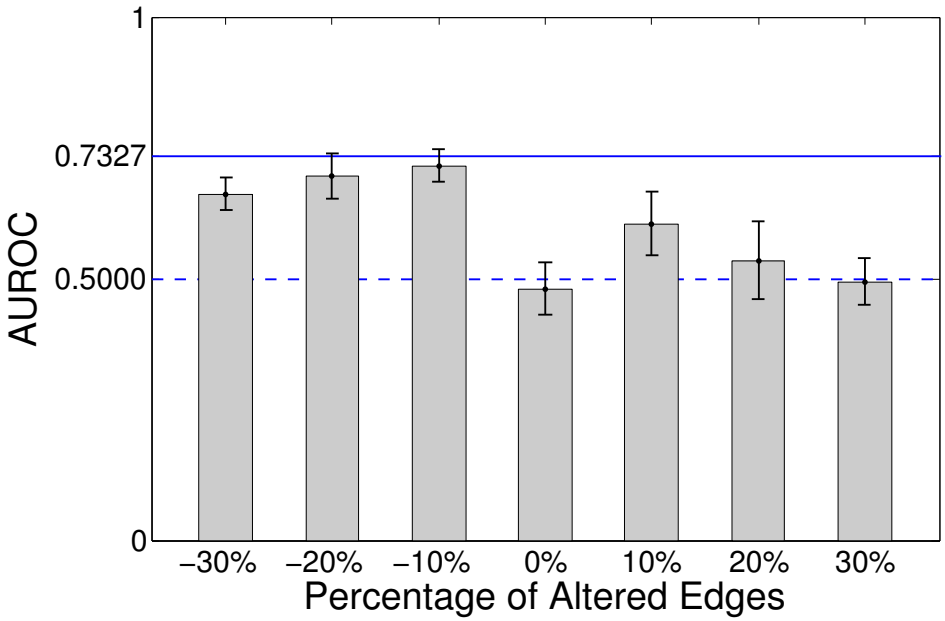

Fig. 4.5. Area Under the ROC Curves (AUROC) in Robustness Test using Randomly Perturbed Networks. In x-axis, negative percentages denote the proportion of edges randomly removed; positive percentages denote random addition of edges; and 0% denotes random shuffle of protein abundance data. In y-axis, the bars and error bars indicate the means and standard deviations of AUROCs from 10 repeated experiments under each type of network perturbations. AUROC = 0.5000 (blue dashed line) indicates the performance of random prediction; and AUROC = 0.7327 (blue solid line) indicates the original performance of our method without network perturbation, as shown in Figure 4.4.

4.4 Conclusion

In this paper, we have presented a computational method, difFBA, based on flux balance analysis to estimate protein fluxes throughout the protein interaction network subject to a balance assumption. We show that the difference in protein quantities can be combined with the protein interactions assuming one-hop balanced diffusion in the network. We also show that the protein flux changes within egocentric networks have a stronger association with the genetic mutational status of the corresponding protein-coding genes than the protein quantity changes. To our knowledge, this is the

first attempt to extend flux balance analysis, which is widely used to study metabolic networks, to network-based analysis of quantitative proteomic data.

In future work, we would like to incorporate multiple *omic* data sets into our framework. And so far, we have assumed the stoichiometric ratio between two binding proteins is 1:1. As stoichiometric data *in vivo* become more available, they can be integrated with higher-level network information about functional modules to refine the estimation of protein fluxes.

5. SIDE PROJECTS

In this Chapter, I will present two side projects: an assessment study of subnetwork detection methods, and my participation of a community-driven competition in systems toxicology.

5.1 Assessment of Subnetwork Detection Methods

Subnetwork detection is often used with differential expression analysis to identify modules or pathways associated with a disease or condition. Many computational methods are available for subnetwork analysis. Here, we compare the results of eight methods: simulated annealingbased jActiveModules, greedy searchbased jActiveModules, DEGAS, BioNet, NetBox, ClustEx, OptDis, and NetWalker. These methods represent distinctly different computational strategies and are among the most widely used. Each of these methods was used to analyze gene expression data consisting of paired tumor and normal samples from 50 breast cancer patients. While the number of genes/proteins and protein interactions detected by the eight methods vary widely, a core set of 60 genes and 50 interactions was found to be shared by the subnetworks identified by five or more of the methods. Within the core set, 12 genes were found to be known breast cancer genes.

5.1.1 Introduction

With the advent of high-throughput measurements in biotechnology, cancer biologists are able to dissect the complicated pathology of cancers from multiple directions. These measured molecular profiles include genetic mutations, copy number variance, messenger RNA (mRNA) expression, microRNA expression, DNA methylation, pro-

tein abundance, etc. [179]. However, multidimensional data also bring a tremendous challenge to the computational biology community. What can these data tell us about cancer? Differential analysis is a straightforward method in which differences in the molecular profiles of tumor and normal cells are identified. These analyses rely on a large number of samples and result in the identification of thousands of differences in molecular profiles. How to interpret these molecular variations as a whole is still under investigation.

Alternatively, molecular interaction data have shown powerful potential for connecting isolated molecular variations into a meaningful framework. These analyses usually start with differential analysis of molecular profiles, e.g., differential gene expression, and score the extent of the difference for each gene. Next, biological network data that indicate the association of genes are collected, and then the scores are overlaid on the network. Now the task is to extract a subset of the network, i.e., a subnetwork of the global network, such that the subnetwork is as small as possible while connecting as many highly scored genes as possible. This subnetwork enriched in differentially expressed genes can be used to discover, for example, that the up-regulation of one gene is caused by the overexpression of its upstream regulator or dysfunction of its suppressor.

Subnetwork detection is a crucial analysis since it is capable of linking multiple individual molecular variations into an insightful wiring diagram showing how one individual variation is related to the others. Many methods for subnetwork detection have been developed. In 2002, Ideker *et al.* first proposed a computational model for subnetwork detection based on simulated annealing [193]. They also proved that subnetwork detection is an NP-Hard problem. As reviewed by Mitra *et al.*, many attempts have been made during recent the decade to solve this problem efficiently using approximation algorithms [147]. Due to the diversity of subnetwork scoring functions used by the different approximation algorithms, it is unlikely that different programs will obtain identical or even very similar subnetworks given the same expression and network data.

In this study, we propose a pipeline to comprehensively evaluate the performance of subnetwork detection methods from multiple aspects. We first select eight methods and assess them equally using an authoritative data set of breast cancer from The Cancer Genome Atlas (TCGA) [179]. Then we perform a differential expression analysis using DESeq [194] and score the significance of expression change for each gene. Next, we extract subnetworks using the eight methods and compare their outputs based on their coverage of significant genes, network modularity, mutual similarities, and functional enrichment. Finally, we compare their computational costs, user friendliness, and discuss their strengths and weaknesses, respectively.

5.1.2 Results

Overview of Subnetwork Detection Methods

Over 40 computational models have been developed during the past decade based on various algorithms, as reviewed by Mitra *et al.* [147], and Berger *et al.* [195]. We selected eight of them (Table 5.1) for further comprehensive assessment based on the following three rules. First, the input of the models must be a network, and an expression set or a list of gene weights based on the expression. The models were ruled out if they required genetic mutation data or integration of co-expression data. Second, the selected models must be accessible either with open source code or a well-maintained online Graphical User Interface (GUI). Third, the selected models must represent diversity of methodology, and similar or integrative models are excluded. We summarize the eight selected methods and discuss their advantages and limitations in Table 5.2.

In order to perform a fair assessment, we kept the input data of the eight models as similar as possible (see Table 5.1). On one hand, we used the proteinprotein interaction network from Human Protein Reference Database (HPRD) [203] as model input if there is no preloaded network data in the models. On the other hand, if the models used their preloaded networks and output a subnetwork including genes not

in the HPRD network, we pruned them from the subnetwork. In terms of expression data, we first utilized DESeq to normalize the raw counts of mRNA sequencing from TCGA breast carcinoma data set. Then we performed differential expression analysis across the 50 case and 50 control samples and assigned each gene an adjusted p-value for its significance of differential expression. Those p-values can be directly used as the input for subnetwork detection, be ranked to select a seed gene set, or be converted into a set of particular weights tailored to the requirement of the model (see Table 5.1). Next, we ran each program to detect subnetworks and tuned the parameters to control the size of subnetworks to be approximately 1,000 genes. Finally, we obtained eight subnetworks from the models and performed an assessment of their coverage of significant genes, network modularity, hits of true breast cancer genes, and functional enrichment in Kyoto Encyclopedia of Genes and Genomes (KEGG) [204] pathways and Gene Ontology (GO) [205] terms.

Assessment of subnetwork quality

We assess the quality of subnetworks output by the eight methods from two aspects: coverage of significant genes and network modularity. First, we prepared volcano plots with $\log_2$(fold change) versus $\log_{10}(p\text{-values})$ for each method and highlighted the found genes in the eight subnetworks in red, as shown in Figure 5.1. We find that jActiveModules using Greedy Search (jAM.GR), BioNet, and NetBox cover most of the significant genes in their subnetworks, while excluding insignificant genes. In contrast, jActiveModules using Simulated Annealing (jAM.SA), ClustEx, and NetWalker cover a large number of genes regardless of their significance. DEGAS covers more upregulated genes, whereas OptDis covers more downregulated genes.

To further examine the specificity and sensitivity of significant gene coverage of each method, we labeled each detected gene as a positive sample for each method and examined whether the expression p-values predict the eight subnetworks well. We plot eight Receiver Operating Characteristic (ROC) curves in Figure 5.2 to show

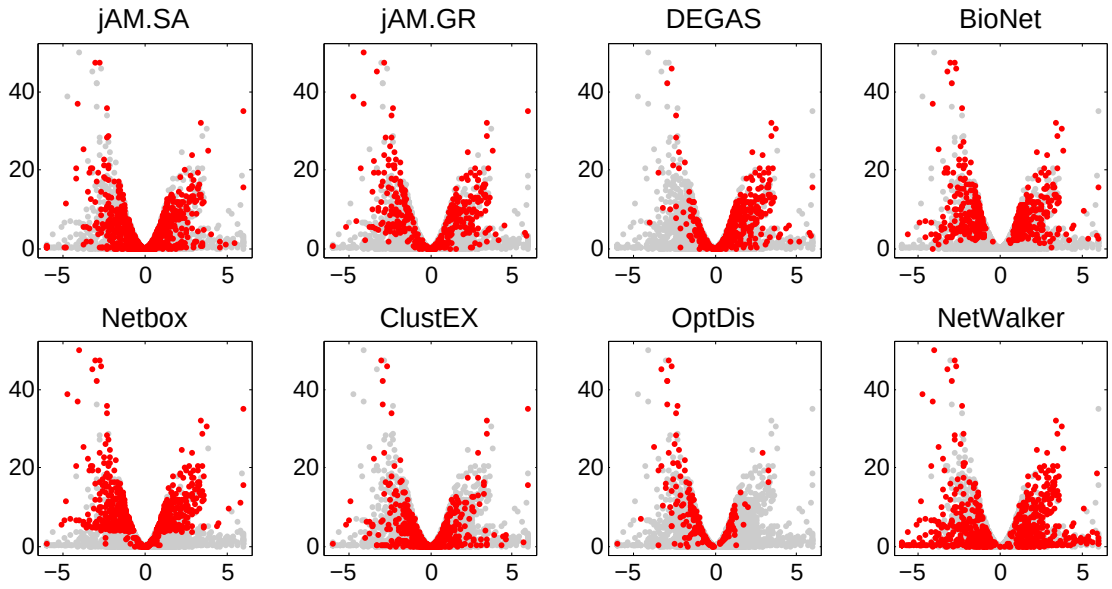

Fig. 5.1. Volcano Plots of Differential Gene Expression. The $\log_2$(fold change) (shown in the $[-6, 6]$ only, 99th percentile) vs. $-\log_{10}(p$-values) evaluated by DESeq. The dots highlighted in red are the genes involving in each subnetwork produced by the eight methods.

the predictability of the p-values for the eight subnetworks. From Figure 5.2, we find that the best performer is BioNet since it achieves an area under the curve (AUC) of 0.93, the highest AUC for any method. This is particularly interesting since BioNet does not depend on a seed gene set. NetBox achieves comparably high AUC (0.89), but there is an obvious kink point on the curve due to the selection of input seed genes based on p-values. The AUC of OptDis ranks the third, probably due to the small size of the subnetwork. jAM.SA detects the largest subnetwork but does not cover low p-value genes very well since it accepts a high p-value gene with a specific probability in simulated annealing to avoid suboptimality. ClustEx does not perform as well as NetBox, even though they use the same seed gene set and network data. This is because we only consider the largest subnetwork (210 seeds out of 801 genes) found by ClustEx as the output and discard the smaller subnetworks, which include 455 seeds.

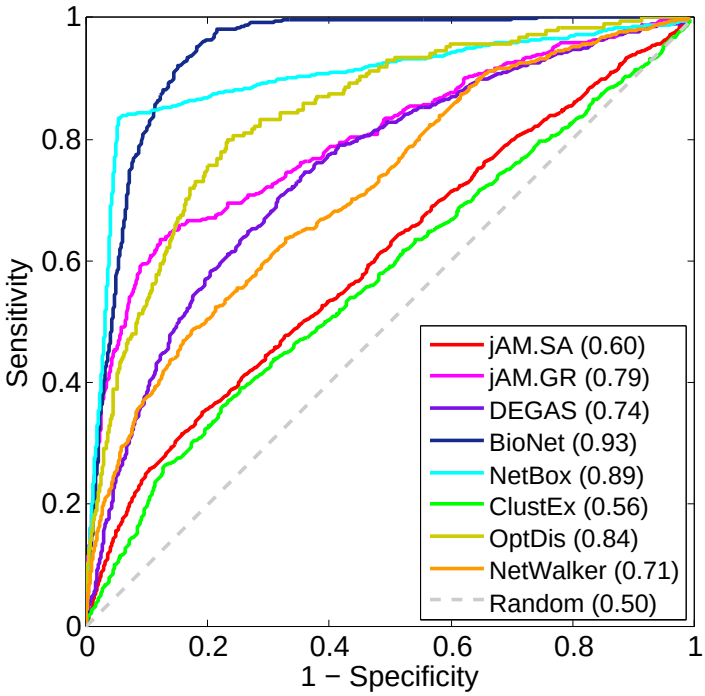

Fig. 5.2. ROC Curves of $-\log_{10}(p\text{-values})$ Predicting the Eight Subnetworks. The numbers in the brackets are the AUCs.

To examine modularity of the eight subnetworks, we used two different measures: Global Clustering Coefficient (GCC) [206] and Cut-Based Ratio (CBR) [207]. GCC measures how close a subnetwork is to a completely connected graph. And CBR measures the degree to which a subnetwork consists of more edges between nodes within the subnetwork and fewer edges between nodes inside and outside the subnetwork. Both modularity scores were scaled to the interval $[0, 1]$ by dividing by the maximum quantities (Figure 5.3). We can see that the OptDis subnetwork has the highest GCC, probably because there are many small (3 to 5 genes) fully connected modules in the subnetwork. In contrast, the ClustEx subnetwork has the highest CBR, probably due to the hierarchical clustering step used before growing the subnetwork within the clusters. The subnetworks of jAM.GR and DEGAS have moderately high modularity scores; both methods search for subnetworks using greedy strategies.

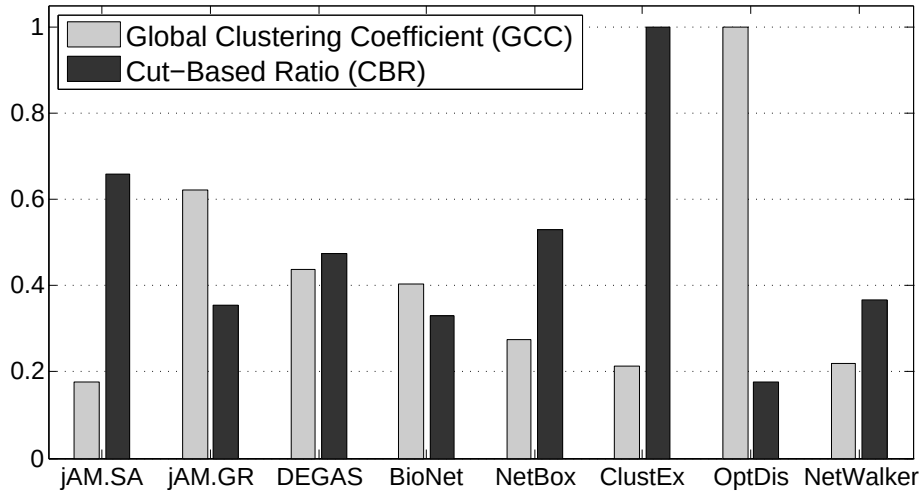

Fig. 5.3. Modularity of the Eight Subnetworks.

Cross-model comparison and functional analysis of subnetworks

To investigate the similarity of the eight output subnetworks detected by the different methods, we first performed a pairwise comparison of the subnetworks using Jaccard similarity, in terms of nodes (Table 5.3) and interactions (Table 5.4). Surprisingly, it was found that the subnetworks of BioNet and NetBox were the most similar even though they used different subnetwork detection strategies. Methods using similar subnetwork detection algorithms have moderate similarities in their output subnetworks, such as jAM.GR and DEGAS. In contrast, methods with the same input expression and network data often detect very dissimilar subnetworks, for instance DEGAS and OptDis, and NetBox and ClustEx. The pairwise similarities of the subnetworks suggest that the use of similar algorithms and/or similar input data do not guarantee a similar output. This is because the different methods use different objective functions to evaluate a subnetwork in optimization.

We tested whether the detected subnetworks contain putative breast cancer genes. First, we collected 462 breast cancer genes from the KEGG Orthology Based Annotation System (KOBAS, [208]) v2.0 functional enrichment list, which integrates Online Mendelian Inheritance in Man (OMIM, [209]), KEGG DISEASE [204], Functional

Disease Ontology (FunDO, [210]), Genetic Association Database (GAD, [211]), and the National Human Genome Research Institute (NHGRI) Genome-Wide Association Studies (GWAS) Catalog [212] disease databases. With those 462 genes as ground truth, we calculated the precision and recall of each of the eight subnetworks (Figure 5.4) and found that the top subnetworks in identifying the true breast cancer genes are those produced by BioNet, NetWalker, NetBox, and jAM.GR. Surprisingly, these four methods use totally different algorithms for subnetwork detection (see Table 5.1). And NetWalker displayed its potential for predicting true disease genes, even though its coverage of significantly differentially expressed genes was relatively poor; this may be due to its use of random walks to diffuse information through the whole network without any restriction to shortest paths and greedy search.

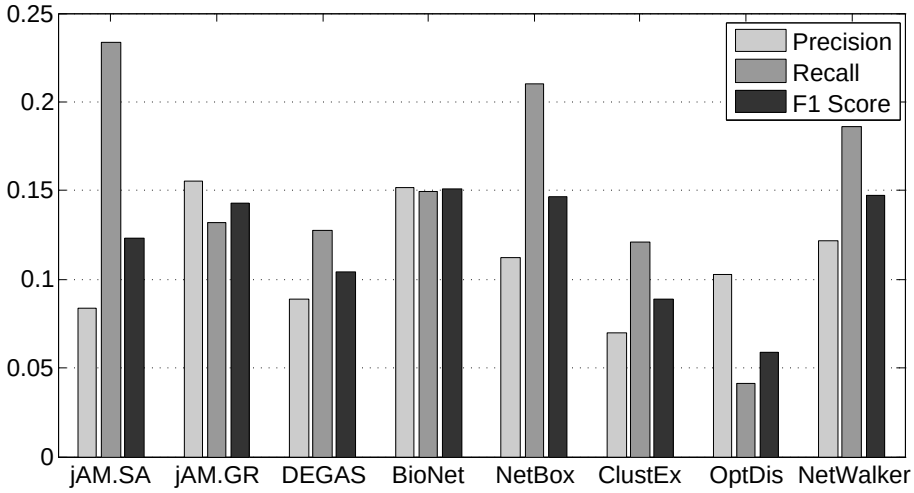

Fig. 5.4. Prediction of the 462 Breast Cancer Genes by the Eight Subnetworks. F1 score is defined as 2 × precision × recall/(precision + recall).

Then we used the list of true breast cancer genes to investigate if cancer-related genes are more likely to be detected by multiple methods. The distribution of all genes and the breast cancer genes is shown in Figure 5.5(a) in terms of how many different methods detect genes in these classes. We can see in Figure 5.5(a) that many genes are detected by only a few methods, whereas a small number of genes are detected

by almost every method. Surprisingly, the percentage of breast cancer genes in the reported subnetworks increases with the number of methods detecting those genes, suggesting that the genes detected by more methods are more likely to be a true breast cancer genes. And also it suggests that an ensemble method that integrates multiple methods may be a better way of detecting subnetworks covering more disease genes. Similarly, we collected $2,058$ interactions enriched in breast cancer pathways using KOBAS [208] from the KEGG pathway [204], Pathway Interaction Database (PID, [213]), BioCarta [214], Reactome [215], BioCyc [216], and Protein ANalysis THrough Evolutionary Relationships (PANTHER, [217]) databases. The distribution of interactions in terms of the number of methods detecting those interactions is shown in Figure 5.5(b). We found that no interactions were commonly detected by more than six methods. The interactions commonly detected by more methods are slightly more likely to be enriched in pathways related to breast cancer.

To examine functional enrichment of commonly detected genes, we used KOBAS to annotate the 553 genes detected by at least three methods (Supplementary Table 1, available online, `DOI:10.4137/CIN.S17641`). The top enriched KEGG pathways of these genes are cell cycle (hsa04110), MicroRNAs in cancer (hsa05206), and Pathways in cancer (hsa05200), all with the corrected p-values less than 0.05. Cancers are enriched as the topmost disease in KEGG DISEASE database with corrected p-values less than 0.1. And the top GO terms enriched in this gene set are extracellular matrix (GO:0031012), cell division (GO:0051301), and their relevant terms. Note that there is no breast cancer-specific term significantly enriched in terms of pathways, diseases, and functions.

Finally, we used Cytoscape v3.0 [218] to visualize a prominent subnetwork in which each interaction is detected by at least five methods. This subnetwork consists of 60 genes and 50 interactions (Figure 5.6). Within those 60 genes, there are 12 true breast cancer genes (red border) detected by KOBAS v2.0 in the multiple databases. Notably, the breast cancer gene Nuclear Receptor Subfamily 3, Group C, Member 2 (NR3C2), a gene encoding the mineralocorticoid receptor, was the only gene detected

by all the eight methods. An RNA interference (RNAi) experiment has verified that the depletion of NR3C2 increases cell death in breast [219]. This evidence is consistent with Figure 5.6 in which NR3C2 is downregulated in breast cancer cells ($\log_2$(fold change) = 2.2). We also found that actin alpha 1 (ACTA1), one of the interactors of NR3C2, was detected by five methods and was downregulated as well. ACTA1 is a highly conserved protein responsible for cell motility and a major constituent of the contractile apparatus [220]. This suggests that downregulation of ACTA1 causes increased cell motility and cancer metastasis. Similarly, inhibin, beta A (INHBA), pleiotrophin (PTN), and seven in absentia homolog family E3 (siah E3) ubiquitin protein ligase 2 (SIAH2), which were detected by seven methods, have been experimentally verified to be associated with breast cancer development. Overexpression of INHBA in mesenchymal cells increases colony formation potential of breast epithelial cells [221]. PTN, a secretory cytokine, has been found to stimulate breast cancer progression through remodeling of the tumor microenvironment [222]. Downregulation of SIAH2 has been found to be associated with resistance to endocrine therapy in breast cancer [223].

5.1.3 Conclusion

We have performed a comprehensive assessment of a broad spectrum of state-of-the-art methods for subnetwork detection using up-to-date gene expression data specific for breast cancer. The key findings in this study can be summarized in the following three main points.

- First, based on the functional enrichment analysis, the subnetworks detected by the individual methods offer only limited information on breast cancer pathology. However, the prominent subnetwork detected by the majority of the methods offers a very specific and relevant result that is clearly related to breast cancer pathology. The data used here are probably as good as or better than what is currently available for most kinds of tumors and are therefore represen-

tative of typical situations. Even though each of the eight methods were claimed to be effective in their original publications, based on the data sets they used, the subnetwork detection problem still cannot be considered to be solved and needs further investigation.

- Second, the enrichment in known breast cancer-related genes in the set of genes identified by many independent methods suggests that investigators should use several different methods based on different principles. For the data set used here, we suggest that a combination of BioNet, jAM.GR, NetBox, and NetWalker could be used, although it is not clear that this would be true for all data sets or types.

- Third, in terms of ease of use, some of the methods are available only as source code, which must be compiled and installed, typically on a UNIX-based system; this may be an obstacle for some experimental biologists. A GUI is highly recommended for the purpose of wide use, or perhaps implementation within a widely used system such as R.

We suggest that the definition of subnetwork needs to be refined to be something more than a simple subset of a global network. Interactome data need to be dissected and reorganized using high-level structures, such as pathways and protein complexes. Those interactome structures ensure that the output subnetworks are biologically meaningful and guide subnetwork detection methods to prune a global network without losing the important biological structures.

5.1.4 Methods

Data preprocessing

Subnetwork detection usually requires two input data sets, a gene expression data set and a network data set. In this study, gene expression was measured by mRNA sequencing (RNA-Seq), and were obtained from TCGA breast invasive carcinoma cat-

egory [179]. The expression data consist of raw counts, normalized median transcript lengths, and Reads Per Kilobase of transcript per Million mapped reads for 20,532 genes in 50 tumor samples, paired with 50 normal samples paired with the same patients. The network data set was downloaded from HPRD [203]. After gene ID matching using BioNet, 7,369 nonredundant genes remained (Supplementary Table 2, available online, `DOI:10.4137/CIN.S17641`) and 28,571 interactions were recorded among the encoded proteins after removal of self-loops and isolated interactions (Supplementary Table 3, available online, `DOI:10.4137/CIN.S17641`). DESeq [194] was used to normalize the raw counts and to detect differentially expressed genes between the tumor and normal samples based on a negative binomial model. The p-values were then adjusted for multiple testing with Benjamini-Hochberg procedure [224] (Supplementary Table 1, available online, `DOI:10.4137/CIN.S17641`).

Subnetwork detection methods

Unless further specified, we used default setting of parameters for all eight models. The input expression and network data are summarized in Table 1, and the gene and interaction lists of the eight subnetworks are in shown Supplementary Tables 2 and 3 (available online, `DOI:10.4137/CIN.S17641`), respectively.

jActiveModules [193, 196] requires a weighted gene list with the weights ranging from 0 to 1. Hence, we directly used the adjusted p-values from DESeq as the weights. Within jActiveModules, there are two different search strategies for subnetworks: simulated annealing [193] and greedy search [196]. For simulated annealing, we increased the default number of iterations from 2,500 to 10,000. Default parameter settings were used for greedy search. For both kinds of searches, we set the maximum number of modules as 1.

DEGAS [197] has multiple optional algorithms, and we used the CUSP (Covering Using Shortest Paths) heuristic algorithm to detect subnetworks. Dysregulation direction was selected to be `DIFF`, and maximum number of modules was set to 1. The

number of covered genes k was set to increase from 100 to $1,000$ with a step size of 100. The other parameters were kept at their default values.

BioNet [198] requires the raw p-values (not adjusted for multiple testing) as the input from differential expression analysis by DESeq. Intrinsically, BioNet first aggregates two lists of p-values from two pairs of comparisons (case 1 vs. control and case 2 vs. control) into one list. Since we only had one comparison between tumor and normal samples, we input one more replicate list of p-values to meet the requirement. We set the False Discovery Rate (FDR) cutoff as 0.00001 other than the default value 0.001. A low FDR cutoff has effects on reducing the size of an output subnetwork.

NetBox [199] is provided with a preloaded Human Interaction Network, and therefore, the only input data needed are a list of seed genes. We used only the genes with the p-value less than 0.0001 in the differential expression analysis as the seed gene set, which selected $1,063$ (14.4%) out of $7,369$ genes. The shortest path threshold was set to 2 rather than the default value 1.

ClustEx [200] provides preloaded network data and also supports customized network uploading. For comparative purposes, we used the trimmed HPRD network described above. It also requires a seed gene set; we used the same set used with NetBox. We considered only the largest output cluster (801 genes) as the final output subnetwork, since all the other 354 clusters contained less than 40 genes.

OptDis [201] needs three input data sets: a network, a gene expression profile, and a gene ID conversion list linking the network and expression sets. As shown in Table 5.1, OptDis ran slowly. To keep the computational cost tractable, we set the maximum size of modules to 10. OptDis returned 50 modules, all with sizes less than 10 genes. We consider the union of these modules to be a single subnetwork in our analysis.

NetWalker [202] has a preloaded network database called the NetWalker Interactome Knowledgebase (NIK). After matching our $7,369$ genes with the $13,328$ genes in the preloaded network, we obtained $7,354$ matched genes. NetWalker requires an expression ratio for each gene centered around 1. We defined the ra-

tio as $r = 2 \cdot \text{logit}(\log_2(\text{FC}))$, where FC denoted the fold change of gene expression in tumor over that in normal cells, and the `logit()` function was defined as $\text{logit}(x) = 1/(1 + \exp(x))$. The unmatched genes were assigned expression ratios of 1, denoting no significant expression change. After running, NetWalker returned an Edge Flux value ranging from 10.04 to 2.41 for each of the 327,599 interactions in the preloaded network. We selected 2,210 (0.67%) interactions with the values lower than 5.5 or higher than 1.5 as the output subnetwork. Then the interactions not present in the HPRD network were removed, and there remained 795 interactions as the final subnetwork produced by NetWalker.

Subnetwork quality assessment and functional enrichment analysis

Majority of network analysis and graphing were done using `MATLAB`. And the functional enrichment analysis of subnetworks was performed by KOBAS v2.0 [208]. We identified 462 breast cancer genes out of the 7,369 genes (Supplementary Table 2, available online, `DOI:10.4137/CIN.S17641`) in multiple disease databases using KOBAS, and used them as the ground truth to evaluate the predictability of the eight subnetworks (see Figures 5.4, 5.5(a), and 5.6). Similarly, we combined the 462 breast cancer genes with 227 genes enriched in cancer pathways to query the HPRD network and found 2,058 interactions (Supplementary Table 3, available online, `DOI:10.4137/CIN.S17641`) that connect the 689 genes in the querying list as a positive set of breast cancer pathways (see Figure 5.5(b)). For the functional analysis of commonly detected genes by at least three methods, we input those genes in KOBAS and set the 7,369 genes to the background gene set (Supplementary Table 1, available online, `DOI:10.4137/CIN.S17641`).

Table 5.1
Overview of the Eight Methods

Method	**Algorithm**	**Tool Type**	**Ref.**	**Input Network**	**Input Expression**	**Running Time (min)**
jAM.SA	Simulated annealing	Cytoscape	[193]	HPRD	Adjusted p-values	∼40
jAM.GR	Greedy search	Cytoscape	[196]	HPRD	Adjusted p-values	∼4
DEGAS	Greedy heuristic	GUI	[197]	HPRD	Normalized counts	∼3
BioNet	Integer-linear programming	R package	[198]	HPRD	p-values	∼7
NetBox	Shortest path	Python, Java	[199]	Preload	Seed genes	∼100
ClustEx	Clustering, shortest path	C & GUI	[200]	HPRD	Seed genes	∼150
OptDis	Color coding	C	[201]	HPRD	Normalized counts	∼1560
NetWalker	Random walks	GUI	[202]	Preload	Adjusted p-values	∼0.1

Table 5.2
Performance Summary of the Eight Methods.

Method	**Description**	**Advantage**	**Limitation**
jAM.SA	Use simulated annealing to search for the most highly scored subnetwork	Accept low-scored genes with a certain probability	Too large subnetwork; Slow
jAM.GR	Maximize a mutual informationbased objective function by growing the subnetwork from seed set	Fast; uses mutual information to evaluate subnetwork quality	Exclude low-scored genes, suboptimal solution only.
DEGAS	Model subnetwork detection as a Connected Set Cover problem and solves it using a greedy heuristic	Fast; able to detect differentially expressed genes; no gene weight required	Many parameters need to be tuned
BioNet	Formulate as a Prize-Collecting Steiner Tree problem and solves it using Integer Linear Programming	Fast; produces a single small subnetwork with high coverage of significant genes	Single small output sub-network with a high false-negative rate
NetBox	Use shortest paths to connect seed setand refine by adding fewest linker genes	High coverage of significant genes, fewest insignificant genes	Produce multiple small and isolated subnetworks
ClustEx	Hierarchical clustering of co-expression network, and refine by shortest by shortest paths	Combines clustering and shortest paths to detect highly co-expressed subnetworks	Produce multiple isolated subnetworks involving many genes
OptDis	Uses color coding technique to search for optimally discriminative subnetworks	Good coverage over significant genes, with small subnetworks	Cannot detect large subnetworks (over 20 genes); very slow
NetWalker	Use random walks to prioritize important genes and interactions in the stationary state	Very fast, friendly GUI	Only produces scores for interactions, no subnetwork search, per se,

Table 5.3
Common Genes Identified by the Eight Methods

	jAM.SA	**jAM.GR**	**DEGAS**	**BioNet**	**NetBox**	**ClustEx**	**OptDis**	**NetWalker**
jAM.SA	**1290**	144	182	164	285	158	52	160
jAM.GR	0.0936	**393**	137	168	213	63	40	146
DEGAS	0.1025	0.1484	**667**	143	247	85	57	136
BioNet	0.1038	0.2474	0.1462	**454**	356	78	64	190
NetBox	0.1526	0.2042	0.1925	0.3704	**863**	162	107	246
ClustEx	0.0817	0.0557	0.0615	0.0663	0.1079	**801**	34	115
OptDis	0.0365	0.0743	0.0717	0.1113	0.1137	0.0357	**185**	50
NetWalker	0.0872	0.1534	0.1100	0.1961	0.1861	0.0827	0.0595	**705**

Table 5.4
Common Interactions Identified by the Eight Methods

	jAM.SA	**jAM.GR**	**DEGAS**	**BioNet**	**NetBox**	**ClustEx**	**OptDis**	**NetWalker**
jAM.SA	**2141**	118	152	105	234	97	26	90
jAM.GR	0.0433	**702**	133	123	178	18	15	82
DEGAS	0.0446	0.0668	**1421**	105	256	34	27	84
BioNet	0.0397	0.1035	0.0545	**609**	429	39	46	173
NetBox	0.0686	0.0878	0.0960	0.2549	**1503**	100	94	215
ClustEx	0.0318	0.0107	0.0142	0.0248	0.0415	**1004**	12	51
OptDis	0.0110	0.0160	0.0164	0.0567	0.0567	0.0097	**249**	34
NetWalker	0.0316	0.0580	0.0394	0.1405	0.1032	0.0292	0.0337	**795**

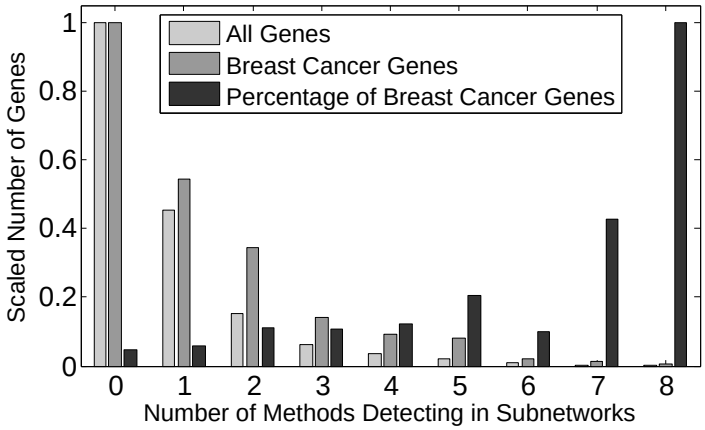

(a) Commonly Detected Genes.

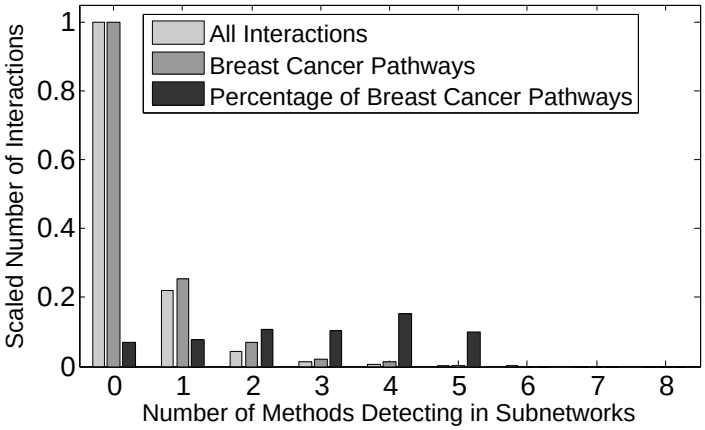

(b) Commonly Detected Interactions.

Fig. 5.5. Number of Methods Detecting Breast Cancer Genes and Interactions in Subnetworks. Histograms of the number of genes (a) and interaction counts (b) versus the number of methods that detect them. (a) All genes denote the $7,369$ genes in the HPRD network. Breast cancer genes are the 462 genes found by KOBAS in multiple disease databases. Both the gene counts are scaled to $[0, 1]$ by dividing by the maximum count. The percentage of breast cancer genes is the breast cancer gene count divided by the count of all the genes in each category (genes found by a certain number of methods). (b) All interactions denote the $28,571$ interactions in the HPRD network. Breast cancer pathways are the $2,058$ interactions found by KOBAS in multiple pathway databases. Both the interaction counts are scaled to $[0, 1]$ by dividing by the maximum count. The percentage of breast cancer pathways is the interaction count in breast cancer pathways divided by the total interaction count in each category.

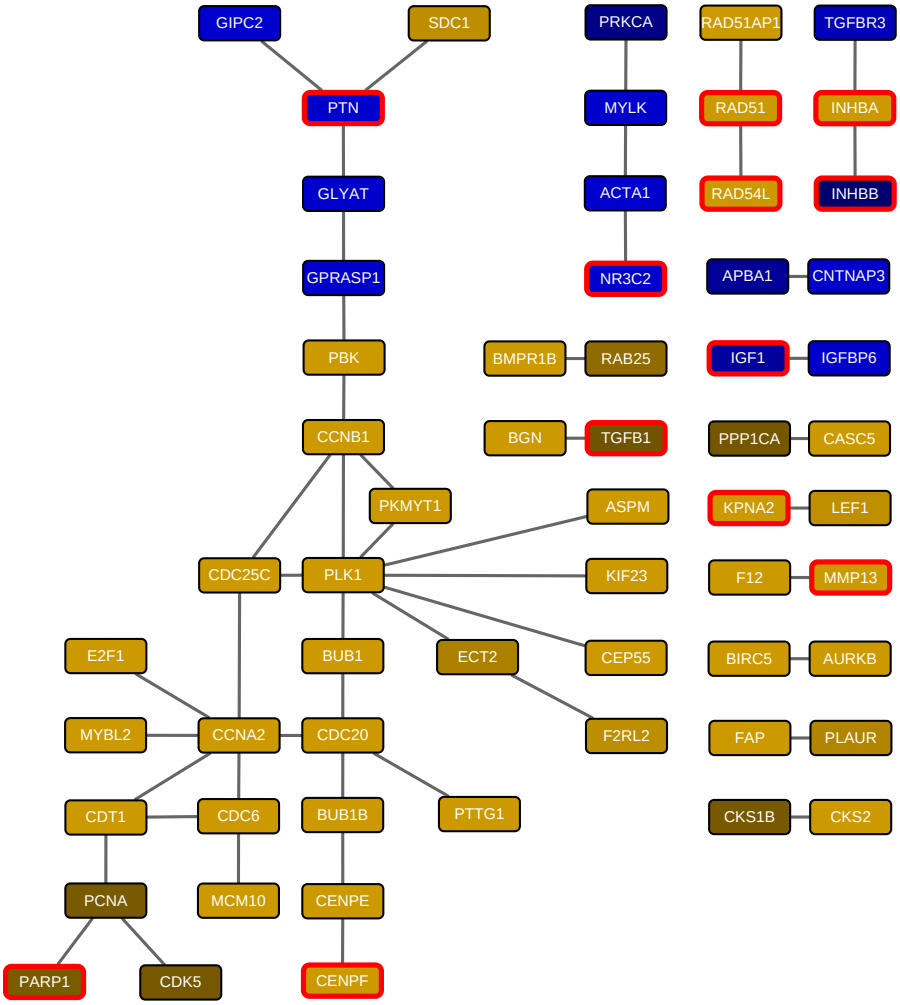

Fig. 5.6. Prominent Subnetwork Whose Interactions are Detected by at least Five Methods. Node color indicates $\log_2$(fold change) of differential expression (yellow: upregulated in tumor samples; blue: downregulated in tumor samples). The 12 genes in red border are in the list of 462 known breast cancer genes. Visualized by Cytoscape v3.0 [218].

5.2 SysTox Challenge: Classification of Smoking Exposure

In this challenge, we are tasked to predict smoking exposure (smoker vs. non-current smoker) or cessation (former smoker vs. never smoker) status using gene expression data of human whole blood. The expression data, measured by microarrays, consist of $18,604$ genes in 224 samples for training and $1,340$ samples for testing. Each samples are labeled as smoker, former smoker or never smoker. Generally, this task can be considered as a classical classification problem in machine learning. We employ three state-of-the-art classification methods to fulfill this task: Support Vector Machine (SVM), Random Forests (RF) and Artificial Neural Networks (ANN). As a result, we report that SVM is the best performer again RF and ANN in two-fold cross validation.

5.2.1 Introduction

Smoking is a primary risk factor for the development of various diseases, such as lung cancer [225], Alzheimer's disease [226], Parkinson's disease [227], coronary heart disease [228], inflammatory bowel disease [229], and so on. There are thousands of chemicals in cigarettes. Some of those chemicals can enter the blood circulatory system, which provides a way to monitor the smoking exposure of an individual subject using gene expression of whole blood.

The whole challenge consists of two parts: sub-challenge 1 for human samples, and sub-challenge 2 for mouse samples. In particular, sub-challenge 2 aims to verify whether the human gene signatures derived in sub-challenge 1 can be used to predict smoking exposure status in mouse samples. In this section, we report only the result of sub-challenge 1 in predicting smoker

There are three given data sets, one for training and the other two for testing. All the expression data are generated by microarrays consisting of $18,604$ human genes and their expression in 224 training samples with labels, and $1,340$ testing samples without labels (638 and 702 samples for round 1 and 2 tests, respectively). The

expression intensities are positive continuous values less than 20. We divided them by 20 to scale them into $[0, 1]$ before feeding them into the classifiers.

5.2.2 Methods: SVM, RF and ANN

Support vector machine, random forests and artificial neural networks are all classical machine learning methods with many successful applications in various fields of studies.

Support Vector Machines

Support vector machine (SVM) seeks a classification boundary with maximum margin between different classes of objects. The boundary is, in fact, determined by a set of support vectors (SVs), i.e., the set of objects closest to the boundary. This makes SVM a robust classifier to outliers, since non-SV objects far away from the boundary do not contribute to the determination of the boundary, and therefore do not affect the final classification accuracy. For more complicated cases where two classes of objects are not linear separable, SVM can adapt to these non-linear cases by integrating various kernels in order to map the original feature space to a higher-order separable space. The most complicated case is that the objects are still not separable after being mapped to a high-order space using kernel trick. The current standard version of SVM overcomes this challenge by introducing *soft margin* which can tolerate a small portion of classification errors. This idea was proposed by Corinna Cortes and Vladimir Vapnik in 1993 and was published in 1995 [230].

Random Forests

Random forest (RF) is an ensemble learning method that applies a *voting* strategy to the classification results of many individual decision trees. It is simple to obtain a satisfying and robust result using RF, since the only parameter to tune is the

number of trees. Normally, the more trees we grow, the better results we have. Remarkably, RF is resistant to overfitting [231], which is an advantage compared to neural networks, when the number of samples is much smaller than the number of features. RF performs a bootstrap sampling from the training set to grow each tree, which lowers the correlation among the trees and maximizes the forest diversity so as to decrease overfitting. This advantage makes RF one of the most popular classifiers in molecular diagnosis, since the number of patients is normally less than the number of measured genes.

Artificial Neural Networks

Artificial Neural networks (ANN) and its extension, Deep learning, are a bioinspired model that mimics how brains recognize objects and memorize information. It is a much more suitable approach for big data challenges than SVM and RF due to its versatile infrastructure of hidden neurons. Its successful applications span various fields of study in artificial intelligence, such as image classification, speech recognition, and recently, computer gaming (see AlphaGO [232]). Deep learning rebuilds the fame of ANN by avoiding overfitting using advanced techniques such as max-pooling (induction, [233]) and dropout (like *amnesia*, [234]). One of its extensions, a deep convolution neural network (CNN) with 8 layers of neurons, trumped SVM in image classification under the standard test using the largest image database, ImageNET [235] with an error rate of 15.3% (CNN) compared to 26.2% (SVM) on October 13, 2012. This is just the beginning of the deep learning era. However, training a deep neural network is computationally expensive, since there are many free parameters corresponding to the connections within and between the layers of hidden neurons.

5.2.3 Results: Two-fold Cross Validation

We randomly split the given training samples into two sets, each of which consists of 112 samples. Then we trained the three classifiers using one set and tested their performances using the other, then we switched the two sets for a two-fold cross validation.

For SVM, we downloaded LIBSVM, A Library for Support Vector Machines [236], from the website: `https://www.csie.ntu.edu.tw/~cjlin/libsvm/`. This library provides users with four different kernels: linear, polynomial, radial basis, and sigmoid. We tested the performances of these four kernels using two-fold cross validations with 3 repeats. The result demonstrates that the linear kernel has the best performance (Figure 5.7), since the feature space is already very high, and therefore non-linear kernels contribute little to the prediction.

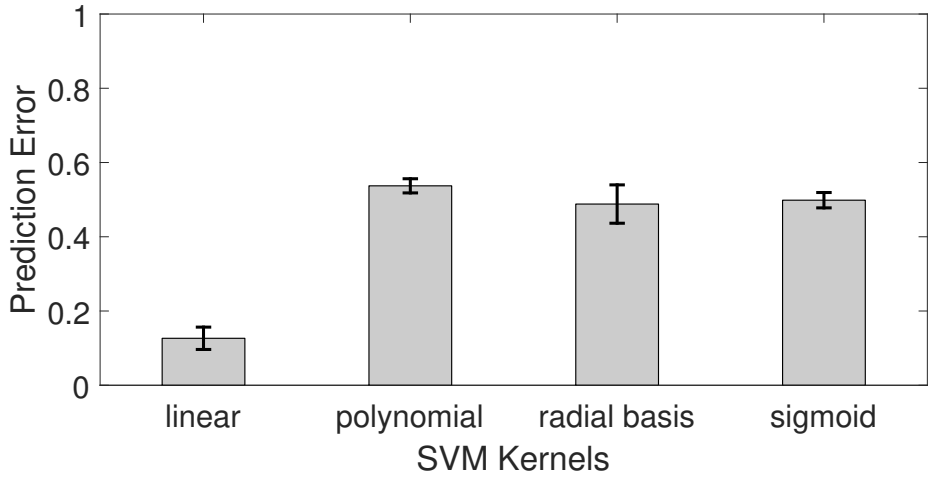

Fig. 5.7. Performances of SVMs with Different Kernels. The error bars represent the standard deviations of prediction errors from 5 repeats of cross-validation experiments.

For RF, we used the MATLAB built-in toolbox, *TreeBagger* to conduct the experiment. More details about this toolbox can be found from the official website: `http://www.mathworks.com/help/stats/treebagger.html`. We tested the performances of RFs with different number of trees, 10, 100, and 1000, respectively, and

examined whether more trees resulted in overfitting. Based on our experimental setting, the result confirms Leo Breiman's claim that RF is resistant to overfitting (Figure 5.8). The prediction error keeps decreasing as the number of trees increases.

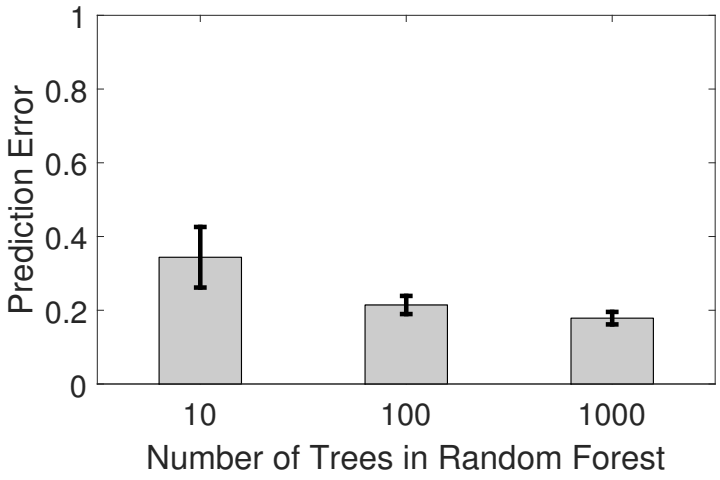

Fig. 5.8. Performances of RF with Different Trees. The error bars represent the standard deviations of prediction errors from 5 repeats of cross-validation experiments.

For ANN, we downloaded a Matlab deep learning toolbox written by Rasmus Berg Palm from his GitHub: `https://github.com/rasmusbergpalm/DeepLearnToolbox`. Even though we utilized several techniques developed for deep learning to avoid overfitting during our model training, we constructed a traditional ANN with only two hidden layers with 100 neurons at each layer (Table 5.5), due to the small size of our training date. Thus, we consider our ANN as a *shallow* network other than a deep neural network. The detailed setting of our ANN model is listed in Table 5.5.

The fraction of dropout means we randomly shut down a hidden neuron with a certain probability (0.25 is used in our model) to avoid overfitting during training [234]. The *sigmoid* function is a commonly used activation function in ANN and deep learning, even though many other activation functions have been developed in the past 10 years. The learning rate, ranging from 0 to 1, represents the step size of the stochastic gradient descent (SGD) search. A small learning rate can help capture the optima at the expense of slowing down the search. Setting the learning rate as 1

Table 5.5
Parameter Setting of ANN

ANN parameters	Setting
Number of hidden layers	2
Number of neurons at each layer	100
Dropout fraction	0.25
Activation function	sigmoid
Learning rate	1
Number of epochs	25
Batch size	35

in our model saves our computational time, but does not guarantee the training error to reach the optima in our experiment (Figure 5.9). The number of epochs denotes how many times the data propagate throughout the entire ANN during training. And the batch size is a parameter of SGD indicating the sample size of a mini-batch over which the gradient is averaged.

Figure 5.9 illustrates one of our training experiments using the parameter setting listed in Table 5.5. The training error quickly reaches almost zero after 25 epochs. However, a training error of zero in ANN does not guarantee an equally perfect error rate in testing.

Taken together, we put the best performance of each method into Figure 5.10 for comparison. We found that SVM with linear kernel is the best performer over RF and ANN, with an averaged testing error of 12.65%. RF with 1000 trees has the most stable performance with an averaged testing error of 17.86% and the smallest standard deviation. ANN does not perform as well as SVM and RF due to overfitting with an averaged testing error of 21.13%.

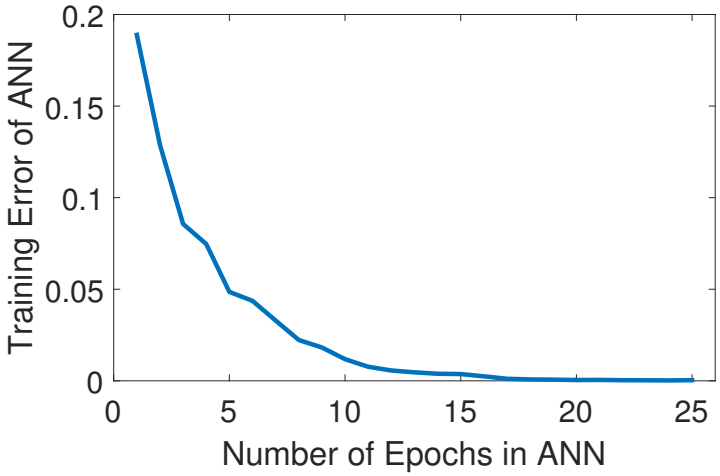

Fig. 5.9. Training Error of ANN.

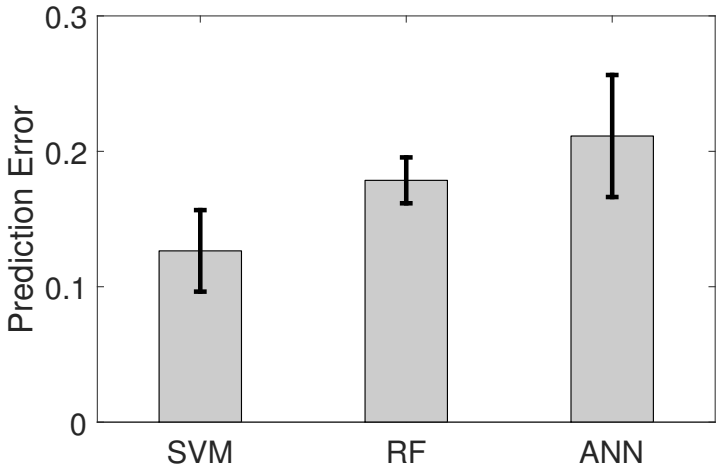

Fig. 5.10. Performance Comparison of the Three Methods. The error bars represent the standard deviations of prediction errors from 5 repeats of cross-validation experiments.

5.2.4 Conclusion

We utilize three state-of-the-art classification algorithms to predict whether an individual is a smoker or non-current smoker using the gene expression data in whole blood. Our experiment demonstrates that SVM with a linear kernel is the best tool in a two-fold cross validation with 224 samples and $18,604$ features. We conclude that

SVM and RF still have competitive performance in small data sets, whereas deep learning requires large data sets to release its power.

Pick the right tool, a scissor or a mower.

6. SUMMARY

6.1 Discussion

In this thesis, I have developed three computational tools to label, partition, and balance molecular networks, respectively. The results suggest that integrating heterogeneous datasets into molecular networks can provide deeper insight into the functional organization and behavior of biological molecules. Raw data of molecular networks offer limited information for scientists to understand complex functional behaviors. Those data show only which molecules directly interact with each other, but they cannot be used to answer the following questions: (1) why are they connected to each other, (2) how does the connection play a role in a complex biological process, and (3) how does the connection change in different physiological conditions. The success of AptRank in protein function prediction validates the hypothesis that proteins with similar functions tend to interact with each other. BioSweeper reveals the functional organization of molecule networks, and demonstrates how a team of molecules performs a complex process by their connections. DifFBA uncovers connections are not constant but dynamic, and these changes provide more insight in understanding the molecular mechanism of phenotypic formation than the changes of molecular quantities alone.

6.2 Future Direction

6.2.1 All-in-One: Differential Pathway Analysis (DiPAna)

In the future, I will incorporate the three models developed in this thesis, AptRank, BioSweeper and difFBA, into a unified model to perform Differential Pathway Analysis (DiPAna) using quantitative proteomic data from complex diseases.

In particular, I will first use AptRank to obtain a "full" protein functional profile given the incomplete functional annotations. Next, with the "full" functional profile, BioSweeper will detect functionally enriched modules (protein complexes and pathways) which set up the boundaries of protein fluxes in a protein-protein interaction network. Finally, I will generalize difFBA into a non-negative least squares model, and solve it by robust regression algorithms to obtain a pathway-activity score for each pathway. A differential analysis of this score between case and control samples will indicate the extent to which a pathway is perturbed in diseased conditions, which can highlight the pathways of interest for further pathological study. Interestingly, *dipana* in Italian means disentangle, which fits the function of DiPAna: to disentangle a molecular network into a dynamic modular diagram.

6.2.2 Perspective

In terms of biology, I believe that molecular networks are the language of molecular function, but our current network models are still insufficient to explain complicated biological processes. Integrating heterogeneous data is one of the most powerful ways to enrich molecular networks. As more and more data on DNA methylation, non-coding RNA expression, protein post-translational modification and metabolic profiling become available, it will one day be feasible to construct a global molecular map of an advanced organism. To come back to the ultimate question: why does one molecule choose to interact with another? This question cannot be answered without the light of evolution. Evolutionary game theory attempts to answer this kind of question: why does one molecule decide to act cooperatively, and does the disruption of this molecular cooperation lead to diseases. Are molecules *selfish*?

In terms of computer science, current advanced machine learning methods enable automatic image classification, language translation, speech recognition and many other complicated tasks. However, those techniques are still too young to understand the world of biology. For example, using deep learning can successfully find a cat in

tons of images, or even videos. However, to identify causal genetic mutations from genomic data to facilitate disease diagnosis is still a daunting challenge for current artificial intelligence. Genomic medicine is becoming one of the most challenging stages for scientists in artificial intelligence. And undoubtedly, finding an efficient biomarker for disease diagnosis is more meaningful than finding a cat in videos.

LIST OF REFERENCES

LIST OF REFERENCES

[1] K.-I. Goh, M. E. Cusick, D. Valle, B. Childs, M. Vidal, and A.-L. Barabási, "The human disease network," *Proceedings of the National Academy of Sciences*, vol. 104, no. 21, pp. 8685–8690, 2007.

[2] M. A. Yıldırım, K.-I. Goh, M. E. Cusick, A.-L. Barabási, and M. Vidal, "Drug-target network," *Nature Biotechnology*, vol. 25, no. 10, pp. 1119–1126, 2007.

[3] G. W. Beadle and E. L. Tatum, "Genetic control of biochemical reactions in neurospora," *Proceedings of the National Academy of Sciences*, vol. 27, no. 11, pp. 499–506, 1941.

[4] H. Kitano, "Biological robustness," *Nature Reviews Genetics*, vol. 5, no. 11, pp. 826–837, 2004.

[5] M. Delbrück, "Unités biologiques douées de continuité génétique colloques internationaux du centre national de la recherche scientifique," *Paris: CNRS*, 1949.

[6] M. Vidal, "A unifying view of 21st century systems biology," *FEBS letters*, vol. 583, no. 24, pp. 3891–3894, 2009.

[7] C. Y. Logan and R. Nusse, "The Wnt signaling pathway in development and disease," *Annual Review of Cell and Developmental Biology*, vol. 20, pp. 781–810, 2004.

[8] J. D. Orth, I. Thiele, and B. Ø. Palsson, "What is flux balance analysis?," *Nature Biotechnology*, vol. 28, no. 3, pp. 245–248, 2010.

[9] M. Watson, "Metabolic maps for the apple II," *Biochemical Society Transactions*, vol. 12, no. 6, pp. 1093–1094, 1984.

[10] J. R. Karr, J. C. Sanghvi, D. N. Macklin, M. V. Gutschow, J. M. Jacobs, B. Bolival, N. Assad-Garcia, J. I. Glass, and M. W. Covert, "A whole-cell computational model predicts phenotype from genotype," *Cell*, vol. 150, no. 2, pp. 389–401, 2012.

[11] N. J. Krogan, S. Lippman, D. A. Agard, A. Ashworth, and T. Ideker, "The cancer cell map initiative: Defining the hallmark networks of cancer," *Molecular Cell*, vol. 58, no. 4, pp. 690–698, 2015.

[12] G. Ciriello, E. Cerami, C. Sander, and N. Schultz, "Mutual exclusivity analysis identifies oncogenic network modules," *Genome Research*, vol. 22, no. 2, pp. 398–406, 2012.

[13] J. Wang, H. Khiabanian, D. Rossi, G. Fabbri, V. Gattei, F. Forconi, L. Laurenti, R. Marasca, G. Del Poeta, R. Foà, L. Pasqualucci, G. Gaidano, and R. Rabadan, "Tumor evolutionary directed graphs and the history of chronic lymphocytic leukemia," *eLife*, vol. 3, no. e02869, 2015.

[14] C. J. Ryan, P. Cimermančič, Z. A. Szpiech, A. Sali, R. D. Hernandez, and N. J. Krogan, "High-resolution network biology: connecting sequence with function," *Nature Reviews Genetics*, vol. 14, no. 12, pp. 865–879, 2013.

[15] Q. Zhong, N. Simonis, Q.-R. Li, B. Charloteaux, F. Heuze, N. Klitgord, S. Tam, H. Yu, K. Venkatesan, D. Mou, V. Swearingen, M. A. Yildirim, H. Yan, A. Dricot, D. Szeto, C. Lin, T. Hao, C. Fan, S. Milstein, D. Dupuy, R. Brasseur, D. E. Hill, M. E. Cusick, and M. Vidal, "Edgetic perturbation models of human inherited disorders," *Molecular Systems Biology*, vol. 5, no. 321, 2009.

[16] T. Pawson and R. Linding, "Network medicine," *FEBS letters*, vol. 582, no. 8, pp. 1266–1270, 2008.

[17] A.-L. Barabási, N. Gulbahce, and J. Loscalzo, "Network medicine: a network-based approach to human disease," *Nature Reviews Genetics*, vol. 12, no. 1, pp. 56–68, 2011.

[18] J. M. Irish, R. Hovland, P. O. Krutzik, O. D. Perez, Ø. Bruserud, B. T. Gjertsen, and G. P. Nolan, "Single cell profiling of potentiated phospho-protein networks in cancer cells," *Cell*, vol. 118, no. 2, pp. 217–228, 2004.

[19] K. Komurov, J.-T. Tseng, M. Muller, E. G. Seviour, T. J. Moss, L. Yang, D. Nagrath, and P. T. Ram, "The glucose-deprivation network counteracts lapatinib-induced toxicity in resistant ErbB2-positive breast cancer cells," *Molecular Systems Biology*, vol. 8, no. 596, 2012.

[20] M. J. Lee, S. Y. Albert, A. K. Gardino, A. M. Heijink, P. K. Sorger, G. MacBeath, and M. B. Yaffe, "Sequential application of anticancer drugs enhances cell death by rewiring apoptotic signaling networks," *Cell*, vol. 149, no. 4, pp. 780–794, 2012.

[21] R. Aebersold and M. Mann, "Mass spectrometry-based proteomics," *Nature*, vol. 422, no. 6928, pp. 198–207, 2003.

[22] S.-E. Ong and M. Mann, "Mass spectrometry-based proteomics turns quantitative," *Nature Chemical Biology*, vol. 1, no. 5, pp. 252–262, 2005.

[23] V. Lange, P. Picotti, B. Domon, and R. Aebersold, "Selected reaction monitoring for quantitative proteomics: a tutorial," *Molecular Systems Biology*, vol. 4, no. 222, 2008.

[24] A. Maiolica, M. A. Jünger, I. Ezkurdia, and R. Aebersold, "Targeted proteome investigation via selected reaction monitoring mass spectrometry," *Journal of Proteomics*, vol. 75, no. 12, pp. 3495–3513, 2012.

[25] P. Mallick and B. Kuster, "Proteomics: a pragmatic perspective," *Nature Biotechnology*, vol. 28, no. 7, pp. 695–709, 2010.

[26] M.-S. Kim, S. M. Pinto, D. Getnet, R. S. Nirujogi, S. S. Manda, R. Chaerkady, A. K. Madugundu, D. S. Kelkar, R. Isserlin, S. Jain, *et al.*, "A draft map of the human proteome," *Nature*, vol. 509, no. 7502, pp. 575–581, 2014.

[27] M. Uhlén, L. Fagerberg, B. M. Hallström, C. Lindskog, P. Oksvold, A. Mardinoglu, Å. Sivertsson, C. Kampf, E. Sjöstedt, A. Asplund, I. Olsson, K. Edlund, E. Lundberg, S. Navani, C. A. Szigyarto, J. Odeberg, D. Djureinovic, J. O. Takanen, S. Hober, T. Alm, P. H. Edqvist, H. Berling, H. Tegel, J. Mulder, J. Rockberg, P. Nilsson, J. M. Schwenk, M. Hamsten, K. von Feilitzen, M. Forsberg, L. Persson, F. Johansson, M. Zwahlen, G. von Heijne, J. Nielsen, and F. Pontén, "Tissue-based map of the human proteome," *Science*, vol. 347, no. 6220, p. 394, 2015.

[28] J. Li, Y. Lu, R. Akbani, Z. Ju, P. L. Roebuck, W. Liu, J.-Y. Yang, B. M. Broom, R. G. Verhaak, D. W. Kane, C. Wakefield, J. N. Weinstein, G. B. Mills, and H. Liang, "TCPA: a resource for cancer functional proteomics data," *Nature Methods*, vol. 10, no. 11, pp. 1046–1047, 2013.

[29] Z. Wang, M. Gerstein, and M. Snyder, "RNA-Seq: a revolutionary tool for transcriptomics," *Nature Reviews Genetics*, vol. 10, no. 1, pp. 57–63, 2009.

[30] T. Steijger, J. F. Abril, P. G. Engström, F. Kokocinski, T. J. Hubbard, R. Guigó, J. Harrow, P. Bertone, and RGASP Consortium, "Assessment of transcript reconstruction methods for RNA-Seq," *Nature Methods*, vol. 10, no. 12, pp. 1177–1184, 2013.

[31] N. L. Bray, H. Pimentel, P. Melsted, and L. Pachter, "Near-optimal probabilistic RNA-seq quantification," *Nature Biotechnology*, vol. 34, no. 5, pp. 525–527, 2016.

[32] R. Wang-Sattler, Z. Yu, C. Herder, A. C. Messias, A. Floegel, Y. He, K. Heim, M. Campillos, C. Holzapfel, B. Thorand, H. Grallert, T. Xu, E. Bader, C. Huth, K. Mittelstrass, A. Döring, C. Meisinger, C. Gieger, C. Prehn, W. Roemisch-Margl, M. Carstensen, L. Xie, H. Yamanaka-Okumura, G. Xing, U. Ceglarek, J. Thiery, G. Giani, H. Lickert, X. Lin, Y. Li, H. Boeing, H. G. Joost, M. H. de Angelis, W. Rathmann, K. Suhre, H. Prokisch, A. Peters, T. Meitinger, M. Roden, H. E. Wichmann, T. Pischon, J. Adamski, and T. Illig, "Novel biomarkers for pre-diabetes identified by metabolomics," *Molecular Systems Biology*, vol. 8, no. 615, 2012.

[33] D. S. Wishart, D. Tzur, C. Knox, R. Eisner, A. C. Guo, N. Young, D. Cheng, K. Jewell, D. Arndt, S. Sawhney, C. Fung, L. Nikolai, M. Lewis, M. A. Coutouly, I. Forsythe, P. Tang, S. Shrivastava, K. Jeroncic, P. Stothard, G. Amegbey, D. Block, D. D. Hau, J. Wagner, J. Miniaci, M. Clements, M. Gebremedhin, N. Guo, Y. Zhang, G. E. Duggan, G. D. Macinnis, A. M. Weljie, R. Dowlatabadi, F. Bamforth, D. Clive, R. Greiner, L. Li, T. Marrie, B. D. Sykes, H. J. Vogel, and L. Querengesser, "HMDB: the human metabolome database," *Nucleic Acids Research*, vol. 35, no. suppl 1, pp. D521–D526, 2007.

[34] I. Thiele, N. Swainston, R. M. Fleming, A. Hoppe, S. Sahoo, M. K. Aurich, H. Haraldsdottir, M. L. Mo, O. Rolfsson, M. D. Stobbe, S. G. Thorleifsson, R. Agren, C. Bölling, S. Bordel, A. K. Chavali, P. Dobson, W. B. Dunn, L. Endler, D. Hala, M. Hucka, D. Hull, D. Jameson, N. Jamshidi, J. J. Jonsson, N. Juty, S. Keating, I. Nookaew, N. Le Novère, N. Malys, A. Mazein, J. A. Papin, N. D. Price, E. Selkov, M. I. Sigurdsson, E. Simeonidis, N. Sonnenschein, K. Smallbone, A. Sorokin, J. H. van Beek, D. Weichart, I. Goryanin, J. Nielsen, H. V. Westerhoff, D. B. Kell, P. Mendes, and B. Ø. Palsson, "A community-driven global reconstruction of human metabolism," *Nature Biotechnology*, vol. 31, no. 5, pp. 419–425, 2013.

[35] R. Chen, G. I. Mias, J. Li-Pook-Than, L. Jiang, H. Y. Lam, E. Miriami, K. J. Karczewski, M. Hariharan, F. E. Dewey, Y. Cheng, M. J. Clark, H. Im, L. Habegger, S. Balasubramanian, M. O'Huallachain, J. T. Dudley, S. Hillenmeyer, R. Haraksingh, D. Sharon, G. Euskirchen, P. Lacroute, K. Bettinger, A. P. Boyle, M. Kasowski, F. Grubert, S. Seki, M. Garcia, M. Whirl-Carrillo, M. Gallardo, M. A. Blasco, P. L. Greenberg, P. Snyder, T. E. Klein, R. B. Altman, A. J. Butte, E. A. Ashley, M. Gerstein, K. C. Nadeau, H. Tang, and M. Snyder, "Personal omics profiling reveals dynamic molecular and medical phenotypes," *Cell*, vol. 148, no. 6, pp. 1293–1307, 2012.

[36] S. Fields and O.-k. Song, "A novel genetic system to detect protein protein interactions," *Nature*, vol. 340, no. 6230, pp. 245–246, 1989.

[37] P. Uetz, L. Giot, G. Cagney, T. A. Mansfield, R. S. Judson, J. R. Knight, D. Lockshon, V. Narayan, M. Srinivasan, P. Pochart, A. Qureshi-Emili, Y. Li, B. Godwin, D. Conover, T. Kalbfleisch, G. Vijayadamodar, M. Yang, M. Johnston, S. Fields, and J. M. Rothberg, "A comprehensive analysis of protein–protein interactions in Saccharomyces cerevisiae," *Nature*, vol. 403, no. 6770, pp. 623–627, 2000.

[38] A. J. Walhout, R. Sordella, X. Lu, J. L. Hartley, G. F. Temple, M. A. Brasch, N. Thierry-Mieg, and M. Vidal, "Protein interaction mapping in C. elegans using proteins involved in vulval development," *Science*, vol. 287, no. 5450, pp. 116–122, 2000.

[39] L. Giot, J. S. Bader, C. Brouwer, A. Chaudhuri, B. Kuang, Y. Li, Y. Hao, C. E. Ooi, B. Godwin, E. Vitols, G. Vijayadamodar, P. Pochart, H. Machineni, M. Welsh, Y. Kong, B. Zerhusen, R. Malcolm, Z. Varrone, A. Collis, M. Minto, S. Burgess, L. McDaniel, E. Stimpson, F. Spriggs, J. Williams, K. Neurath, N. Ioime, M. Agee, E. Voss, K. Furtak, R. Renzulli, N. Aanensen, S. Carrolla, E. Bickelhaupt, Y. Lazovatsky, A. DaSilva, J. Zhong, C. A. Stanyon, R. L. Finley, K. P. White, M. Braverman, T. Jarvie, S. Gold, M. Leach, J. Knight, R. A. Shimkets, M. P. McKenna, J. Chant, and J. M. Rothberg, "A protein interaction map of Drosophila melanogaster," *Science*, vol. 302, no. 5651, pp. 1727–1736, 2003.

[40] J.-F. Rual, K. Venkatesan, T. Hao, T. Hirozane-Kishikawa, A. Dricot, N. Li, G. F. Berriz, F. D. Gibbons, M. Dreze, N. Ayivi-Guedehoussou, N. Klitgord, C. Simon, M. Boxem, S. Milstein, J. Rosenberg, D. S. Goldberg, L. V. Zhang, S. L. Wong, G. Franklin, S. Li, J. S. Albala, J. Lim, C. Fraughton, E. Llamosas, S. Cevik, C. Bex, P. Lamesch, R. S. Sikorski, J. Vandenhaute, H. Y. Zoghbi, A. Smolyar, S. Bosak, R. Sequerra, L. Doucette-Stamm, M. E. Cusick, D. E. Hill, F. P. Roth, and M. Vidal, "Towards a proteome-scale map of the human protein–protein interaction network," *Nature*, vol. 437, no. 7062, pp. 1173–1178, 2005.

[41] H. Yu, P. Braun, M. A. Yıldırım, I. Lemmens, K. Venkatesan, J. Sahalie, T. Hirozane-Kishikawa, F. Gebreab, N. Li, N. Simonis, T. Hao, J. F. Rual, A. Dricot, A. Vazquez, R. R. Murray, C. Simon, L. Tardivo, S. Tam, N. Svrzikapa, C. Fan, A. S. de Smet, A. Motyl, M. E. Hudson, J. Park, X. Xin, M. E. Cusick, T. Moore, C. Boone, M. Snyder, F. P. Roth, A.-L. Barabási, J. Tavernier, D. E. Hill, and M. Vidal, "High-quality binary protein interaction map of the yeast interactome network," *Science*, vol. 322, no. 5898, pp. 104–110, 2008.

[42] S. V. Rajagopala, P. Sikorski, A. Kumar, R. Mosca, J. Vlasblom, R. Arnold, J. Franca-Koh, S. B. Pakala, S. Phanse, A. Ceol, R. Häuser, G. Siszler, S. Wuchty, A. Emili, M. Babu, P. Aloy, R. Pieper, and P. Uetz, "The binary protein-protein interaction landscape of Escherichia coli," *Nature Biotechnology*, vol. 32, no. 3, pp. 285–290, 2014.

[43] T. Rolland, M. Taşan, B. Charloteaux, S. J. Pevzner, Q. Zhong, N. Sahni, S. Yi, I. Lemmens, C. Fontanillo, R. Mosca, A. Kamburov, S. D. Ghiassian, X. Yang, L. Ghamsari, D. Balcha, B. E. Begg, P. Braun, M. Brehme, M. P. Broly, A. R. Carvunis, D. Convery-Zupan, R. Corominas, J. Coulombe-Huntington, E. Dann, M. Dreze, A. Dricot, C. Fan, E. Franzosa, F. Gebreab, B. J. Gutierrez, M. F. Hardy, M. Jin, S. Kang, R. Kiros, G. N. Lin, K. Luck, A. MacWilliams, J. Menche, R. R. Murray, A. Palagi, M. M. Poulin, X. Rambout, J. Rasla, P. Reichert, V. Romero, E. Ruyssinck, J. M. Sahalie, A. Scholz, A. A. Shah, A. Sharma, Y. Shen, K. Spirohn, S. Tam, A. O. Tejeda, S. A. Trigg, J. C. Twizere, K. Vega, J. Walsh, M. E. Cusick, Y. Xia, A.-L. Barabási, L. M. Iakoucheva, P. Aloy, J. De Las Rivas, J. Tavernier, M. A. Calderwood, D. E. Hill, T. Hao, F. P. Roth, and M. Vidal, "A proteome-scale map of the human interactome network," *Cell*, vol. 159, no. 5, pp. 1212–1226, 2014.

[44] T. V. Vo, J. Das, M. J. Meyer, N. A. Cordero, N. Akturk, X. Wei, B. J. Fair, A. G. Degatano, R. Fragoza, L. G. Liu, A. Matsuyama, M. Trickey, S. Horibata, A. Grimson, H. Yamano, M. Yoshida, F. P. Roth, J. A. Pleiss, Y. Xia, and H. Yu, "A proteome-wide fission yeast interactome reveals network evolution principles from yeasts to human," *Cell*, vol. 164, no. 1-2, pp. 310–323, 2016.

[45] M. Vidal and S. Fields, "The yeast two-hybrid assay: still finding connections after 25 years," *Nature Methods*, vol. 11, no. 12, pp. 1203–1206, 2014.

[46] A.-C. Gingras, M. Gstaiger, B. Raught, and R. Aebersold, "Analysis of protein complexes using mass spectrometry," *Nature Reviews Molecular Cell Biology*, vol. 8, no. 8, pp. 645–654, 2007.

[47] G. Rigaut, A. Shevchenko, B. Rutz, M. Wilm, M. Mann, and B. Séraphin, "A generic protein purification method for protein complex characterization and proteome exploration," *Nature Biotechnology*, vol. 17, no. 10, pp. 1030–1032, 1999.

[48] A.-C. Gavin, P. Aloy, P. Grandi, R. Krause, M. Boesche, M. Marzioch, C. Rau, L. J. Jensen, S. Bastuck, B. Dümpelfeld, A. Edelmann, M. A. Heurtier, V. Hoffman, C. Hoefert, K. Klein, M. Hudak, A. M. Michon, M. Schelder, M. Schirle, M. Remor, T. Rudi, S. Hooper, A. Bauer, T. Bouwmeester, G. Casari, G. Drewes, G. Neubauer, J. M. Rick, B. Kuster, P. Bork, R. B. Russell, and G. Superti-Furga, "Proteome survey reveals modularity of the yeast cell machinery," *Nature*, vol. 440, no. 7084, pp. 631–636, 2006.

[49] N. J. Krogan, G. Cagney, H. Yu, G. Zhong, X. Guo, A. Ignatchenko, J. Li, S. Pu, N. Datta, A. P. Tikuisis, T. Punna, J. M. Peregrín-Alvarez, M. Shales, X. Zhang, M. Davey, M. D. Robinson, A. Paccanaro, J. E. Bray, A. Sheung, B. Beattie, D. P. Richards, V. Canadien, A. Lalev, F. Mena, P. Wong, A. Starostine, M. M. Canete, J. Vlasblom, S. Wu, C. Orsi, S. R. Collins, S. Chandran, R. Haw, J. J. Rilstone, K. Gandi, N. J. Thompson, G. Musso, P. St Onge, S. Ghanny, M. H. Lam, G. Butland, A. M. Altaf-Ul, S. Kanaya, A. Shilatifard, E. O'Shea, J. S. Weissman, C. J. Ingles, T. R. Hughes, J. Parkinson, M. Gerstein, S. J. Wodak, A. Emili, and J. F. Greenblatt, "Global landscape of protein complexes in the yeast Saccharomyces cerevisiae," *Nature*, vol. 440, no. 7084, pp. 637–643, 2006.

[50] J. R. Hutchins, Y. Toyoda, B. Hegemann, I. Poser, J.-K. Hériché, M. M. Sykora, M. Augsburg, O. Hudecz, B. A. Buschhorn, J. Bulkescher, C. Conrad, D. Comartin, A. Schleiffer, M. Sarov, A. Pozniakovsky, M. M. Slabicki, S. Schloissnig, I. Steinmacher, M. Leuschner, A. Ssykor, S. Lawo, L. Pelletier, H. Stark, K. Nasmyth, J. Ellenberg, R. Durbin, F. Buchholz, K. Mechtler, A. A. Hyman, and J. M. Peters, "Systematic analysis of human protein complexes identifies chromosome segregation proteins," *Science*, vol. 328, no. 5978, pp. 593–599, 2010.

[51] P. C. Havugimana, G. T. Hart, T. Nepusz, H. Yang, A. L. Turinsky, Z. Li, P. I. Wang, D. R. Boutz, V. Fong, S. Phanse, M. Babu, S. A. Craig, P. Hu, C. Wan, J. Vlasblom, V. U. Dar, A. Bezginov, G. W. Clark, G. C. Wu, S. J. Wodak, E. R. Tillier, A. Paccanaro, E. M. Marcotte, and A. Emili, "A census of human soluble protein complexes," *Cell*, vol. 150, no. 5, pp. 1068–1081, 2012.

[52] O. Rozenblatt-Rosen, R. C. Deo, M. Padi, G. Adelmant, M. A. Calderwood, T. Rolland, M. Grace, A. Dricot, M. Askenazi, M. Tavares, S. J. Pevzner, F. Abderazzaq, D. Byrdsong, A. R. Carvunis, A. A. Chen, J. Cheng, M. Correll, M. Duarte, C. Fan, M. C. Feltkamp, S. B. Ficarro, R. Franchi, B. K. Garg, N. Gulbahce, T. Hao, A. M. Holthaus, R. James, A. Korkhin, L. Litovchick, J. C. Mar, T. R. Pak, S. Rabello, R. Rubio, Y. Shen, S. Singh, J. M. Spangle, M. Tasan, S. Wanamaker, J. T. Webber, J. Roecklein-Canfield, E. Johannsen, A.-L. Barabási, R. Beroukhim, E. Kieff, M. E. Cusick, D. E. Hill, K. Münger, J. A. Marto, J. Quackenbush, F. P. Roth, J. A. DeCaprio, and M. Vidal, "Interpreting cancer genomes using systematic host network perturbations by tumour virus proteins," *Nature*, vol. 487, no. 7408, pp. 491–495, 2012.

[53] A. Breitkreutz, H. Choi, J. R. Sharom, L. Boucher, V. Neduva, B. Larsen, Z.-Y. Lin, B.-J. Breitkreutz, C. Stark, G. Liu, J. Ahn, D. Dewar-Darch, T. Reguly, X. Tang, R. Almeida, Z. S. Qin, T. Pawson, A.-C. Gingras, A. I. Nesvizhskii, and M. Tyers, "A global protein kinase and phosphatase interaction network in yeast," *Science*, vol. 328, no. 5981, pp. 1043–1046, 2010.

[54] A.-E. Saliba, I. Vonkova, S. Ceschia, G. M. Findlay, K. Maeda, C. Tischer, S. Deghou, V. van Noort, P. Bork, T. Pawson, J. Ellenberg, and A.-C. Gavin, "A quantitative liposome microarray to systematically characterize protein-lipid interactions," *Nature Methods*, vol. 11, no. 1, pp. 47–50, 2014.

[55] L. Gu, C. Li, J. Aach, D. E. Hill, M. Vidal, and G. M. Church, "Multiplex single-molecule interaction profiling of DNA-barcoded proteins," *Nature*, vol. 515, no. 7528, pp. 554–557, 2014.

[56] D. S. Johnson, A. Mortazavi, R. M. Myers, and B. Wold, "Genome-wide mapping of *in vivo* protein-DNA interactions," *Science*, vol. 316, no. 5830, pp. 1497–1502, 2007.

[57] Q. C. Zhang, D. Petrey, L. Deng, L. Qiang, Y. Shi, C. A. Thu, B. Bisikirska, C. Lefebvre, D. Accili, T. Hunter, T. Maniatis, A. Califano, and B. Honig, "Structure-based prediction of protein-protein interactions on a genome-wide scale," *Nature*, vol. 490, no. 7421, pp. 556–560, 2012.

[58] D. La and D. Kihara, "A novel method for protein–protein interaction site prediction using phylogenetic substitution models," *Proteins: Structure, Function, and Bioinformatics*, vol. 80, no. 1, pp. 126–141, 2012.

[59] M. Bansal, V. Belcastro, A. Ambesi-Impiombato, and D. Di Bernardo, "How to infer gene networks from expression profiles," *Molecular Systems Biology*, vol. 3, no. 78, 2007.

[60] M. B. Eisen, P. T. Spellman, P. O. Brown, and D. Botstein, "Cluster analysis and display of genome-wide expression patterns," *Proceedings of the National Academy of Sciences*, vol. 95, no. 25, pp. 14863–14868, 1998.

[61] B. Zhang and S. Horvath, "A general framework for weighted gene co-expression network analysis," *Statistical Applications in Genetics and Molecular Biology*, vol. 4(1), no. 17, 2005.

[62] N. Friedman, M. Linial, I. Nachman, and D. Pe'er, "Using bayesian networks to analyze expression data," *Journal of Computational Biology*, vol. 7, no. 3-4, pp. 601–620, 2000.

[63] A. J. Butte and I. S. Kohane, "Mutual information relevance networks: functional genomic clustering using pairwise entropy measurements," in *Pacific Symposium on Biocomputing*, vol. 5, pp. 418–429, 2000.

[64] P. D'haeseleer, X. Wen, S. Fuhrman, and R. Somogyi, "Linear modeling of mRNA expression levels during CNS development and injury.," in *Pacific Symposium on Biocomputing*, vol. 4, pp. 41–52, 1999.

[65] D. Marbach, J. C. Costello, R. Küffner, N. M. Vega, R. J. Prill, D. M. Camacho, K. R. Allison, M. Kellis, J. J. Collins, G. Stolovitzky, and DREAM5 Consortium, "Wisdom of crowds for robust gene network inference," *Nature Methods*, vol. 9, no. 8, pp. 796–804, 2012.

[66] C. Boone, H. Bussey, and B. J. Andrews, "Exploring genetic interactions and networks with yeast," *Nature Reviews Genetics*, vol. 8, no. 6, pp. 437–449, 2007.

[67] A. H. Tong, M. Evangelista, A. B. Parsons, H. Xu, G. D. Bader, N. Pagé, M. Robinson, S. Raghibizadeh, C. W. Hogue, H. Bussey, B. Andrews, M. Tyers, and C. Boone, "Systematic genetic analysis with ordered arrays of yeast deletion mutants," *Science*, vol. 294, no. 5550, pp. 2364–2368, 2001.

[68] A. H. Tong, G. Lesage, G. D. Bader, H. Ding, H. Xu, X. Xin, J. Young, G. F. Berriz, R. L. Brost, M. Chang, Y. Chen, X. Cheng, G. Chua, H. Friesen, D. S. Goldberg, J. Haynes, C. Humphries, G. He, S. Hussein, L. Ke, N. Krogan, Z. Li, J. N. Levinson, H. Lu, P. Ménard, C. Munyana, A. B. Parsons, O. Ryan, R. Tonikian, T. Roberts, A. M. Sdicu, J. Shapiro, B. Sheikh, B. Suter, S. L. Wong, L. V. Zhang, H. Zhu, C. G. Burd, S. Munro, C. Sander, J. Rine, J. Greenblatt, M. Peter, A. Bretscher, G. Bell, F. P. Roth, G. W. Brown, B. Andrews, H. Bussey, and C. Boone, "Global mapping of the yeast genetic interaction network," *Science*, vol. 303, no. 5659, pp. 808–813, 2004.

[69] M. Costanzo, A. Baryshnikova, J. Bellay, Y. Kim, E. D. Spear, C. S. Sevier, H. Ding, J. L. Koh, K. Toufighi, S. Mostafavi, J. Prinz, R. P. St Onge, B. VanderSluis, T. Makhnevych, F. J. Vizeacoumar, S. Alizadeh, S. Bahr, R. L. Brost, Y. Chen, M. Cokol, R. Deshpande, Z. Li, Z. Y. Lin, W. Liang, M. Marback, J. Paw, B. J. San Luis, E. Shuteriqi, A. H. Tong, N. van Dyk, I. M. Wallace, J. A. Whitney, M. T. Weirauch, G. Zhong, H. Zhu, W. A. Houry, M. Brudno, S. Ragibizadeh, B. Papp, C. Pál, F. P. Roth, G. Giaever, C. Nislow, O. G. Troyanskaya, H. Bussey, G. D. Bader, A.-C. Gingras, Q. D. Morris, P. M. Kim, C. A. Kaiser, C. L. Myers, B. J. Andrews, and C. Boone, "The genetic landscape of a cell," *Science*, vol. 327, no. 5964, pp. 425–431, 2010.

[70] S. Bandyopadhyay, M. Mehta, D. Kuo, M. K. Sung, R. Chuang, E. J. Jaehnig, B. Bodenmiller, K. Licon, W. Copeland, M. Shales, D. Fiedler, J. Dutkowski, A. Guénolé, H. van Attikum, K. M. Shokat, R. D. Kolodner, W. K. Huh, R. Aebersold, M. C. Keogh, N. J. Krogan, and T. Ideker, "Rewiring of genetic networks in response to DNA damage," *Science*, vol. 330, no. 6009, pp. 1385–1389, 2010.

[71] A. Roguev, D. Talbot, G. L. Negri, M. Shales, G. Cagney, S. Bandyopadhyay, B. Panning, and N. J. Krogan, "Quantitative genetic-interaction mapping in mammalian cells," *Nature Methods*, vol. 10, no. 5, pp. 432–437, 2013.

[72] P. Erdős and A. Rényi, "On random graphs," *Publicationes Mathematicae Debrecen*, vol. 6, pp. 290–297, 1959.

[73] A.-L. Barabási and R. Albert, "Emergence of scaling in random networks," *Science*, vol. 286, no. 5439, pp. 509–512, 1999.

[74] M. P. Stumpf, C. Wiuf, and R. M. May, "Subnets of scale-free networks are not scale-free: sampling properties of networks," *Proceedings of the National Academy of Sciences*, vol. 102, no. 12, pp. 4221–4224, 2005.

[75] R. Khanin and E. Wit, "How scale-free are biological networks," *Journal of Computational Biology*, vol. 13, no. 3, pp. 810–818, 2006.

[76] H. Jeong, S. P. Mason, A.-L. Barabási, and Z. N. Oltvai, "Lethality and centrality in protein networks," *Nature*, vol. 411, no. 6833, pp. 41–42, 2001.

[77] J.-D. J. Han, N. Bertin, T. Hao, D. S. Goldberg, G. F. Berriz, L. V. Zhang, D. Dupuy, A. J. Walhout, M. E. Cusick, F. P. Roth, and M. Vidal, "Evidence for dynamically organized modularity in the yeast protein-protein interaction network," *Nature*, vol. 430, no. 6995, pp. 88–93, 2004.

[78] I. W. Taylor, R. Linding, D. Warde-Farley, Y. Liu, C. Pesquita, D. Faria, S. Bull, T. Pawson, Q. Morris, and J. L. Wrana, "Dynamic modularity in protein interaction networks predicts breast cancer outcome," *Nature Biotechnology*, vol. 27, no. 2, pp. 199–204, 2009.

[79] E. W. Dijkstra, "A note on two problems in connexion with graphs," *Numerische mathematik*, vol. 1, no. 1, pp. 269–271, 1959.

[80] R. Bellman, "On the theory of dynamic programming," *Proceedings of the National Academy of Sciences*, vol. 38, no. 8, pp. 716–719, 1952.

[81] S. Milgram, "The small world problem," *Psychology Today*, vol. 1, no. 1, pp. 60–67, 1967.

[82] J. Guare, *Six degrees of separation: A play*. Vintage Books, New York, 1990.

[83] D. J. Watts and S. H. Strogatz, "Collective dynamics of "small-world" networks," *Nature*, vol. 393, no. 6684, pp. 440–442, 1998.

[84] Q. K. Telesford, K. E. Joyce, S. Hayasaka, J. H. Burdette, and P. J. Laurienti, "The ubiquity of small-world networks," *Brain Connectivity*, vol. 1, no. 5, pp. 367–375, 2011.

[85] L. C. Freeman, "A set of measures of centrality based on betweenness," *Sociometry*, pp. 35–41, 1977.

[86] H. Yu, P. M. Kim, E. Sprecher, V. Trifonov, and M. Gerstein, "The importance of bottlenecks in protein networks: correlation with gene essentiality and expression dynamics," *PLoS Computational Biology*, vol. 3, no. 4, p. e59, 2007.

[87] R. D. Luce and A. D. Perry, "A method of matrix analysis of group structure," *Psychometrika*, vol. 14, no. 2, pp. 95–116, 1949.

[88] L. H. Hartwell, J. J. Hopfield, S. Leibler, and A. W. Murray, "From molecular to modular cell biology," *Nature*, vol. 402, pp. C47–C52, 1999.

[89] E. Ravasz, A. L. Somera, D. A. Mongru, Z. N. Oltvai, and A.-L. Barabási, "Hierarchical organization of modularity in metabolic networks," *Science*, vol. 297, no. 5586, pp. 1551–1555, 2002.

[90] M. Girvan and M. E. Newman, "Community structure in social and biological networks," *Proceedings of the National Academy of Sciences*, vol. 99, no. 12, pp. 7821–7826, 2002.

[91] M. E. Newman and M. Girvan, "Finding and evaluating community structure in networks," *Physical Review E*, vol. 69, no. 2, p. 026113, 2004.

[92] M. E. Newman, "Modularity and community structure in networks," *Proceedings of the National Academy of Sciences*, vol. 103, no. 23, pp. 8577–8582, 2006.

[93] S. Fortunato, "Community detection in graphs," *Physics Reports*, vol. 486, no. 3, pp. 75–174, 2010.

[94] T. Ideker and N. J. Krogan, "Differential network biology," *Molecular Systems Biology*, vol. 8, no. 565, 2012.

[95] M. Dreze, B. Charloteaux, S. Milstein, P.-O. Vidalain, M. A. Yildirim, Q. Zhong, N. Svrzikapa, V. Romero, G. Laloux, R. Brasseur, J. Vandenhaute, M. Boxem, M. E. Cusick, D. E. Hill, and M. Vidal, ""Edgetic" perturbation of a *C. elegans* BCL2 ortholog," *Nature Methods*, vol. 6, no. 11, pp. 843–849, 2009.

[96] X. Wang, X. Wei, B. Thijssen, J. Das, S. M. Lipkin, and H. Yu, "Three-dimensional reconstruction of protein networks provides insight into human genetic disease," *Nature Biotechnology*, vol. 30, no. 2, pp. 159–164, 2012.

[97] N. Sahni, S. Yi, M. Taipale, J. I. F. Bass, J. Coulombe-Huntington, F. Yang, J. Peng, J. Weile, G. I. Karras, Y. Wang, I. A. Kovács, A. Kamburov, I. Krykbaeva, M. H. Lam, G. Tucker, V. Khurana, A. Sharma, Y. Y. Liu, N. Yachie, Q. Zhong, Y. Shen, A. Palagi, A. San-Miguel, C. Fan, D. Balcha, A. Dricot, D. M. Jordan, J. M. Walsh, A. A. Shah, X. Yang, A. K. Stoyanova, A. Leighton, M. A. Calderwood, Y. Jacob, M. E. Cusick, K. Salehi-Ashtiani, L. J. Whitesell, S. Sunyaev, B. Berger, A.-L. Barabási, B. Charloteaux, D. E. Hill, T. Hao, F. P. Roth, Y. Xia, A. J. Walhout, S. Lindquist, and M. Vidal, "Widespread macromolecular interaction perturbations in human genetic disorders," *Cell*, vol. 161, no. 3, pp. 647–660, 2015.

[98] X. Yang, J. Coulombe-Huntington, S. Kang, G. M. Sheynkman, T. Hao, A. Richardson, S. Sun, F. Yang, Y. A. Shen, R. R. Murray, K. Spirohn, B. E. Begg, M. Duran-Frigola, A. MacWilliams, S. J. Pevzner, Q. Zhong, S. A. Trigg, S. Tam, L. Ghamsari, N. Sahni, S. Yi, M. D. Rodriguez, D. Balcha, G. Tan, M. Costanzo, B. Andrews, C. Boone, X. J. Zhou, K. Salehi-Ashtiani, B. Charloteaux, A. A. Chen, M. A. Calderwood, P. Aloy, F. P. Roth, D. E. Hill, L. M. Iakoucheva, Y. Xia, and M. Vidal, "Widespread expansion of protein interaction capabilities by alternative splicing," *Cell*, vol. 164, no. 4, pp. 805–817, 2016.

[99] N. Sahni, S. Yi, Q. Zhong, N. Jailkhani, B. Charloteaux, M. E. Cusick, and M. Vidal, "Edgotype: a fundamental link between genotype and phenotype," *Current Opinion in Genetics and Development*, vol. 23, no. 6, pp. 649–657, 2013.

[100] P. Creixell, A. Palmeri, C. J. Miller, H. J. Lou, C. C. Santini, M. Nielsen, B. E. Turk, and R. Linding, "Unmasking determinants of specificity in the human kinome," *Cell*, vol. 163, no. 1, pp. 187–201, 2015.

[101] P. Creixell, E. M. Schoof, C. D. Simpson, J. Longden, C. J. Miller, H. J. Lou, L. Perryman, T. R. Cox, N. Zivanovic, A. Palmeri, A. Wesolowska-Andersen, M. Helmer-Citterich, J. Ferkinghoff-Borg, H. Itamochi, B. Bodenmiller, J. T. Erler, B. E. Turk, and R. Linding, "Kinome-wide decoding of network-attacking mutations rewiring cancer signaling," *Cell*, vol. 163, no. 1, pp. 202–217, 2015.

[102] M. AlQuraishi, G. Koytiger, A. Jenney, G. MacBeath, and P. K. Sorger, "A multiscale statistical mechanical framework integrates biophysical and genomic data to assemble cancer networks," *Nature Genetics*, vol. 46, no. 12, pp. 1363–1371, 2014.

[103] N. Bisson, D. A. James, G. Ivosev, S. A. Tate, R. Bonner, L. Taylor, and T. Pawson, "Selected reaction monitoring mass spectrometry reveals the dynamics of signaling through the grb2 adaptor," *Nature Biotechnology*, vol. 29, no. 7, pp. 653–658, 2011.

[104] B. C. Collins, L. C. Gillet, G. Rosenberger, H. L. Röst, A. Vichalkovski, M. Gstaiger, and R. Aebersold, "Quantifying protein interaction dynamics by swath mass spectrometry: application to the 14-3-3 system," *Nature Methods*, vol. 10, no. 12, pp. 1246–1253, 2013.

[105] J.-P. Lambert, G. Ivosev, A. L. Couzens, B. Larsen, M. Taipale, Z.-Y. Lin, Q. Zhong, S. Lindquist, M. Vidal, R. Aebersold, T. Pawson, R. Bonner, S. Tate, and A.-C. Gingras, "Mapping differential interactomes by affinity purification coupled with data-independent mass spectrometry acquisition," *Nature Methods*, vol. 10, no. 12, pp. 1239–1245, 2013.

[106] S. Krishnaswamy, M. H. Spitzer, M. Mingueneau, S. C. Bendall, O. Litvin, E. Stone, D. Pe'er, and G. P. Nolan, "Conditional density-based analysis of T cell signaling in single-cell data," *Science*, vol. 346, no. 6213, p. 1250689, 2014.

[107] L. Peŋa-Castillo, M. Taşan, C. L. Myers, H. Lee, T. Joshi, C. Zhang, Y. Guan, M. Leone, A. Pagnani, W. K. Kim, C. Krumpelman, W. Tian, G. Obozinski, Y. Qi, S. Mostafavi, G. N. Lin, G. F. Berriz, F. D. Gibbons, G. Lanckriet, J. Qiu, C. Grant, Z. Barutcuoglu, D. P. Hill, D. Warde-Farley, C. Grouios, D. Ray, J. A. Blake, M. Deng, M. I. Jordan, W. S. Noble, Q. Morris, J. Klein-Seetharaman, Z. Bar-Joseph, T. Chen, F. Sun, O. G. Troyanskaya, E. M. Marcotte, D. Xu, T. R. Hughes, and F. P. Roth, "A critical assessment of Mus musculus gene function prediction using integrated genomic evidence," *Genome Biology*, vol. 9, no. S2, 2008.

[108] P. Radivojac, W. T. Clark, T. R. Oron, A. M. Schnoes, T. Wittkop, A. Sokolov, K. Graim, C. Funk, K. Verspoor, A. Ben-Hur, G. Pandey, J. M. Yunes, A. S. Talwalkar, S. Repo, M. L. Souza, D. Piovesan, R. Casadio, Z. Wang, J. Cheng, H. Fang, J. Gough, P. Koskinen, P. Törönen, J. Nokso-Koivisto, L. Holm, D. Cozzetto, D. W. Buchan, K. Bryson, D. T. Jones, B. Limaye, H. Inamdar, A. Datta, S. K. Manjari, R. Joshi, M. Chitale, D. Kihara, A. M. Lisewski, S. Erdin, E. Venner, O. Lichtarge, R. Rentzsch, H. Yang, A. E. Romero, P. Bhat, A. Paccanaro, T. Hamp, R. Kaßner, S. Seemayer, E. Vicedo, C. Schaefer, D. Achten, F. Auer, A. Boehm, T. Braun, M. Hecht, M. Heron, P. Hönigschmid, T. A. Hopf, S. Kaufmann, M. Kiening, D. Krompass, C. Landerer, Y. Mahlich, M. Roos, J. Björne, T. Salakoski, A. Wong, H. Shatkay, F. Gatzmann, I. Sommer, M. N. Wass, M. J. Sternberg, N. Škunca, F. Supek, M. Bošnjak, P. Panov, S. Džeroski, T. Šmuc, Y. A. Kourmpetis, A. D. van Dijk, C. J. ter Braak, Y. Zhou, Q. Gong, X. Dong, W. Tian, M. Falda, P. Fontana, E. Lavezzo, B. Di Camillo, S. Toppo, L. Lan, N. Djuric, Y. Guo, S. Vucetic, A. Bairoch, M. Linial, P. C. Babbitt, S. E. Brenner, C. Orengo, B. Rost, S. D. Mooney, and F. I., "A large-scale evaluation of computational protein function prediction," *Nature Methods*, vol. 10, no. 3, pp. 221–227, 2013.

[109] S. Mostafavi, D. Ray, D. Warde-Farley, C. Grouios, and Q. Morris, "GeneMANIA: a real-time multiple association network integration algorithm for predicting gene function," *Genome Biology*, vol. 9, no. S4, 2008.

[110] R. Sharan, I. Ulitsky, and R. Shamir, "Network-based prediction of protein function," *Molecular Systems Biology*, vol. 3, no. 88, 2007.

[111] B. Schwikowski, P. Uetz, and S. Fields, "A network of protein–protein interactions in yeast," *Nature Biotechnology*, vol. 18, no. 12, pp. 1257–1261, 2000.

[112] A. J. Enright, S. Van Dongen, and C. A. Ouzounis, "An efficient algorithm for large-scale detection of protein families," *Nucleic Acids Research*, vol. 30, no. 7, pp. 1575–1584, 2002.

[113] G. D. Bader and C. W. Hogue, "An automated method for finding molecular complexes in large protein interaction networks," *BMC Bioinformatics*, vol. 4, no. 2, 2003.

[114] E. Nabieva, K. Jim, A. Agarwal, B. Chazelle, and M. Singh, "Whole-proteome prediction of protein function via graph-theoretic analysis of interaction maps," *Bioinformatics*, vol. 21, no. suppl 1, pp. i302–i310, 2005.

[115] L. Page, S. Brin, R. Motwani, and T. Winograd, "The PageRank citation ranking: bringing order to the web.," *Technical Report, Stanford University, Stanford, CA*, no. 1999-66, 1999.

[116] V. Freschi, "Protein function prediction from interaction networks using a random walk ranking algorithm," in *Proceedings of the 7th IEEE International Conference on Bioinformatics and Bioengineering*, pp. 42–48, IEEE, 2007.

[117] D. Zhou, O. Bousquet, T. N. Lal, J. Weston, and B. Schölkopf, "Learning with local and global consistency," *Advances in Neural Information Processing Systems*, vol. 16, no. 16, pp. 321–328, 2004.

[118] G. Yu, H. Rangwala, C. Domeniconi, G. Zhang, and Z. Yu, "Protein function prediction using multi-label ensemble classification," *IEEE/ACM Transactions on Computational Biology and Bioinformatics*, vol. 10, no. 4, pp. 1–1, 2013.

[119] H. Wang, H. Huang, and C. Ding, "Image annotation using bi-relational graph of images and semantic labels," in *IEEE Conference on Computer Vision and Pattern Recognition*, pp. 793–800, IEEE, 2011.

[120] Gene Ontology Consortium, "The Gene Ontology (GO) database and informatics resource," *Nucleic Acids Research*, vol. 32, no. suppl 1, pp. D258–D261, 2004.

[121] O. D. King, R. E. Foulger, S. S. Dwight, J. V. White, and F. P. Roth, "Predicting gene function from patterns of annotation," *Genome Research*, vol. 13, no. 5, pp. 896–904, 2003.

[122] Z. Barutcuoglu, R. E. Schapire, and O. G. Troyanskaya, "Hierarchical multi-label prediction of gene function," *Bioinformatics*, vol. 22, no. 7, pp. 830–836, 2006.

[123] G. Valentini, "True path rule hierarchical ensembles for genome-wide gene function prediction," *IEEE/ACM Transactions on Computational Biology and Bioinformatics*, vol. 8, no. 3, pp. 832–847, 2011.

[124] G. Valentini, "Hierarchical ensemble methods for protein function prediction," *International Scholarly Research Notices Bioinformatics*, vol. 2014, no. 901419, 2014.

[125] Y. Tao, L. Sam, J. Li, C. Friedman, and Y. A. Lussier, "Information theory applied to the sparse gene ontology annotation network to predict novel gene function," *Bioinformatics*, vol. 23, no. 13, pp. i529–i538, 2007.

[126] G. Pandey, C. L. Myers, and V. Kumar, "Incorporating functional inter-relationships into protein function prediction algorithms," *BMC Bioinformatics*, vol. 10, no. 142, 2009.

[127] D. Lin, "An information-theoretic definition of similarity," in *International Conference on Machine Learning*, vol. 98, pp. 296–304, 1998.

[128] A. Sokolov and A. Ben-Hur, "Hierarchical classification of gene ontology terms using the gostruct method," *Journal of Bioinformatics and Computational Biology*, vol. 8, no. 02, pp. 357–376, 2010.

[129] I. Tsochantaridis, T. Joachims, T. Hofmann, and Y. Altun, "Large margin methods for structured and interdependent output variables," in *Journal of Machine Learning Research*, pp. 1453–1484, 2005.

[130] G. Yu, H. Zhu, C. Domeniconi, and J. Liu, "Predicting protein function via downward random walks on a gene ontology," *BMC Bioinformatics*, vol. 16, no. 271, 2015.

[131] S. Wang, H. Cho, C. Zhai, B. Berger, and J. Peng, "Exploiting ontology graph for predicting sparsely annotated gene function," *Bioinformatics*, vol. 31, no. 12, pp. i357–i364, 2015.

[132] J. Gillis and P. Pavlidis, "The impact of multifunctional genes on "guilt by association" analysis," *PLoS One*, vol. 6(2), no. e17258, 2011.

[133] J. Gillis and P. Pavlidis, ""Guilt by association" is the exception rather than the rule in gene networks," *PLoS Computational Biology*, vol. 8, no. 3, 2012.

[134] P. Pavlidis and J. Gillis, "Progress and challenges in the computational prediction of gene function using networks: 2012-2013 update," *F1000Research*, vol. 2, no. 230, 2013.

[135] J. Gillis, S. Ballouz, and P. Pavlidis, "Bias tradeoffs in the creation and analysis of protein–protein interaction networks," *Journal of Proteomics*, vol. 100, pp. 44–54, 2014.

[136] Gene Ontology Consortium, "Gene Ontology Consortium: going forward," *Nucleic acids research*, vol. 43, no. D1, pp. D1049–D1056, 2015.

[137] H. Tong, "Fast random walk with restart and its applications," in *Proceedings of the 6th IEEE International Conference on Data Mining*, 2006.

[138] G. Jeh and J. Widom, "Scaling personalized web search," in *Proceedings of the 12th international Conference on the World Wide Web*, pp. 271–279, ACM, 2003.

[139] R. Baeza-Yates, P. Boldi, and C. Castillo, "Generalizing PageRank: Damping functions for link-based ranking algorithms," in *Proceedings of the 29th Annual International ACM SIGIR Conference on Research and Development in Information Retrieval*, pp. 308–315, ACM, 2006.

[140] P. G. Constantine and D. F. Gleich, "Random alpha PageRank," *Internet Mathematics*, vol. 6, no. 2, pp. 189–236, 2010.

[141] F. Chung, "The heat kernel as the PageRank of a graph," *Proceedings of the National Academy of Sciences*, vol. 104, no. 50, pp. 19735–19740, 2007.

[142] X. Zhu, W. Nejdl, and M. Georgescu, "An adaptive teleportation random walk model for learning social tag relevance," in *Proceedings of the 37th International ACM SIGIR Conference on Research and Development in Information Retrieval*, pp. 223–232, ACM, 2014.

[143] S. Mostafavi and Q. Morris, "Fast integration of heterogeneous data sources for predicting gene function with limited annotation," *Bioinformatics*, vol. 26, no. 14, pp. 1759–1765, 2010.

[144] H. Cho, B. Berger, and J. Peng, "Diffusion component analysis: unraveling functional topology in biological networks," in *Research in Computational Molecular Biology*, pp. 62–64, Springer, 2015.

[145] C. Stark, B.-J. Breitkreutz, T. Reguly, L. Boucher, A. Breitkreutz, and M. Tyers, "BioGRID: a general repository for interaction datasets," *Nucleic Acids Research*, vol. 34, no. suppl 1, pp. D535–D539, 2006.

[146] W. Verleyen, S. Ballouz, and J. Gillis, "Positive and negative forms of replicability in gene network analysis," *Bioinformatics*, vol. 32, no. 7, pp. 1065–1073, 2015.

[147] K. Mitra, A.-R. Carvunis, S. K. Ramesh, and T. Ideker, "Integrative approaches for finding modular structure in biological networks," *Nature Reviews Genetics*, vol. 14, no. 10, pp. 719–732, 2013.

[148] N. Pržulj, D. A. Wigle, and I. Jurisica, "Functional topology in a network of protein interactions," *Bioinformatics*, vol. 20, no. 3, pp. 340–348, 2004.

[149] G. Palla, I. Derényi, I. Farkas, and T. Vicsek, "Uncovering the overlapping community structure of complex networks in nature and society," *Nature*, vol. 435, no. 7043, pp. 814–818, 2005.

[150] B. Adamcsek, G. Palla, I. J. Farkas, I. Derényi, and T. Vicsek, "CFinder: locating cliques and overlapping modules in biological networks," *Bioinformatics*, vol. 22, no. 8, pp. 1021–1023, 2006.

[151] B. J. Frey and D. Dueck, "Clustering by passing messages between data points," *Science*, vol. 315, no. 5814, pp. 972–976, 2007.

[152] K. Macropol, T. Can, and A. K. Singh, "RRW: repeated random walks on genome-scale protein networks for local cluster discovery," *BMC Bioinformatics*, vol. 10, no. 283, 2009.

[153] Y.-Y. Ahn, J. P. Bagrow, and S. Lehmann, "Link communities reveal multiscale complexity in networks," *Nature*, vol. 466, no. 7307, pp. 761–764, 2010.

[154] A. T. Kalinka and P. Tomancak, "Linkcomm: an R package for the generation, visualization, and analysis of link communities in networks of arbitrary size and type," *Bioinformatics*, vol. 27, no. 14, pp. 2011–2012, 2011.

[155] T. Nepusz, H. Yu, and A. Paccanaro, "Detecting overlapping protein complexes in protein-protein interaction networks," *Nature Methods*, vol. 9, no. 5, pp. 471–472, 2012.

[156] C. Wiwie, J. Baumbach, and R. Röttger, "Comparing the performance of biomedical clustering methods," *Nature methods*, vol. 12, no. 11, pp. 1033–1038, 2015.

[157] Z. Lubovac, J. Gamalielsson, and B. Olsson, "Combining functional and topological properties to identify core modules in protein interaction networks," *Proteins: Structure, Function, and Bioinformatics*, vol. 64, no. 4, pp. 948–959, 2006.

[158] Y.-R. Cho, W. Hwang, M. Ramanathan, and A. Zhang, "Semantic integration to identify overlapping functional modules in protein interaction networks," *BMC Bioinformatics*, vol. 8, no. 265, 2007.

[159] M. T. Dittrich, G. W. Klau, A. Rosenwald, T. Dandekar, and T. Müller, "Identifying functional modules in protein–protein interaction networks: an integrated exact approach," *Bioinformatics*, vol. 24, no. 13, pp. i223–i231, 2008.

[160] D. Boyanova, S. Nilla, G. W. Klau, T. Dandekar, T. Müller, and M. Dittrich, "Functional module search in protein networks based on semantic similarity improves the analysis of proteomics data," *Molecular and Cellular Proteomics*, vol. 13, no. 7, pp. 1877–1889, 2014.

[161] C. M. Taniguchi, B. Emanuelli, and C. R. Kahn, "Critical nodes in signalling pathways: insights into insulin action," *Nature Reviews Molecular Cell Biology*, vol. 7, no. 2, pp. 85–96, 2006.

[162] P. J. Mucha, T. Richardson, K. Macon, M. A. Porter, and J.-P. Onnela, "Community structure in time-dependent, multiscale, and multiplex networks," *Science*, vol. 328, no. 5980, pp. 876–878, 2010.

[163] S. Zhang, Q. Li, J. Liu, and X. J. Zhou, "A novel computational framework for simultaneous integration of multiple types of genomic data to identify microRNA-gene regulatory modules," *Bioinformatics*, vol. 27, no. 13, pp. i401–i409, 2011.

[164] W. Li, S. Zhang, C.-C. Liu, and X. J. Zhou, "Identifying multi-layer gene regulatory modules from multi-dimensional genomic data," *Bioinformatics*, vol. 28, no. 19, pp. 2458–2466, 2012.

[165] B. Wang, A. M. Mezlini, F. Demir, M. Fiume, Z. Tu, M. Brudno, B. Haibe-Kains, and A. Goldenberg, "Similarity network fusion for aggregating data types on a genomic scale," *Nature Methods*, vol. 11, no. 3, pp. 333–337, 2014.

[166] D. F. Gleich and K. Kloster, "Seeded PageRank solution paths," *European Journal of Applied Mathematics*, vol. FirstView, pp. 1–34, Published online: July 1, 2016. DOI:10.1017/S0956792516000280.

[167] K. Kloster and D. F. Gleich, "Heat kernel based community detection," in *Proceedings of the 20th ACM SIGKDD International Conference on Knowledge Discovery and Data Mining*, pp. 1386–1395, ACM, 2014.

[168] H. Nassar, K. Kloster, and D. F. Gleich, "Strong localization in personalized PageRank vectors," in *Algorithms and Models for the Web Graph*, pp. 190–202, Springer, 2015.

[169] R. Andersen, F. Chung, and K. Lang, "Local graph partitioning using PageRank vectors," in *The 47th Annual IEEE Symposium on Foundations of Computer Science*, pp. 475–486, IEEE, 2006.

[170] J. M. Cherry, C. Adler, C. Ball, S. A. Chervitz, S. S. Dwight, E. T. Hester, Y. Jia, G. Juvik, T. Roe, M. Schroeder, S. Weng, and D. Botstein, "SGD: Saccharomyces genome database," *Nucleic Acids Research*, vol. 26, no. 1, pp. 73–79, 1998.

[171] H.-W. Mewes, C. Amid, R. Arnold, D. Frishman, U. Güldener, G. Mannhaupt, M. Münsterkötter, P. Pagel, N. Strack, V. Stümpflen, J. Warfsmann, and A. Ruepp, "MIPS: analysis and annotation of proteins from whole genomes," *Nucleic Acids Research*, vol. 32, no. suppl 1, pp. D41–D44, 2004.

[172] H. W. Kuhn, "The hungarian method for the assignment problem," *Naval Research Logistics Quarterly*, vol. 2, no. 1-2, pp. 83–97, 1955.

[173] D. F. Gleich, *Models and Algorithms for PageRank Sensitivity*. PhD thesis, Stanford University, September 2009. Chapter 7 on MatlabBGL.

[174] M. N. Djekidel, Z. Liang, Q. Wang, Z. Hu, G. Li, Y. Chen, and M. Q. Zhang, "3CPET: finding co-factor complexes from ChIA-PET data using a hierarchical Dirichlet process," *Genome Biology*, vol. 16, no. 288, 2015.

[175] E. S. Lein, M. J. Hawrylycz, N. Ao, M. Ayres, A. Bensinger, A. Bernard, A. F. Boe, M. S. Boguski, K. S. Brockway, E. J. Byrnes, L. Chen, T. M. Chen, M. C. Chin, J. Chong, B. E. Crook, A. Czaplinska, C. N. Dang, S. Datta, N. R. Dee, A. L. Desaki, T. Desta, E. Diep, T. A. Dolbeare, M. J. Donelan, H. W. Dong, J. G. Dougherty, B. J. Duncan, A. J. Ebbert, G. Eichele, L. K. Estin, C. Faber, B. A. Facer, R. Fields, S. R. Fischer, T. P. Fliss, C. Frensley, S. N. Gates, K. J. Glattfelder, K. R. Halverson, M. R. Hart, J. G. Hohmann, M. P. Howell, D. P. Jeung, R. A. Johnson, P. T. Karr, R. Kawal, J. M. Kidney, R. H. Knapik, C. L. Kuan, J. H. Lake, A. R. Laramee, K. D. Larsen, C. Lau, T. A. Lemon, A. J. Liang, Y. Liu, L. T. Luong, J. Michaels, J. J. Morgan, R. J. Morgan, M. T. Mortrud, N. F. Mosqueda, L. L. Ng, R. Ng, G. J. Orta, C. C. Overly, T. H. Pak, S. E. Parry, S. D. Pathak, O. C. Pearson, R. B. Puchalski, Z. L. Riley, H. R. Rockett, S. A. Rowland, J. J. Royall, M. J. Ruiz, N. R. Sarno, K. Schaffnit, N. V. Shapovalova, T. Sivisay, C. R. Slaughterbeck, S. C. Smith, K. A. Smith, B. I. Smith, A. J. Sodt, N. N. Stewart, K. R. Stumpf, S. M. Sunkin, M. Sutram, A. Tam, C. D. Teemer, C. Thaller, C. L. Thompson, L. R. Varnam, A. Visel, R. M. Whitlock, P. E. Wohnoutka, C. K. Wolkey, V. Y. Wong, M. Wood, *et al.*, "Genome-wide atlas of gene expression in the adult mouse brain," *Nature*, vol. 445, no. 7124, pp. 168–176, 2007.

[176] Y. Shen, F. Yue, D. F. McCleary, Z. Ye, L. Edsall, S. Kuan, U. Wagner, J. Dixon, L. Lee, V. V. Lobanenkov, and B. Ren, "A map of the cis-regulatory sequences in the mouse genome," *Nature*, vol. 488, no. 7409, pp. 116–120, 2012.

[177] S. Haider, B. Ballester, D. Smedley, J. Zhang, P. Rice, and A. Kasprzyk, "BioMart central portal–unified access to biological data," *Nucleic Acids Research*, vol. 37, no. suppl 2, pp. W23–W27, 2009.

[178] A. R. Quinlan and I. M. Hall, "BEDTools: a flexible suite of utilities for comparing genomic features," *Bioinformatics*, vol. 26, no. 6, pp. 841–842, 2010.

[179] The Cancer Genome Atlas Network, "Comprehensive molecular portraits of human breast tumours," *Nature*, vol. 490, no. 7418, pp. 61–70, 2012.

[180] Cancer Genome Atlas Research Network, "Comprehensive genomic characterization of squamous cell lung cancers," *Nature*, vol. 489, no. 7417, pp. 519–525, 2012.

[181] Cancer Genome Atlas Network, "Comprehensive molecular characterization of human colon and rectal cancer," *Nature*, vol. 487, no. 7407, pp. 330–337, 2012.

[182] L. Ding, G. Getz, D. A. Wheeler, E. R. Mardis, M. D. McLellan, K. Cibulskis, C. Sougnez, H. Greulich, D. M. Muzny, M. B. Morgan, L. Fulton, R. S. Fulton, Q. Zhang, M. C. Wendl, M. S. Lawrence, D. E. Larson, K. Chen, D. J. Dooling, A. Sabo, A. C. Hawes, H. Shen, S. N. Jhangiani, L. R. Lewis, O. Hall, Y. Zhu, T. Mathew, Y. Ren, J. Yao, S. E. Scherer, K. Clerc, G. A. Metcalf, B. Ng, A. Milosavljevic, M. L. Gonzalez-Garay, J. R. Osborne, R. Meyer, X. Shi, Y. Tang, D. C. Koboldt, L. Lin, R. Abbott, T. L. Miner, C. Pohl, G. Fewell, C. Haipek, H. Schmidt, B. H. Dunford-Shore, A. Kraja, S. D. Crosby, C. S. Sawyer, T. Vickery, S. Sander, J. Robinson, W. Winckler, J. Baldwin, L. R. Chirieac, A. Dutt, T. Fennell, M. Hanna, B. E. Johnson, R. C. Onofrio, R. K. Thomas, G. Tonon, B. A. Weir, X. Zhao, L. Ziaugra, M. C. Zody, T. Giordano, M. B. Orringer, J. A. Roth, M. R. Spitz, I. I. Wistuba, B. Ozenberger, P. J. Good, A. C. Chang, D. G. Beer, M. A. Watson, M. Ladanyi, S. Broderick, A. Yoshizawa, W. D. Travis, W. Pao, M. A. Province, G. M. Weinstock, H. E. Varmus, S. B. Gabriel, E. S. Lander, R. A. Gibbs, M. Meyerson, and R. K. Wilson, "Somatic mutations affect key pathways in lung adenocarcinoma," *Nature*, vol. 455, no. 7216, pp. 1069–1075, 2008.

[183] Y. Setty, A. E. Mayo, M. G. Surette, and U. Alon, "Detailed map of a cis-regulatory input function," *Proceedings of the National Academy of Sciences*, vol. 100, no. 13, pp. 7702–7707, 2003.

[184] J. J. Li, C.-R. Jiang, J. B. Brown, H. Huang, and P. J. Bickel, "Sparse linear modeling of next-generation mRNA sequencing (RNA-seq) data for isoform discovery and abundance estimation," *Proceedings of the National Academy of Sciences*, vol. 108, no. 50, pp. 19867–19872, 2011.

[185] Y. Wang, T. Joshi, X.-S. Zhang, D. Xu, and L. Chen, "Inferring gene regulatory networks from multiple microarray datasets," *Bioinformatics*, vol. 22, no. 19, pp. 2413–2420, 2006.

[186] N. C. Duarte, S. A. Becker, N. Jamshidi, I. Thiele, M. L. Mo, T. D. Vo, R. Srivas, and B. Ø. Palsson, "Global reconstruction of the human metabolic network based on genomic and bibliomic data," *Proceedings of the National Academy of Sciences*, vol. 104, no. 6, pp. 1777–1782, 2007.

[187] L. Akoglu, M. McGlohon, and C. Faloutsos, "Oddball: Spotting anomalies in weighted graphs," in *Advances in Knowledge Discovery and Data Mining*, pp. 410–421, Springer, 2010.

[188] D. F. Gleich and C. Seshadhri, "Vertex neighborhoods, low conductance cuts, and good seeds for local community methods," in *Proceedings of the 18th ACM SIGKDD International Conference on Knowledge Discovery and Data Mining*, pp. 597–605, ACM, 2012.

[189] J. R. Wiśniewski, P. Ostasiewicz, K. Duś, D. F. Zielińska, F. Gnad, and M. Mann, "Extensive quantitative remodeling of the proteome between normal colon tissue and adenocarcinoma," *Molecular Systems Biology*, vol. 8, no. 611, 2012.

[190] J. Zhang, S. Haider, J. Baran, A. Cros, J. M. Guberman, J. Hsu, Y. Liang, L. Yao, and A. Kasprzyk, "BioMart: a data federation framework for large collaborative projects," *Database*, vol. 2011, no. bar038, 2011.

[191] J. Renegar, "A polynomial-time algorithm, based on Newton's method, for linear programming," *Mathematical Programming*, vol. 40, no. 1-3, pp. 59–93, 1988.

[192] A. Petitjean, M. Achatz, A. Borresen-Dale, P. Hainaut, and M. Olivier, "TP53 mutations in human cancers: functional selection and impact on cancer prognosis and outcomes," *Oncogene*, vol. 26, no. 15, pp. 2157–2165, 2007.

[193] T. Ideker, O. Ozier, B. Schwikowski, and A. F. Siegel, "Discovering regulatory and signalling circuits in molecular interaction networks," *Bioinformatics*, vol. 18, no. Suppl 1, pp. S233–S240, 2002.

[194] S. Anders and W. Huber, "Differential expression analysis for sequence count data," *Genome Biology*, vol. 11(10), no. R106, 2010.

[195] B. Berger, J. Peng, and M. Singh, "Computational solutions for omics data," *Nature Reviews Genetics*, vol. 14, no. 5, pp. 333–346, 2013.

[196] H.-Y. Chuang, E. Lee, Y.-T. Liu, D. Lee, and T. Ideker, "Network-based classification of breast cancer metastasis," *Molecular Systems Biology*, vol. 3, no. 140, 2007.

[197] I. Ulitsky, A. Krishnamurthy, R. M. Karp, and R. Shamir, "DEGAS: *De novo* discovery of dysregulated pathways in human diseases," *PLoS One*, vol. 5, no. 10, 2010.

[198] D. Beisser, G. W. Klau, T. Dandekar, T. Müller, and M. T. Dittrich, "BioNet: an R-package for the functional analysis of biological networks," *Bioinformatics*, vol. 26, no. 8, pp. 1129–1130, 2010.

[199] E. Cerami, E. Demir, N. Schultz, B. S. Taylor, and C. Sander, "Automated network analysis identifies core pathways in glioblastoma," *PLoS One*, vol. 5, no. 2, 2010.

[200] J. Gu, Y. Chen, S. Li, and Y. Li, "Identification of responsive gene modules by network-based gene clustering and extending: application to inflammation and angiogenesis," *BMC Systems Biology*, vol. 4, p. 47, 2010.

[201] P. Dao, K. Wang, C. Collins, M. Ester, A. Lapuk, and S. C. Sahinalp, "Optimally discriminative subnetwork markers predict response to chemotherapy," *Bioinformatics*, vol. 27, no. 13, pp. i205–i213, 2011.

[202] K. Komurov, S. Dursun, S. Erdin, and P. T. Ram, "NetWalker: a contextual network analysis tool for functional genomics," *BMC Genomics*, vol. 13, no. 282, 2012.

[203] T. S. Keshava Prasad, R. Goel, K. Kandasamy, S. Keerthikumar, S. Kumar, S. Mathivanan, D. Telikicherla, R. Raju, B. Shafreen, A. Venugopal, L. Balakrishnan, A. Marimuthu, S. Banerjee, D. S. Somanathan, A. Sebastian, S. Rani, S. Ray, C. J. Harrys Kishore, S. Kanth, M. Ahmed, M. K. Kashyap, R. Mohmood, Y. L. Ramachandra, V. Krishna, B. A. Rahiman, S. Mohan, P. Ranganathan, S. Ramabadran, R. Chaerkady, and A. Pandey, "Human protein reference database–2009 update," *Nucleic Acids Research*, vol. 37, no. Suppl 1, pp. D767–D772, 2009.

[204] M. Kanehisa and S. Goto, "Kyoto encyclopedia of genes and genomes," *Nucleic Acids Research*, vol. 28, no. 1, pp. 27–30, 2000.

[205] M. A. Harris, J. Clark, A. Ireland, J. Lomax, M. Ashburner, R. Foulger, K. Eilbeck, S. Lewis, B. Marshall, C. Mungall, J. Richter, G. M. Rubin, J. A. Blake, C. Bult, M. Dolan, H. Drabkin, J. T. Eppig, D. P. Hill, L. Ni, M. Ringwald, R. Balakrishnan, J. M. Cherry, K. R. Christie, M. C. Costanzo, S. S. Dwight, S. Engel, D. G. Fisk, J. E. Hirschman, E. L. Hong, R. S. Nash, A. Sethuraman, C. L. Theesfeld, D. Botstein, K. Dolinski, B. Feierbach, T. Berardini, S. Mundodi, S. Y. Rhee, R. Apweiler, D. Barrell, E. Camon, E. Dimmer, V. Lee, R. Chisholm, P. Gaudet, W. Kibbe, R. Kishore, E. M. Schwarz, P. Sternberg, M. Gwinn, L. Hannick, J. Wortman, M. Berriman, V. Wood, N. de la Cruz, P. Tonellato, P. Jaiswal, T. Seigfried, and R. White, "The Gene Ontology (GO) database and informatics resource," *Nucleic Acids Research*, vol. 32, no. Suppl 1, pp. D258–D261, 2004.

[206] R. D. Luce and A. D. Perry, "A method of matrix analysis of group structure," *Psychometrika*, vol. 14, no. 2, pp. 95–116, 1949.

[207] J. J. Whang, D. F. Gleich, and I. S. Dhillon, "Overlapping community detection using seed set expansion," *Proceedings of the 22nd ACM International Conference on Information and Knowledge Management*, pp. 2099–2108, 2013.

[208] C. Xie, X. Mao, J. Huang, Y. Ding, J. Wu, S. Dong, L. Kong, G. Gao, C. Y. Li, and L. Wei, "KOBAS 2.0: A web server for annotation and identification of enriched pathways and diseases," *Nucleic Acids Research*, vol. 39, no. Suppl 2, pp. W316–W322, 2011.

[209] A. Hamosh, A. F. Scott, J. S. Amberger, C. A. Bocchini, and V. A. McKusick, "Online Mendelian Inheritance in Man (OMIM), a knowledgebase of human genes and genetic disorders," *Nucleic Acids Research*, vol. 33, no. Suppl 1, pp. D514–D517, 2005.

[210] P. Du, G. Feng, J. Flatow, J. Song, M. Holko, W. A. Kibbe, and S. M. Lin, "From disease ontology to disease-ontology lite: Statistical methods to adapt a general-purpose ontology for the test of gene-ontology associations," vol. 25, no. 12, pp. i63–i68, 2009.

[211] K. G. Becker, K. C. Barnes, T. J. Bright, and S. A. Wang, "The genetic association database," *Nature Genetics*, vol. 36, no. 5, pp. 431–432, 2004.

[212] D. Welter, J. MacArthur, J. Morales, T. Burdett, P. Hall, H. Junkins, A. Klemm, P. Flicek, T. Manolio, L. Hindorff, and H. Parkinson, "The NHGRI GWAS Catalog, a curated resource of SNP-trait associations," *Nucleic Acids Research*, vol. 42, no. D1, pp. D1001–D1006, 2014.

[213] C. F. Schaefer, K. Anthony, S. Krupa, J. Buchoff, M. Day, T. Hannay, and K. H. Buetow, "PID: The pathway interaction database," *Nucleic Acids Research*, vol. 37, no. Suppl 1, pp. D674–D679, 2009.

[214] D. Nishimura, "BioCarta," *Biotech Software and Internet Report*, vol. 2, no. 3, pp. 117–120, 2001.

[215] G. Joshi-Tope, M. Gillespie, I. Vastrik, P. D'Eustachio, E. Schmidt, B. de Bono, B. Jassal, G. R. Gopinath, G. R. Wu, L. Matthews, S. Lewis, E. Birney, and L. Stein, "Reactome: A knowledgebase of biological pathways," *Nucleic Acids Research*, vol. 33, no. Suppl 1, pp. D428–D432, 2005.

[216] R. Caspi, T. Altman, R. Billington, K. Dreher, H. Foerster, C. A. Fulcher, T. A. Holland, I. M. Keseler, A. Kothari, A. Kubo, M. Krummenacker, M. Latendresse, L. A. Mueller, Q. Ong, S. Paley, P. Subhraveti, D. S. Weaver, D. Weerasinghe, P. Zhang, and P. D. Karp, "The MetaCyc database of metabolic pathways and enzymes and the BioCyc collection of pathway/genome databases," *Nucleic Acids Research*, vol. 42, no. D1, pp. D459–D471, 2014.

[217] H. Mi, B. Lazareva-Ulitsky, R. Loo, A. Kejariwal, J. Vandergriff, S. Rabkin, N. Guo, A. Muruganujan, O. Doremieux, M. J. Campbell, H. Kitano, and P. D. Thomas, "The PANTHER database of protein families, subfamilies, functions and pathways," *Nucleic Acids Research*, vol. 33, no. Suppl 1, pp. D284–D288, 2005.

[218] R. Saito, M. E. Smoot, K. Ono, J. Ruscheinski, P.-L. Wang, S. Lotia, A. R. Pico, G. D. Bader, and T. Ideker, "A travel guide to Cytoscape plugins.," *Nature Methods*, vol. 9, no. 11, pp. 1069–1076, 2012.

[219] J. M. Silva, K. Marran, J. S. Parker, J. Silva, M. Golding, M. R. Schlabach, S. J. Elledge, G. J. Hannon, and K. Chang, "Profiling essential genes in human mammary cells by multiplex RNAi screening.," *Science*, vol. 319, no. 5863, pp. 617–620, 2008.

[220] M. R. Sajnani, A. K. Patel, V. D. Bhatt, A. K. Tripathi, V. B. Ahir, V. Shankar, S. Shah, T. M. Shah, P. G. Koringa, S. J. Jakhesara, and C. G. Joshi, "Identification of novel transcripts deregulated in buccal cancer by RNA-seq," *Gene*, vol. 507, no. 2, pp. 152–158, 2012.

[221] S. Duss, H. Brinkhaus, A. Britschgi, E. Cabuy, D. M. Frey, D. J. Schaefer, and M. Bentires-Alj, "Mesenchymal precursor cells maintain the differentiation and proliferation potentials of breast epithelial cells," *Breast Cancer Research*, vol. 16(3), no. R60, 2014.

[222] Y. Chang, M. Zuka, P. Perez-Pinera, A. Astudillo, J. Mortimer, J. R. Berenson, and T. F. Deuel, "Secretion of pleiotrophin stimulates breast cancer progression through remodeling of the tumor microenvironment," *Proceedings of the National Academy of Sciences*, vol. 104, no. 26, pp. 10888–10893, 2007.

[223] M. P. H. M. Jansen, K. Ruigrok-Ritstier, L. C. J. Dorssers, I. L. Van Staveren, M. P. Look, M. E. Meijer-Van Gelder, A. M. Sieuwerts, J. Helleman, S. Sleijfer, J. G. M. Klijn, J. A. Foekens, and E. M. J. J. Berns, "Downregulation of SIAH2, an ubiquitin E3 ligase, is associated with resistance to endocrine therapy in breast cancer," *Breast Cancer Research and Treatment*, vol. 116, no. 2, pp. 263–271, 2009.

[224] Y. Benjamini and Y. Hochberg, "Controlling the false discovery rate: A practical and powerful approach to multiple testing," *Journal of the Royal Statistical Society. Series B (Methodological)*, vol. 57, no. 1, pp. 289–300, 1995.

[225] S. Sun, J. H. Schiller, and A. F. Gazdar, "Lung cancer in never smokers–a different disease," *Nature Reviews Cancer*, vol. 7, no. 10, pp. 778–790, 2007.

[226] P. Lee, "Smoking and alzheimer's disease: a review of the epidemiological evidence," *Neuroepidemiology*, vol. 13, no. 4, pp. 131–144, 1994.

[227] M. F. Allam, M. J. Campbell, A. Hofman, A. S. Del Castillo, and R. Fernández-Crehuet Navajas, "Smoking and parkinson's disease: systematic review of prospective studies," *Movement Disorders*, vol. 19, no. 6, pp. 614–621, 2004.

[228] J. A. Critchley and S. Capewell, "Mortality risk reduction associated with smoking cessation in patients with coronary heart disease: a systematic review," *JAMA*, vol. 290, no. 1, pp. 86–97, 2003.

[229] T. Birrenbach and U. Böcker, "Inflammatory bowel disease and smoking. a review of epidemiology, pathophysiology, and therapeutic implications," *Inflammatory Bowel Diseases*, vol. 10, no. 6, pp. 848–859, 2004.

[230] C. Cortes and V. Vapnik, "Support-vector networks," *Machine learning*, vol. 20, no. 3, pp. 273–297, 1995.

[231] L. Breiman, "Random forests," *Machine Learning*, vol. 45, no. 1, pp. 5–32, 2001.

[232] D. Silver, A. Huang, C. J. Maddison, A. Guez, L. Sifre, G. Van Den Driessche, J. Schrittwieser, I. Antonoglou, V. Panneershelvam, M. Lanctot, S. Dieleman, D. Grewe, J. Nham, N. Kalchbrenner, I. Sutskever, T. Lillicrap, M. Leach, K. Kavukcuoglu, T. Graepel, and D. Hassabis, "Mastering the game of Go with deep neural networks and tree search," *Nature*, vol. 529, no. 7587, pp. 484–489, 2016.

[233] Y. Zhou and R. Chellappa, "Computation of optical flow using a neural network," in *Neural Networks, 1988., IEEE International Conference on*, pp. 71–78, IEEE, 1988.

[234] G. E. Hinton, N. Srivastava, A. Krizhevsky, I. Sutskever, and R. R. Salakhutdinov, "Improving neural networks by preventing co-adaptation of feature detectors," *arXiv:1207.0580*, 2012.

[235] J. Deng, W. Dong, R. Socher, L.-J. Li, K. Li, and L. Fei-Fei, "Imagenet: A large-scale hierarchical image database," in *IEEE Conference on Computer Vision and Pattern Recognition*, pp. 248–255, IEEE, 2009.

[236] C.-C. Chang and C.-J. Lin, "LIBSVM: a library for support vector machines," *ACM Transactions on Intelligent Systems and Technology*, vol. 2(3), no. 27, 2011.

VITA

VITA

Biaobin Jiang was born in Nanning, Guangxi, China, on March 5th, 1986. He began to study pharmaceutical engineering in Beijing Institute of Technology in September 2005, and completed a Bachelor of Engineering in July 2009. He worked as a research intern Academy of Mathematics and Systems Science, Chinese Academy of Sciences from 2009 to 2010. He started his graduate study in August 2010, and received his Ph.D. in computational biology from Department of Biological Sciences, Purdue University (West Lafayette, IN) in August 2016. His graduate research focuses on modeling molecular networks using machine learning techniques. He entered Department of Genetics and Genomic Sciences, Icahn School of Medicine at Mount Sinai (New York, NY) as a postdoctoral researcher in September 2016.

Publication

[1] B. Jiang and M. Gribskov. *Assessment of subnetwork detection methods for breast cancer.* Cancer Informatics, 13 (Suppl 6), pp.15-23, 2014.

[2] B. Jiang, D.F. Gleich, and M. Gribskov. *Differential flux balance analysis of quantitative proteomic data on protein interaction networks.* IEEE Global Conference on Signal and Information Processing, pp.977-981, Dec. 2015.

[3] B. Jiang, K. Kloster, D.F. Gleich, and M. Gribskov. *AptRank: an adaptive PageRank model for protein function prediction on bi-relational graphs.* (under review).

[4] B. Jiang, K. Kloster, D.F. Gleich, M. Gribskov, and Y. Wang. *BioSweeper: a joint clustering method for functional module detection on multi-layer networks.* (in preparation).

[5] B. Jiang, D.F. Gleich, and M. Gribskov. *DiPAna: differential pathway analysis.* (in preparation)